EXPERIMENTAL STRAIN ANALYSIS TECHNIQUE FOR LARGE DEFORMATIONS BASED ON THE OPTICAL PROPERTIES OF A THIN METALLIC FILM DEPOSITED ON A STRUCTURAL SUBSTRATE

by

Jerry Gene Williams

Thesis submitted to the Graduate Faculty of the

Virginia Polytechnic Institute

in candidacy for the degree of

DOCTOR OF PHILOSOPHY

in

Engineering Mechanics

APPROVED: Daniel Frederick
Chairman, Dr. Daniel Frederick

Prof. Charles W. Smith

Dr. George A. Gray

Dr. Halbert F. Brinson

Dr. John W. Layman

May 1970

Blacksburg, Virginia

EXPERIMENTAL STRAIN ANALYSIS TECHNIQUE FOR LARGE DEFORMATIONS BASED ON THE OPTICAL PROPERTIES OF A THIN METALLIC FILM DEPOSITED ON A STRUCTURAL SUBSTRATE

by

Jerry Gene Williams

Thesis submitted to the Graduate Faculty of the

Virginia Polytechnic Institute

in candidacy for the degree of

DOCTOR OF PHILOSOPHY

Engineering Mechanics

APPROVED:

Chairman, Dr. Daniel Frederick

Prof. Charles W. Smith

Dr. George A. Gray

Dr. Halbert F. Brinson

Dr. John W. Layman

May 1970

Blacksburg, Virginia

EXPERIMENTAL STRAIN ANALYSIS TECHNIQUE FOR LARGE DEFORMATIONS BASED ON THE OPTICAL PROPERTIES OF A THIN METALLIC FILM DEPOSITED ON A STRUCTURAL SUBSTRATE

By Jerry Gene Williams

ABSTRACT

The optical response to loading of a thin metallic film deposited on a low modulus structural substrate is studied both analytically and experimentally. Two fundamental types of transmittance and reflectance properties are shown to be related to the mechanical state of the substrate. The first property called total transmittance (or total reflectance) is defined as the total energy of incident light which is transmitted (or reflected) by the material. A change in the total transmittance (or reflectance) as a result of a change in the mechanical state of the substrate is caused by two factors: First, due to a change in the film effective thickness; and second, due to the development of microfractures. The second property called central image transmittance (or central image reflectance) is associated with the formation in the thin metallic film of a periodic set of closely spaced wrinkles with which light interacts to create a diffraction grating. The diffraction grating spacially redistributes the incident light energy by deflecting energy out of the central image component and into side bands. Such a set of wrinkles and consequently the diffraction effect occurs only if the thin film is subjected to a compressive strain field. Otherwise,

the central image property reverts to the total transmittance (or total reflectance) case.

An analytical approach is developed to relate the optical properties of the metallic film to the mechanical properties of the substrate. A set of empirical optical-mechanics relationships are proposed between the total and central image transmittance and reflectance properties and the strain field of a general biaxial problem.

Experimental results are presented for the total and central image transmittance response for thin films of aluminum, copper and indium deposited on a silicone rubber substrate subjected to uniaxial loading Microscopic surface examinations of gold, aluminum and indium on a silicone rubber substrate clearly demonstrate the characteristic microfracture and wrinkle geometric patterns. The total and central image transmittance responses of a silicone rubber rectangular plate with a centrally located hole subjected to uniaxial loading are used to calculate the principal strain field for the cross section of minimum area. The plate was coated with a thin film of aluminum prior to loading. It is shown that principal strain directions may be determined from the microfracture pattern and when the strain in a principal direction is compressive, also from the spectral diffraction pattern.

The experimental results presented are in general in good agreement with the analytical models proposed. The technique requires more development, but does show promise as a new approach for the experimental determination of the strain field, especially, for large deformation problems.

TABLE OF CONTENTS

CHAPTER PAGE

LIST OF FIGURES

LIST OF TABLES

LIST OF SYMBOLS

A	area
$\mathring{A}$	angstrom, 10^{-10} meters
a	absorption
b	width
c	velocity of light
$\vec{D}$	electric displacement vector
d	thin film thickness
$\vec{E}$	electric force vector
F	force
f_o	grating frequency
G_1, G_2, G_3, G_4	proportionality functions associated with the development of microfractures
$\vec{H}$	magnetic force vector
J_1, J_2, J_3, J_4	proportionality functions associated with diffraction
J_q	Bessel function of first kind and of order q
k	absorption coefficient
l	length
m	peak-to-peak change in amplitude transmitted across the grating
mm	millimeter
n	refractive index
$\bar{n}$	complex refractive index
p	peak-to-peak excursion of the phase delay
R	reflectance

r	radius
s	transmittance function
T	transmittance
t	time
u	general displacement or displacement in x-direction
V	volume
v	displacement in y-direction
W_1, W_2	proportionality function associated with total transmittance
W_3, W_4	proportionality function associated with total reflectance
W_5	proportionality constant associated with total transmittance
W_6	proportionality constant associated with total reflectance
w	displacement in z-direction
x, y, z	rectangular Cartesian coordinates
ΔR	change in reflectance between initial and final conditions
ΔT	change in transmittance between initial and final conditions
ϵ	strain
ϵ^L	conventional Lagrangian strain
$\tilde{\epsilon}$	natural strain
$\epsilon_{xx}, \epsilon_{yy}$	principal strains
η	specific conductivity
λ	wavelength of light
μ	magnetic permeability
ν	Poisson's ratio

$\bar{\nu}$	Poisson's ratio associated with natural strain
ξ	dielectric constant
ρ	electric charge density
σ	stress
$\tilde{\sigma}$	true stress
σ_a	uniform stress applied to a rectangular plate with a centrally located hole

Subscript

f	final
i	initial
x,y,z	corresponding to x, y, or z rectangular Cartesian coordinate

I. INTRODUCTION

Modern structural materials for civil and aerospace applications includes many materials whose response to loading results in large deformations. The solution of problems from classical elasticity is made extremely difficult under these circumstances due to the necessity for the retention of higher order terms in the strain displacement equations, complicated constitutive equations, and because the resulting state of strain may depend on the rate and order of application of the loads and on preceding load history. The strain distribution in bodies subjected to large deformations has been analytically determined in a very small number of cases but always for relatively simple problems (ref. 1).

On the other hand, certain existing experimental methods and that developed herein by this writer seem to be well suited to obtaining the solution of some of these large deformation problems. A review of existing experimental methods including grid, moire, and photoelasticity techniques may be found in reference 2. The theory and applications of brittle coatings are covered in reference 3. The new experimental stress analysis technique proposed in this paper is based on the change in optical properties between initial and final conditions of a thin metallic film deposited on a structural substrate. The discovery of this new technique was made during the course of the writer's development of a flexible window concept for application in manned expandable space structures (refs. 4 and 5). The window utilizes steel or fiber

glass reinforcement placed in an open grid pattern in a flexible polymeric matrix. A thin transparent metallic coating was vapor deposited on the window matrix material to investigate its spectral transmission response and to provide ultraviolet light protection to the window and viewer. While stretching the silicone rubber substrate, it was observed that the thin metallic film acted as a light shutter; that is, tensile deformations increased the intensity of light transmitted by the window. It was also observed that the phenomenon was reversible.

The possibility of utilizing such a phenomenon in an experimental stress analysis technique was subsequently considered by the writer and the results of the ensuing investigation are described herein. A review is presented of the pertinent literature; a theoretical explanation is proposed for the changes in total and central image transmittance and reflectance of a thin metallic film resulting from a change in the mechanical state of the substrate on which it is deposited; and the results of an experimental study for the case of uniaxial loading are presented Experimental results include transmittance data for a variety of metallic thin film coating materials, thicknesses and conditions; and photomicrographs of the film microfracture and wrinkle patterns. Finally, the theory is extended to a biaxial case and the problem of a uniaxially loaded rectangular plate with a centrally located hole is experimentally investigated using the new technique. The technique does show promise as an experimental stress analysis technique, especially for problems involving large deformations.

II. LITERATURE REVIEW

2.0 Large Deformation Theory

The difficulty in analyzing problems with large deformations is primarily a result of nonlinearities in the governing equations. These nonlinearities are a result of material properties (nonlinear constitutive relations) and/or geometric considerations (finite deformations). A review of this subject may be found in references 6, 7, 8, and 9.

The results of Hooke's law are applicable for materials for which there exists a linear relationship between the applied stress and the resulting strain. To this end, some large deformation experimental stress analysts (refs. 10, 11, and 12) have found it convenient to assume new definitions for strain and stress other than the conventional Lagrangian or engineering definitions.

Natural strain is defined as the integral of the instantaneous (or incremental) change in length divided by the length the fiber has at each level of incremental deformation.

$$\begin{aligned} \bar{\epsilon} &= \int \frac{dl}{l} \\ &= \ln \frac{l_f}{l_i} \\ &= \ln(1 + \epsilon^L) \end{aligned} \tag{2.1}$$

where ϵ^L is the conventional Lagrangian definition of strain

$$\epsilon^L = \lim_{l_1 \to 0} \frac{l_f - l_1}{l_i} \tag{2.2}$$

Stress is conventionally defined as the applied load divided by the initial cross-sectional area. True stress defined as the applied load divided by the final cross-sectional area is commonly used to define stress for problems involving large deformations.

$$\bar{\sigma} = \frac{\text{applied load}}{\text{final cross-sectional area}} \tag{2.3}$$

Another definition, natural stress, is defined to parallel the concept of natural strain and is the sum between initial and final conditions of all the instantaneous (or incremental) loads divided by the corresponding area at that instant. Mathematically it is expressed by:

$$\bar{\sigma} = \int_{m=1}^{m=f} \frac{dF}{A_m} \tag{2.4}$$

Reference 12 cautions, however, that natural stress values in the deformed state do not satisfy equilibrium conditions. Using true stress and natural strain definitions, reference 10 shows for a polyurethane material (Solithane 113), that the stress-strain relationship is linear for Lagrangian strains up to 15 percent.

Using natural stress and natural strain definitions, reference 12 shows that for another polyurethane material (MP600, manufactured by Easthampton Rubber, Easthampton, Massachusetts) that the stress-strain plot is linear up to a Lagrangian strain of on the order of 100 percent.

The technique used in these extensions of Hooke's law to problems with large deformations is to observe the linearity between stress and strain in a uniaxial load test and to assume that the results hold true for a general state of stress.

Theories which relate the strains and deformations of a body usually begin by considering the motions of the body under load. One may approach the problem from either a Lagrangian (deformations expressed in terms of initial positions) or Eulerian (deformations expressed in terms of instantaneous positions) viewpoint. The Lagrangian viewpoint is the more common in elasticity and is the approach chosen for discussion in this paper.

An assumption commonly made in the development of elasticity for small deformations is that the partial derivative of the displacements are small such that the products and powers of the derivatives can be neglected with respect to the derivatives and that the derivatives can be neglected with respect to unity. Based on this assumption the so-called infinitesimal strain displacement relationship is developed (ref. 13)

$$\epsilon_{ij} = \frac{1}{2}(u_{i,j} + u_{j,i}) \tag{2.5}$$

Several expressions appear in the literature for the general or finite strain-displacement relations (refs. 9, 11, 13). The differences are a result of the different geometric and mathematical assumptions made in the derivation.

An expression derived for the strain-displacement relations in which differential displacement and position vectors are expanded in a Taylor series and terms of order higher than two are dropped is of the following form:

$$\epsilon_{ij} = \frac{1}{2}(u_{i,j} + u_{j,i} + u_{r,i}\, u_{r,j}) \tag{2.6}$$

Parks and Durelli (ref. 11) use geometric considerations in their derivation to obtain the relationships:

$$\left.\begin{aligned}
\epsilon_{xx} &= \sqrt{1 + 2\frac{\partial u}{\partial x} + \left(\frac{\partial u}{\partial x}\right)^2 + \left(\frac{\partial v}{\partial x}\right)^2 + \left(\frac{\partial w}{\partial x}\right)^2} - 1 \\
\epsilon_{yy} &= \sqrt{1 + 2\frac{\partial v}{\partial y} + \left(\frac{\partial u}{\partial y}\right)^2 + \left(\frac{\partial v}{\partial y}\right)^2 + \left(\frac{\partial w}{\partial y}\right)^2} - 1 \\
\epsilon_{zz} &= \sqrt{1 + 2\frac{\partial w}{\partial z} + \left(\frac{\partial u}{\partial z}\right)^2 + \left(\frac{\partial v}{\partial z}\right)^2 + \left(\frac{\partial w}{\partial z}\right)^2} - 1
\end{aligned}\right\} \tag{2.7}$$

$$\left.\begin{aligned}
\epsilon_{xy} &= \arcsin \frac{\frac{\partial u}{\partial y} + \frac{\partial v}{\partial x} + \frac{\partial u}{\partial x}\frac{\partial u}{\partial y} + \frac{\partial v}{\partial x}\frac{\partial v}{\partial y} + \frac{\partial w}{\partial x}\frac{\partial w}{\partial y}}{(1 + \epsilon_{xx})(1 + \epsilon_{yy})} \\
\epsilon_{yz} &= \arcsin \frac{\frac{\partial v}{\partial z} + \frac{\partial w}{\partial y} + \frac{\partial u}{\partial y}\frac{\partial u}{\partial z} + \frac{\partial v}{\partial y}\frac{\partial v}{\partial z} + \frac{\partial w}{\partial y}\frac{\partial w}{\partial z}}{(1 + \epsilon_{yy})(1 + \epsilon_{zz})} \\
\epsilon_{zx} &= \arcsin \frac{\frac{\partial w}{\partial x} + \frac{\partial u}{\partial z} + \frac{\partial u}{\partial x}\frac{\partial u}{\partial z} + \frac{\partial v}{\partial x}\frac{\partial v}{\partial z} + \frac{\partial w}{\partial x}\frac{\partial w}{\partial z}}{(1 + \epsilon_{xx})(1 + \epsilon_{zz})}
\end{aligned}\right\}$$

The normal strains (ϵ_{xx}, ϵ_{yy}, ϵ_{zz}) from equation (2.7) reduce to those of equation (2.6) if it is assumed that the strains are small enough so that second order powers of strain can be neglected with respect to the strain itself. Further, the shear strains (ϵ_{xy}, ϵ_{xz}, ϵ_{yz}) from equations (2.7) reduce to those of equation (2.6) if it is assumed that the sine of the shear strain is equal to the shear strain, and as before, the normal strains are assumed small and can be neglected with respect to unity. A discussion of the errors introduced by these and other assumptions may be found in reference 11.

Biot (ref 9) separates the displacement of a body into one of pure deformation followed by rigid body rotation and neglects third-order terms to obtain the relationships:

$$\epsilon_{ij} = \frac{1}{2}(u_{i,j} + u_{j,i}) + \frac{1}{8}(3\, u_{r,i}u_{r,j} - u_{j,r}u_{i,r} - u_{r,i}u_{j,r} - u_{r,j}u_{i,r}) \tag{2.8}$$

2.1 Thin Film Optical Theory

A thin film may be defined as a material extending in two directions with the third direction, the thickness, being on the order of the magnitude of the wavelength of the incident light. A very thin film may be defined as one whose thickness $d < \frac{\lambda}{100}$. A "thick" thin film is defined as one which transmits less than 10 percent of the incident light. A thin film is characterized by a refractive index "n" and if absorption is present, by a coefficient of absorption "k." The total energy of the light incident upon a thin film is either transmitted, reflected, or absorbed by it.

$$T + R + a = 1 \tag{2.9}$$

Diffraction also may occur in which case the total energy may assume a different spacial distribution than would otherwise occur.

Studies of the optical properties of thin films date back to the early 18th century when Newton (ref. 14) wrote concerning his observations on the reflections, refractions, and colors of thin transparent bubbles of glass and water. Faraday (ref. 15) wrote in the mid-18th century of the optical and physical properties of gold beaten into thin transparent film as well as of other metals.

The theory for the optical properties of a thin film based on the laws of electromagnetism is well established in the literature (refs. 16, 17, 18, 19, and 20) The laws of electromagnetism for an isotropic medium may be expressed mathematically:

$$\text{div } \vec{D} = \xi \text{ div } \vec{E} = 4\pi\rho \tag{2.10}$$

$$\text{div } \vec{D} = \mu \text{ div } \vec{H} = 0 \tag{2.11}$$

$$\text{curl } \vec{E} = -\frac{\mu}{c}\frac{\partial \vec{H}}{\partial t} \tag{2.12}$$

$$\text{curl } \vec{H} = \frac{4\pi\eta\vec{E}}{c} + \frac{\xi}{c}\frac{\partial \vec{E}}{\partial t} \tag{2.13}$$

where

C - velocity of light

$\vec{D}$ - electric displacement vector

$\vec{E}$ - electric force vector

$\vec{H}$ - magnetic force vector

t - time

μ - magnetic permeability

ξ - dielectric constant

ρ - electric charge density

η - specific conductivity

For a medium in which there is no space-charge, these relations lead directly to Maxwell's equations representing the propagation of an electromagnetic disturbance in the medium.

$$\nabla^2\vec{E} = \frac{\xi\mu}{c^2}\frac{\partial^2\vec{E}}{\partial t^2} + \frac{4\pi\mu\eta}{c^2}\frac{\partial\vec{E}}{\partial t} \qquad (2\ 14)$$

$$\nabla^2\vec{H} = \frac{\xi\mu}{c^2}\frac{\partial^2\vec{H}}{\partial t^2} + \frac{4\pi\mu\eta}{c^2}\frac{\partial\vec{H}}{\partial t} \qquad (2\ 15)$$

If the medium is nonconducting ($\eta = 0$), these equations reduce to

$$\nabla^2\vec{E} = \frac{\xi\mu}{c^2}\frac{\partial^2\vec{E}}{\partial t^2} \qquad (2.16)$$

$$\nabla^2\vec{H} = \frac{\xi\mu}{c^2}\frac{\partial^2\vec{H}}{\partial t^2} \qquad (2.17)$$

each of which is the well-known wave equation.

The problem of determining the reflected and transmitted light amplitude and intensities at a boundary separating two media is solved by applying appropriate boundary conditions to the solution of Maxwell's equations.

Extension of the electromagnetic theory for the transmittance and reflectance of multilayer thin films reduce basically to the determination of the steady-state amplitudes of the electric and magnetic field vectors at the successive interfaces of the multilayers arising from an incident light wave of specified characteristics. In general the equations for the propagation of light in a nonabsorbing medium may be extended to an absorbing medium by replacing the refractive index n by a complex refractive index $\bar{n} = (n - ik)$ where "k" represents the energy absorption of the medium.

The optical problem of particular interest in this paper is that of the transmittance and reflectance of a metallic film deposited on a transparent polymeric substrate. Metallic films are by nature highly absorbing in the visible spectrum as can be seen by observing typical values for "n" and "k" in table 1 (from refs. 21 and 22) for thin films of silver, gold, copper, and aluminum.

Two types of solutions are found in the literature for this problem. Hadley and Dennison (ref. 23), Berning (ref. 24), and Heavens (ref. 25), give a solution to the problem based on the application of Maxwell's equations subject to appropriate boundary conditions. Harris, Beasley, and Loeb (ref. 26) present a solution based on the additions of intensities of the multiple reflections from the two surfaces of the transparent plate (one surface exposed to air and the other covered by the thin metallic film). Jenkins and White (ref. 27) show that intensity superposition is justified if the light source is incoherent.

The solution by Harris, Beasley, and Loeb (refs. 26 and 28) for the transmittance and reflectance of light normally incident upon a metal film (n,k) deposited on a thick nonabsorbing substrate (n_2) is presented below.

$$R = R_{oa} + \frac{R_{ob}T_{oa}^2}{1 - R_{ob}R_{ba}} \qquad (2.18(a))$$

$$T = T_{oa}\frac{1 - R_{ob}}{1 - R_{ob}R_{ba}} \qquad (2.18(b))$$

TABLE 1.- VALUES OF INDEX OF REFRACTION "n" AND ABSORPTION COEFFICIENT "k" FOR SILVER, GOLD, COPPER, AND ALUMINUM

λ, Å	SILVER		GOLD		COPPER		ALUMINUM	
	n	k	n	k	n	k	n	k
4000	0 075	1.93	1.45	....	0.85	....	0 40	3.92
4500	0.055	2.42	1.40	1.88	0.87	2.20	0.49	4.32
5000	0.050	2.87	0.84	1.84	0.88	2.42	0.62	4.80
5500	0.055	3.32	0.34	2.37	0.72	2.42	0.76	5.32
6000	0.060	3.75	0.23	2.97	0.17	3.07	0.97	6.00
6500	0.070	4.20	0.19	3.50	0.13	3.65	1.24	6.60
7000	0.075	4.62	0.17	3.97	0.12	4.17	1.55	7.00
7500	0.080	5.05	0.16	4.42	0.12	4.62	1.80	7.12
8000	0.090	5.45	0.16	4.84	0.12	5.07	1.99	7.05
8500	0.100	5.85	0.17	5.30	0.12	5.47	2.08	7.15
9000	0 105	6.22	0.18	5.72	0.13	5.86	1.96	7.70
9500	0.110	6.56	0.19	6.10	0.13	6.22	1.75	8.50

$$R' = R_{ob} + \frac{R_{ba}(1 - R_{ob})^2}{1 - R_{ob}R_{ba}} \qquad (2\ 18(c))$$

where

$$R_{oa} = \frac{\left|(n_2 - 1)\cos\left\{\frac{2\pi}{\lambda}(n + ik)d\right\} + \left(\frac{n_2}{n + ik} - n - ik\right) i \sin\left\{\frac{2\pi}{\lambda}(n + ik)d\right\}\right|^2}{\left|(n_2 + 1)\cos\left\{\frac{2\pi}{\lambda}(n + ik)d\right\} - \left(\frac{n_2}{n + ik} + n - ik\right) i \sin\left\{\frac{2\pi}{\lambda}(n + ik)d\right\}\right|^2}$$

$$T_{oa} = \frac{4n_2}{\left|(n_2 + 1)\cos\left\{\frac{2\pi}{\lambda}(n + ik)d\right\} - \left(\frac{n_2}{n + ik} + n + ik\right) i \sin\left\{\frac{2\pi}{\lambda}(n + ik)d\right\}\right|^2}$$

$$R_{ba} = \frac{\left|(n_2 - 1)\cos\left\{\frac{2\pi}{\lambda}(n + ik)d\right\} - \left(\frac{n_2}{n + ik} - n - ik\right) i \sin\left\{\frac{2\pi}{\lambda}(n + ik)d\right\}\right|^2}{\left|(n_2 + 1)\cos\left\{\frac{2\pi}{\lambda}(n + ik)d\right\} - \left(\frac{n_2}{n + ik} + n + ik\right) i \sin\left\{\frac{2\pi}{\lambda}(n + ik)d\right\}\right|^2}$$

$$R_{ob} = \frac{(n_2 - 1)^2}{(n_2 + 1)^2}$$

The index of refraction of the medium of incidence (n_o) is assumed to be unity. Reflectance "R" is for light initially incident upon the metal side and reflectance "R'" is for light initially incident upon the nonabsorbing substrate side. It is interesting to observe that the transmittance is identical regardless of whether the light is initially incident upon the metal or the nonabsorbing substrate side. This result is not true, however, for reflectance.

The solution by Heavens (ref. 25) for the reflectance and transmittance of normally incident light upon an absorbing film (n,k) deposited on a nonabsorbing substrate (n_2) is given below. The refractive index of the medium of incidence (n_o) is assumed to be unity.

$$R = \frac{A' \cosh \alpha + \beta' \sinh \alpha - C' \cos \zeta + D' \sin \zeta}{E' \cosh \alpha + F' \sinh \alpha - G' \cos \zeta + H' \sin \zeta} \qquad (2.19(a))$$

$$T = \frac{8n_2(n^2 + k^2)}{E' \cosh \alpha + F' \sinh \alpha - G' \cos \zeta + H' \sin \zeta} \qquad (2.19(b))$$

where

$$\alpha = \frac{4\pi kd}{\lambda}$$

$$\zeta = \frac{4\pi nd}{\lambda}$$

and,

$$A' = (n^2 + k^2 + 1)(n^2 + k^2 + n_2^2) - 4n^2n_2$$

$$B' = 2n\left[n_2(n^2 + k^2 + 1) - (n^2 + k^2 + n_2^2)\right]$$

$$C' = (n^2 + k^2 - 1)(n^2 + k^2 - n_2^2) + 4k^2n_2$$

$$D' = 2k\left[n_2(n^2 + k^2 - 1) - (n^2 + k^2 - n_2^2)\right]$$

$$E' = (n^2 + k^2 + 1)(n^2 + k^2 + n_2^2) + 4n^2n_2$$

$$F' = 2n\left[n_2(n^2 + k^2 + 1) + (n^2 + k^2 + n_2^2)\right]$$

$$G' = (n^2 + k^2 - 1)(n^2 + k^2 - n_2^2) - 4k^2n_2$$

$$H' = 2k\left[n_2(n^2 + k^2 - 1) + (n^2 + k^2 - n_2^2)\right]$$

Heavens presents the solution for the transmittance and reflectance of an absorbing film versus the ratio of the film thickness to the wavelength of the incident light in graphical form in reference 19. This graph is reproduced herein as figure 1. The effect of increasing absorption (increasing k) is to reduce the amplitude of successive maxima in the reflectance and transmittance curves. When the absorption is sufficiently high, as is the case for metals (see table 1), the curves of transmittance versus thickness fall rapidly and smoothly. Experimentally measured values of transmittance and reflectance do indeed follow this form as shown by the transmittance and reflectance versus film thickness graphs for aluminum as given in figure 2 (also taken from reference 19).

An approximate solution for the transmittance of an absorbing film deposited on a transparent substrate is proposed by Heavens in reference 19. This equation is presented below and a graph of the equation versus film thickness for incident light with a wavelength of 5000 $\mathring{A}$ is presented in figure 3 for several values of k characteristic of the materials presented in table 1.

$$T = \frac{n_2}{n_o} e^{-\frac{4\pi k d}{\lambda}} \qquad (2\ 20)$$

This solution is limited to highly absorbing films such that multiple reflections can be neglected. Comparison of the data for $k = 4.80$ with that of figure 2 shows that the results of the approximate solution are high relative to experimental data.

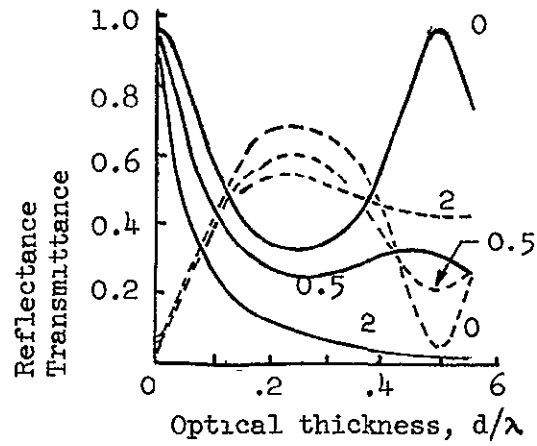

Figure 1.- Theoretical solution for variation of reflectance and transmittance versus ratio of absorbing film thickness to light wavelength for various values of "k" (from Heavens (ref. 19))

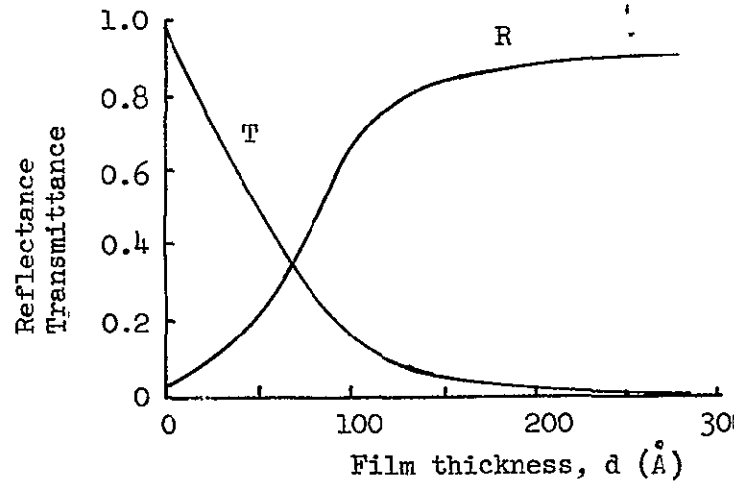

Figure 2.- Experimental data for the variation of reflectance and transmittance with thickness for an aluminum film and for a light wavelength of 5,000 Å (from Heavens (ref. 19)).

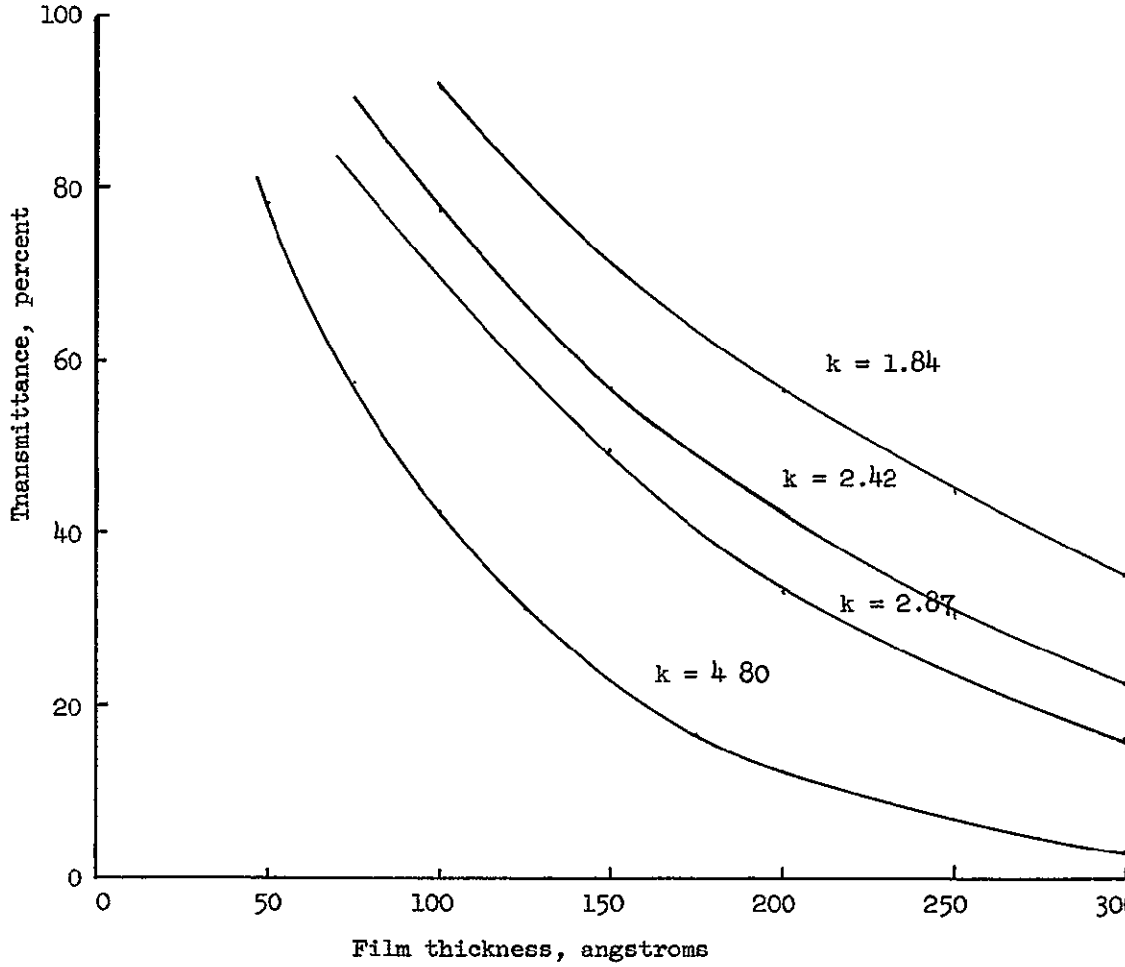

Figure 3.- Approximate solution for variation of transmittance with film thickness for λ = 5,000 Å, n_o = 1.0, and n_2 = 1.43 (eq. 2.20).

2.2 Diffraction Grating

Huygens proposed in 1690 (ref. 29) the principle that each point of a wave front can be regarded as a new source of waves. When a light wave is transmitted or reflected by a periodic set of apertures, reinforcement (constructive diffraction) or reduction (destructive diffraction) in intensity occurs yielding alternate light and dark regions. Diffraction is wavelength dependent and if the apertures are closely spaced, the spectral distribution is distinctly separated. Fraunhofer is credited with the first investigations of diffraction gratings and his name is usually associated with this type of diffraction.

The diffraction grating of primary interest in this paper is a sinusoidal type grating. Goodman (ref. 30) presents solutions for the intensities of light diffracted by a sinusoidal amplitude grating and a sinusoidal phase grating.

The transmittance of a sinusoidal amplitude grating is defined by the transmittance function

$$s(x,y) = \left[\frac{1}{2} + \frac{m}{2}\cos(2\pi f_o x)\right] \text{rect}\left(\frac{x}{l}\right) \text{rect}\left(\frac{y}{l}\right) \qquad (2.21)$$

where

$$\text{rect } x = \begin{cases} 1 & |x| \leq \frac{1}{2} \\ 0 & \text{otherwise} \end{cases}$$

where the grating structure is bounded by a square aperture of width l. The parameter m represents the peak-to-peak change of amplitude

transmitted across the grating, and f_o is the grating frequency Figure 4 shows a cross section of this transmittance function

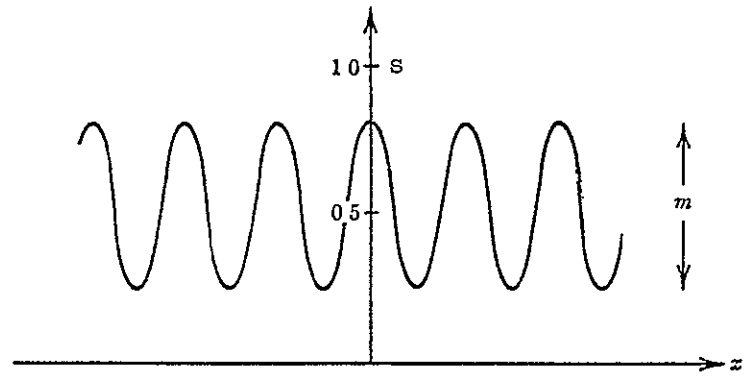

Figure 4.- Transmittance function of a sinusoidal amplitude grating (from Goodman (ref. 30)).

Assuming that the grating frequency is small, then the transmittance light intensity in a plane (x_o,y_o) parallel to the plane of the grating (x,y) and z distance from it is found to be:

$$I(x_o,y_o) = \left[\frac{l^2}{2\lambda z}\right]^2 \operatorname{sinc}^2\left(\frac{l y_o}{\lambda z}\right)\left\{\operatorname{sinc}^2\left(\frac{l x_o}{\lambda z}\right) + \frac{m^2}{4}\operatorname{sinc}^2\left[\frac{l}{\lambda z}(x_o + f_o\lambda z)\right] + \frac{m^2}{4}\operatorname{sinc}^2\left[\frac{l}{\lambda z}(x_o - f_o\lambda z)\right]\right\} \tag{2.22}$$

where

$$\operatorname{sinc}(x) = \frac{\sin \pi x}{\pi x}$$

A plot of this intensity function taken from reference 30 is shown in figure 5. The central diffraction pattern is the zero-order component of the Fraunhofer pattern and the patterns on either side are

the first-order components. The effect of the sinusoidal amplitude grating on energy distribution is to shift energy out of the central pattern and into the two side patterns. The separation of the zero and first-order components is $f_o \lambda z$ where z is the perpendicular distance from the grating to the plane of observation. The width of each component is proportional to $\frac{\lambda z}{l}$ and the resolving ability of the grating can be shown to be equal to the number of sinusoidal fringes on the grating $(f_o l)$.

A sinusoidal phase grating is defined by the transmittance function

$$s(x_1,y_1) = e^{\left[1 \frac{p}{2} \sin(2\pi f_o x_1)\right]} \operatorname{rect}\left(\frac{x_1}{l}\right) \operatorname{rect}\left(\frac{y_1}{l}\right) \quad (2.23)$$

where p is the peak-to-peak excursion of the phase delay If it is again assumed that $f_o \gg \frac{2}{l}$, then the diffraction intensity pattern in the plane (x_o,y_o) is found to be

$$I(x_o,y_o) = \left(\frac{l^2}{\lambda z}\right)^2 \sum_{q=-\infty}^{\infty} J_q^2\left(\frac{p}{2}\right) \operatorname{sinc}^2\left[\frac{l}{\lambda z}(x_o - q f_o \lambda z)\right] \operatorname{sinc}^2\left(\frac{l y_o}{\lambda z}\right) \quad (2.24)$$

where J_q is a Bessel function of the first kind and order q.

The sinusoidal phase grating deflects energy out of the zero order component into a multitude of higher order components. The peak intensity of the qth-order component is $\left[\frac{l^2 J_q\left(\frac{p}{2}\right)}{\lambda z}\right]^2$ and the displacement of that component from the center of the diffraction pattern is $q f_o \lambda z$.

Figure 6 (taken from ref. 30) presents a cross section of the intensity pattern when the peak-to-peak phase delay (p) is 8 radians. When $\frac{p}{2}$ is a root of J_o it can be shown that the zero-order fringe vanishes entirely.

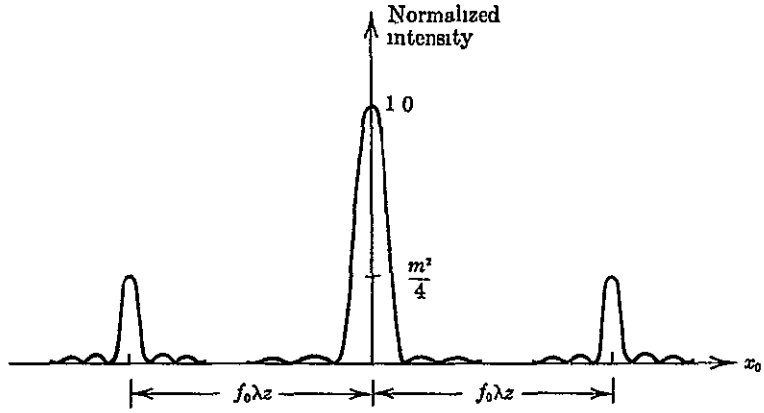

Figure 5.- Cross section of Fraunhofer diffraction pattern of sinusoidal amplitude grating (from Goodman (ref. 30)).

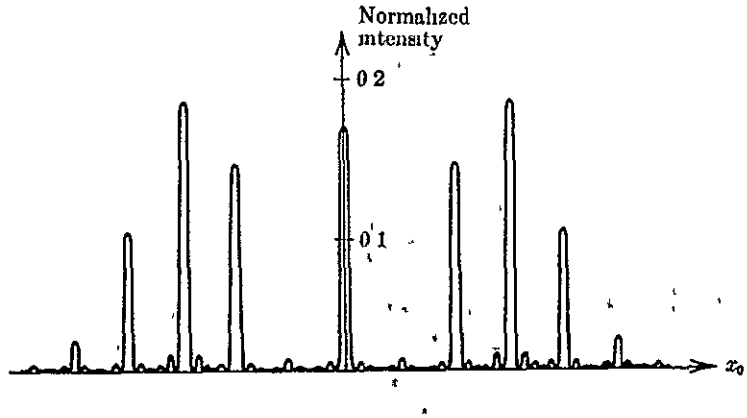

Figure 6.- Cross section of the Fraunhofer diffraction pattern of a sinusoidal phase grating for $p = 8$ (from Goodman (ref. 30))

III. THE INVESTIGATION

3.0 Theoretical

It was hypothesized early in the investigation based on information in the literature on the optical properties of thin films and on preliminary experimental evidence that the change between initial and final conditions in the total light intensity transmitted or reflected by a thin metallic film on a structural substrate was primarily caused by two factors.

(1) The change in the effective thickness of the film due to a redistribution of the coating material over a new surface area.

(2) The development of microfractures in the metallic film.

The first factor assumes that a redistribution of the coating material occurs due either to plastic deformation and cold working of the coating or as a result of molecular migration. It was believed that the relative importance of these two factors depended on the mechanical properties of the metal and the film, the thickness of the film, and the magnitude of the deformations.

For loadings which in a principal direction result in negative or compressive strain of the thin metallic film relative to initial conditions, it was hypothesized that the critical buckling load of the film would be exceeded at relatively low magnitudes of strain. If the resulting wrinkle pattern was periodic and of very short period, it was conceived that the ensuing periodic transmission function might set up a diffraction phenomenon which would reveal additional independent information.

These hypotheses are used in the following paragraphs to formulate strain-optic laws to relate the total and central image intensities of light transmitted and reflected to the mechanical state of the structural substrate. Large deformations are of primary interest in this investigation; consequently, large deformation strain-displacement relations are used in this development. It is assumed that the surface area of the thin film is identical with that of the substrate on which it is deposited and that surface strains occurring on the substrate are transmitted to the coating without magnification or attenuation and that the coating strains are uniform throughout the thickness of the thin film. The case of a uniaxially applied load is developed in depth and the theory is extended to a general biaxial case.

3.0.1 Total Transmittance

It is assumed that the change between initial and final mechanical conditions in the total light energy transmitted (or reflected) by a multilayer film (defined as total transmittance (or total reflectance)) is influenced by two factors as proposed in the preceding section.

(1) By the change in the thin film effective thickness.

(2) By the development of thin film microfractures.

An expression for the change in transmittance (or reflectance) for normally incident light resulting from thin film thickness changes alone may be developed from the equations presented in Section 2.1.

$$(\Delta T)_{\text{thickness change}} = T_{\text{final}} - T_{\text{initial}} \qquad (3.1)$$

$$(\Delta R)_{\text{thickness change}} = R_{\text{final}} - R_{\text{initial}} \qquad (3.2)$$

where T and R are calculated based on known optical properties and the thin film thickness "d." Unfortunately, this is complicated in that optical properties may also vary with film thickness.

Microfractures in thin metallic films probably develop along directions perpendicular to the directions of principal tensile strain as in brittle coating techniques. A critical strain level exists below which the film is either elastically or plastically deformed without the development of microfractures. Above this critical strain value, microfractures are developed. It is reasonable to assume that the microfracture density will continue to increase as the imposed strain is continuously increased. It may be assumed then that the change in transmittance (or reflectance) due to the development of microfracture light apertures is related to the principal strains.

$$(\Delta T)_{microfractures} = G_1 \epsilon'_{xx} + G_2 \epsilon'_{yy} \tag{3.3}$$

$$(\Delta R)_{microfractures} = G_3 (\epsilon'_{xx})^{-1} + G_4 (\epsilon'_{yy})^{-1} \tag{3.4}$$

where

$\epsilon'_{xx}, \epsilon'_{yy}$ = principal strains

G_1, G_2, G_3, G_4 = proportionality functions associated with the development of microfractures

$G_1, G_3 = 0$ if ϵ'_{xx} is negative (compressive)

$G_2, G_4 = 0$ if ϵ'_{yy} is negative (compressive)

This assumption introduces error for small strains, but is a reasonable expression for the average influence over a wide range of

strains. For greater precision for small strains, one could subtract out the expression for the range up to where thin film fractures were believed to initiate.

It now remains to obtain a relationship for the change in thin film thickness based on mechanical considerations. Such an expression is developed in the following paragraphs based on the assumption that the metallic film occupies a constant volume. The validity of this assumption may be questioned based on the experimental measurements by Hartman of the variation of density with thickness of thin films of aluminum (ref. 31). It is, however, a quantitative rather than qualitative density factor which is important from the standpoint of light transmission, and it is the total number of molecules per unit area which is significant rather than the density itself. Based on this argument, an effective thickness is used which is defined as the thickness to which the light responds, assuming a constant number of molecules per unit area.

Consider an initial coating volume V_i uniformly deposited over an area A_1 and with thickness d_1. If one assumes that as a result of a substrate deformation that the coating follows this deformation and redistributes uniformly over the new area without the development of microfractures, then a new coating area A_f and thickness d_f results. Assuming constant volume of coating material, then

$$V_i = V_f$$

and

$$A_i d_1 = A_f d_f$$

Then,

$$d_f = \frac{A_i}{A_f} d_1 \tag{3.5}$$

or the change in thickness is

$$\Delta d = d_1\left(1 - \frac{A_i}{A_f}\right) \tag{3.6}$$

Expressions for the area ratio required in equation (3.5) are developed from continuum mechanics considerations in the following section for the case of a uniaxially applied load.

3.0.1.1 Change in Surface Area for Case of Uniaxially Applied Load

The strain displacement relations from equations (2.7) and (2.8) for the case of a uniaxially applied load reduce to the following.

$$\epsilon_{xx} = \frac{\partial u}{\partial x}$$
$$\epsilon_{yy} = \frac{\partial v}{\partial y} \tag{3.7}$$

Similarly, equation (2.6) gives an additional second-order term.

$$\epsilon_{xx} = \frac{\partial u}{\partial x} + \frac{1}{2}\left(\frac{\partial u}{\partial x}\right)^2$$
$$\epsilon_{yy} = \frac{\partial v}{\partial y} + \frac{1}{2}\left(\frac{\partial v}{\partial y}\right)^2 \tag{3.8}$$

Since for this problem there are no rotations, the shear strains are zero.

Conventional Lagrangian strains are then by equation (3.7) simply,

$$\epsilon^{L}_{xx} = \frac{u}{l_x}$$
$$\epsilon^{L}_{yy} = \frac{v}{l_y} \tag{3.9}$$

Or from equations (3.8),

$$\epsilon^{L}_{xx} = \frac{u}{l_x} + \frac{1}{2}\left(\frac{u}{l_x}\right)^2$$
$$\epsilon^{L}_{yy} = \frac{v}{l_y} + \frac{1}{2}\left(\frac{v}{l_y}\right)^2 \tag{3.10}$$

From the definition of Poisson's ratio,

$$\nu = -\frac{\epsilon_{yy}}{\epsilon_{xx}} \tag{3.11}$$

one may obtain an expression for the displacement v in terms of the displacement u. Equations (3.10) and (3.11) then yield, respectively,

$$v = -\nu u \frac{l_y}{l_x} \tag{3.12}$$

and

$$v = -l_y\left(1 \pm \sqrt{1 - \frac{\nu u}{l_x{}^2}(u + 2l_x)}\right) \tag{3.13}$$

The ratio of initial to final surface area may be mathematically defined by the following:

$$\text{Area ratio} = \frac{A_i}{A_f}$$

$$= \frac{l_x l_y}{(l_x + u)(l_y + v)} \qquad (3.14)$$

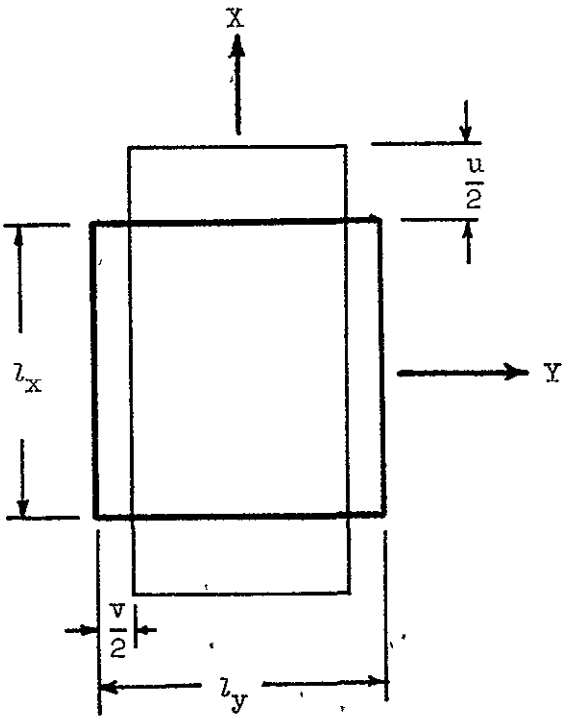

Substituting for v from equation (3.12), the area ratio becomes

$$\text{Area ratio} = \frac{l_x}{(l_x + u)\left(1 - \frac{\nu u}{l_x}\right)} \qquad (3.15)$$

Similarly, substituting for v from equation (3.13),

$$\text{Area ratio} = \frac{l_x}{(l_x + u)\left(\sqrt{1 - \frac{\nu u}{l_x^2}(u + 2l_x)}\right)} \tag{3.16}$$

An expression for the area ratio may also be developed using the natural strain definition (eq. (2.1)). Using the conventional strain displacement relations from equation (3.9), one obtains

$$\begin{aligned} \bar{\epsilon}_{xx} &= \ln\left(1 + \frac{u}{l_x}\right) \\ \bar{\epsilon}_{yy} &= \ln\left(1 + \frac{v}{l_y}\right) \end{aligned} \tag{3.17}$$

Similarly, using equation (3.10), one obtains

$$\begin{aligned} \bar{\epsilon}_{xx} &= \ln\left(1 + \frac{u}{l_x} + \frac{1}{2}\left(\frac{u}{l_x}\right)^2\right) \\ \bar{\epsilon}_{yy} &= \ln\left(1 + \frac{v}{l_y} + \frac{1}{2}\left(\frac{v}{l_y}\right)^2\right) \end{aligned} \tag{3.18}$$

Poisson's ratio may then be defined in terms of natural strains,

$$\bar{\nu} = -\frac{\bar{\epsilon}_{yy}}{\bar{\epsilon}_{xx}} \tag{3.19}$$

Substituting equations (3.17) into equation (3.19) to solve for v in terms of u, one obtains·

$$v = -l_y\left[1 - \left(1 + \frac{u}{l_x}\right)^{-\bar{\nu}}\right] \tag{3.20}$$

Similarly, using equations (3.18) and (3.19), one obtains

$$v = -l_y\left\{1 \pm \sqrt{2\left(1 + \frac{u}{l_x} + \frac{1}{2}\left(\frac{u}{l_x}\right)^2\right)^{-\bar{\nu}} - 1}\right\} \tag{3.21}$$

The ratio of initial to final surface area based on a natural strain formulation is then, using equation (3.20),

$$\text{Area ratio} = \left(\frac{l_x}{l_x + u}\right)\left(1 + \frac{u}{l_x}\right)^{\bar{\nu}} \tag{3.22}$$

And similarly, using equation (3.21),

$$\text{Area ratio} = \frac{l_x}{(l_x + u)\left(\sqrt{2\left(1 + \frac{u}{l_x} + \frac{1}{2}\left(\frac{u}{l_x}\right)^2\right)^{-\bar{\nu}} - 1}\right)} \tag{3.23}$$

A graphical solution to equations (3.15), (3.16), (3.22), and (3 23) is presented in figure 7. In this solution the area ratio is plotted versus Lagrangian strain (eq. (3.9) in the direction of the applied load. Unit length is assumed for the original dimension "l_x" and Poisson's ratio is taken from the data presented in figure 15 for the silicone rubber substrate material used in experimental investigations. Equation (3.22) yields very nearly a linear relationship between the area ratio and conventional strain.

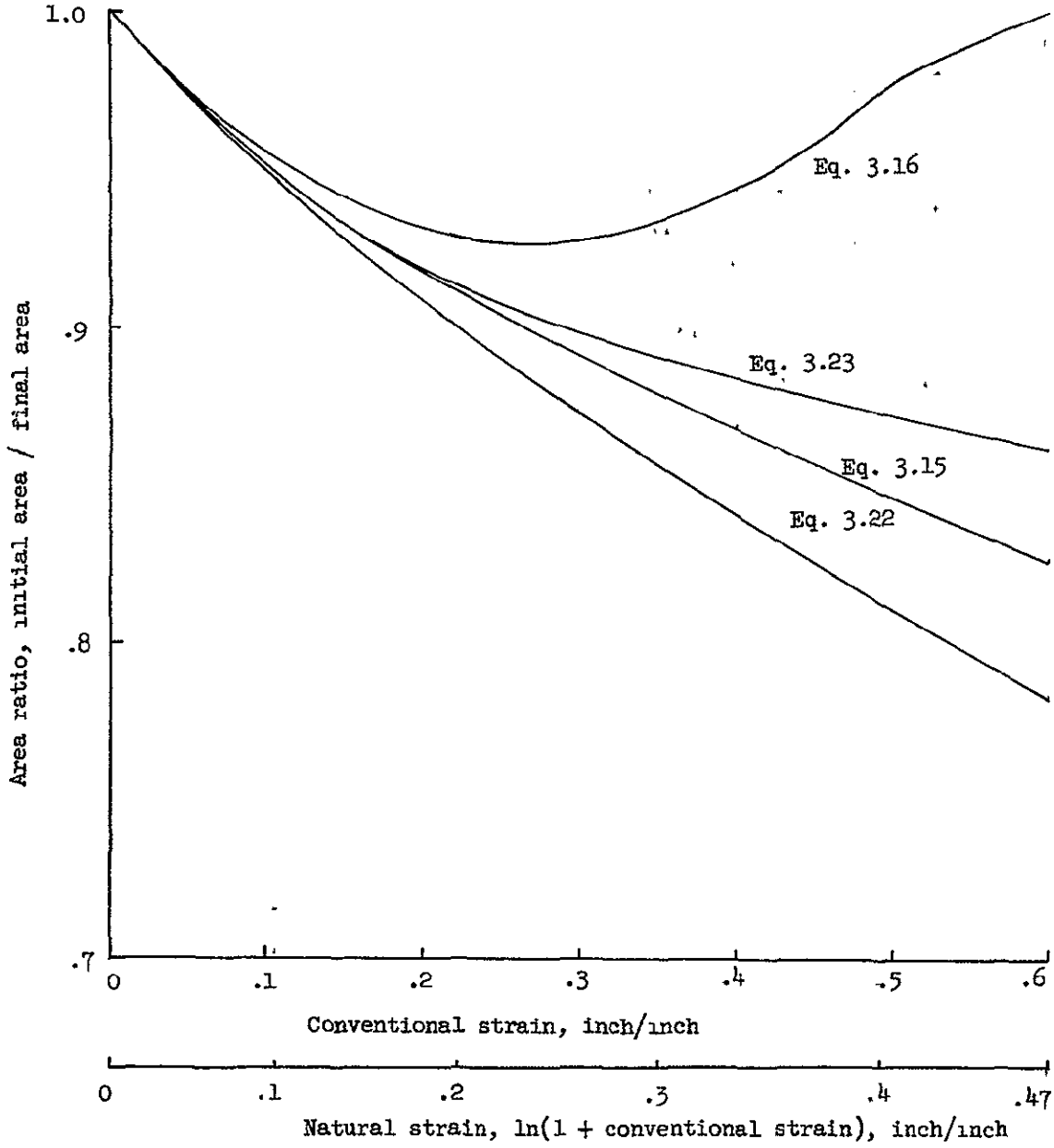

Figure 7.– Area ratio versus conventional and natural Lagrangian strain of case of uniaxial load.

3 0.1.2 Total Transmittance Optical-Mechanics Law for Uniaxial Loading

An optical-mechanics law may now be expressed for the change in total transmittance (or total reflectance) of a thin metallic coating deposited on a uniaxially loaded structural substrate by using expressions of the preceding paragraphs. This is accomplished by substituting one of the expressions for area ratio from Section 3.0.1.1 (eqs. (3.15), (3.16), (3.22), or (3.23)) into equation (3.5) for the final thin film thickness and using this value together with the initial thickness in equation (3.1) (or (3.2)) for the change in transmittance (or reflectance) due to the effective thickness change. The total change is then obtained by adding to this expression the expression for the change due to the development of microfractures (eqs. (3.3) or (3.4)) and a term to be explained in the next section due to an effective thickness change resulting from wrinkling. The latter term exists only in the event of a negative (compressive) strain field.

$$(\Delta T)_{total} = (\Delta T)_{\substack{\text{thickness} \\ \text{change due} \\ \text{to area} \\ \text{change}}} + (\Delta T)_{\substack{\text{thickness} \\ \text{change due} \\ \text{to wrinkling}}} + (\Delta T)_{microfracture} \tag{3.24}$$

$$(\Delta R)_{total} = (\Delta R)_{\substack{\text{thickness} \\ \text{change due} \\ \text{to area} \\ \text{change}}} + (\Delta R)_{\substack{\text{thickness} \\ \text{change due} \\ \text{to wrinkling}}} + (\Delta R)_{microfracture} \tag{3.25}$$

3.0.2 Central Image Transmittance

3.0.2.1 Compressive Wrinkling of Thin Metallic Film on Thick Elastic Substrate

Since the stiffness of a typical thin metallic coating is so small (i.e., on the order of 10^{-12} b inch-pound for a 250 Å thick aluminum film where b is the width), the film may be expected to wrinkle with a high periodic frequency when subjected to compressive loading. A model of such a pattern is shown schematically in figure 8. Microfractures tend to make such a pattern discontinuous. Deformations of the film are, of course, restrained by the structural substrate. This problem closely resembles that of the buckling of a beam on an elastic foundation. Hetenyi presents a solution in reference 32 for the critical buckling load of a straight bar on an elastic foundation for cases of a bar with free ends, pinned ends, and fixed ends. Budiansky, Seide, and Weinberger present a solution in reference 33 for the buckling of a column with two, three, four, or an infinite number of equally spaced intermediate deflection and rotational springs.

Thin film wrinkling is of interest in this discussion, as it affects the transmission of light as will be shown in the next section.

3.0.2.2 Diffraction by a Pattern of Closely Spaced Periodic Thin Film Wrinkles

The central image of a diffraction grating is the center portion of the transmitted (or reflected) light. The light is diffracted to both sides of this center to form reinforcing light and dark fringe patterns. If diffraction is not present, the central image contains the total transmitted (or reflected) light energy. When diffraction

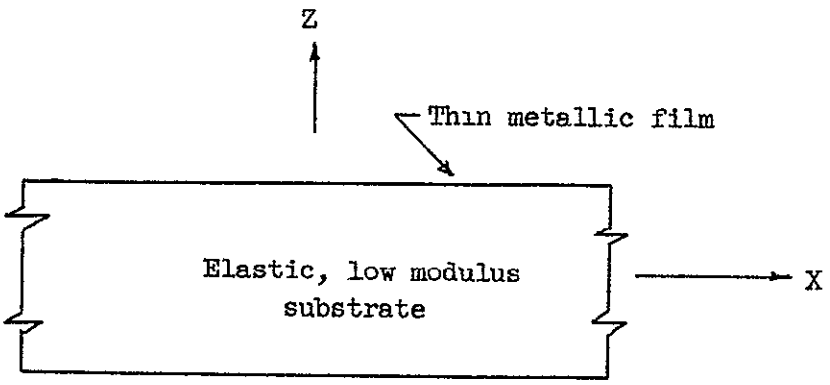

(a) Initial cross section.

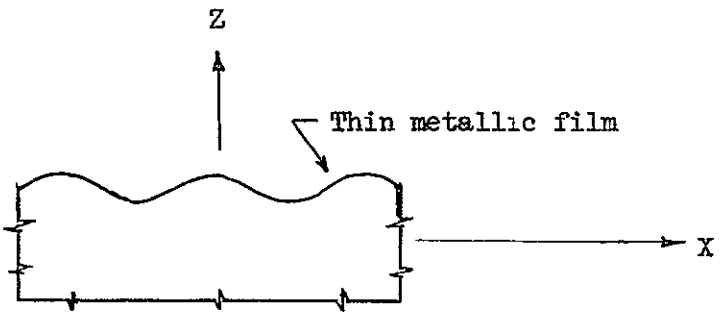

(b) Deformed cross section.

Figure 8.- Model for compressive wrinkling of thin metallic film on thick low modulus substrate

is present, the central image energy is reduced by the amount diffracted to the right and to the left of the central image.

A closely spaced periodic pattern of metallic thin film wrinkles as proposed in Section 3.0.2.1 would act in essence as a diffraction grating. Light striking the thin film peaks and valleys at normal incidence is transmitted (or reflected) as if the film were not wrinkled. Light, however, which strikes the wrinkled thin film at non-normal incidence is refracted, and the thickness of the absorbing thin film traversed by the light is different than the unwrinkled nominal thickness of the film. The magnitude of the effective thickness and, consequently, the intensity of light transmitted, is dependent on the angle between the incidence light path and the normal to the thin film surface. It is reasonable to assume that the wrinkle pattern is approximately sinusoidal in shape and, correspondingly, that the transmission function is also approximately sinusoidal in nature. The diffraction of light by a sinusoidal amplitude grating and by a sinusoidal phase grating were presented in Section 2.2 as developed by Goodman (ref. 30).

3.0.2.3 Central Image Transmittance Optical-Mechanics Law

The change in the central image transmittance between initial and final mechanical conditions for a thin metallic film deposited on a structural substrate is influenced by three factors.

(1) By the change in thin film effective thickness.

(2) By the development of thin film microfractures.

(3) By diffraction set up by compressive wrinkling of the metallic thin film.

The effective thickness of the thin film is, in turn, influenced by two factors.

(1) By the redistribution of coating material over the new surface area.

(2) By the change in light path length through the thin film due to the wrinkle geometry.

The change in central image transmittance (or central image reflectance) then is of the following form:

$$(\Delta T)_{\text{central image}} = (\Delta T)_{\substack{\text{thickness change} \\ \text{due to area change}}} + (\Delta T)_{\substack{\text{thickness change} \\ \text{due to wrinkling}}} + (\Delta T)_{\text{microfractures}} - (\Delta T)_{\text{diffraction}} \tag{3.26}$$

$$(\Delta R)_{\text{central image}} = (\Delta R)_{\substack{\text{thickness change} \\ \text{due to area change}}} + (\Delta R)_{\substack{\text{thickness change} \\ \text{due to wrinkling}}} + (\Delta R)_{\text{microfractures}} - (\Delta R)_{\text{diffraction}}$$

The first three terms on the right are precisely the quantities proposed in Section 3.0.1.2 responsible for the change in total transmittance (or total reflectance). The change in central image transmittance (or central image reflectance) is therefore the difference between the change in total transmittance (or total reflectance) and the change in transmittance (or reflectance) due to diffraction.

$$(\Delta T)_{\text{central image}} = (\Delta T)_{\text{total}} - (\Delta T)_{\text{diffraction}}$$

$$(\Delta R)_{\text{central image}} = (\Delta R)_{\text{total}} - (\Delta R)_{\text{diffraction}} \qquad (3.27)$$

An expression for the change in transmittance (or reflectance) due to diffraction could conceivably be developed around the equations for the diffraction by a sinusoidal-type transmission grating from Section 2.2. Two variables appear in each of these two intensity distribution solutions. (1) the peak-to-peak amplitude "m" and (2) the grating frequency "f_o" in equation (2.22); and (1) the peak-to-peak excursion of the phase delay "p" and (2) the grating frequency "f_o" in equation (2.24). It is reasonable to expect the wrinkle geometry to be influenced by the mechanical state of the structure. This, in turn, would directly influence the grating frequency and possibly the other parameters as well.

The work necessary to establish the exact form of the equation relating the mechanical state of the structure to the change in transmittance due to diffraction is of sufficient magnitude to merit independent study. It is believed that the solution would involve considerable experimental study as well as new theoretical considerations including thin film wrinkle theory and even the solution for diffraction for an alternate transmittance function to that proposed above.

3.0.3 General Biaxial Optical-Mechanics Law

One could conceivably obtain the solution for the deformations of a general biaxial problem based on the solution for the change in

total and central image transmittances from a set of equations similar to that proposed in the preceding paragraphs. The approach would be to use transmittance data to determine the change in effective film thickness which, in turn, would be used to calculate displacements using an expression formulated on surface area change considerations. In this approach one would have to independently assess the contribution of microfractures, wrinkling, and diffraction. From deformations, the strain displacement relations would be used to obtain strains and the constitutive relations to obtain stresses.

The work involved in obtaining a solution in this manner would indeed be a laborious task. It is further complicated by the fact that optical properties are, in general, also functions of the film thickness.

A far simpler approach, if it can be developed, would be to formulate an empirical relationship between the changes in transmittance (or reflectance) and the mechanical state of the structure based on physical considerations. In this approach, calibration tests would be used to provide the proportionality functions required. Such an approach is proposed below for the general biaxial problem.

The two factors proposed in Section 3.0 as influencing the change in the total transmittance intensity were effective thickness changes and the development of microfractures. Both the effective thickness change resulting from area changes and the development of microfractures work constructively; that is, they both increase transmittance corresponding to positive strains. One might, therefore, propose a relationship between the change in total transmittance (or total reflectance) and strain of the following form:

$$(\Delta T)_{total} = W_1 \epsilon'_{xx} + W_2 \epsilon'_{yy}$$

$$(\Delta R)_{total} = W_3 \epsilon'_{xx} + W_4 \epsilon'_{yy} \qquad (3.28)$$

where

W_1, W_2 = proportionality functions associated with total transmittance

W_3, W_4 = proportionality functions associated with total reflectance

$\epsilon'_{xx}, \epsilon'_{yy}$ = principal strains

The transmittance of aluminum was shown in figure 2 to be linearly related to film thickness for thicknesses less than approximately 100 Å. It is also reasonable to assume that the relationship between transmittance and the density of microfractures will also be approximately linear. In a problem for which the materials behave in this manner and for which the properties are isotropic, equation (3.28) will reduce to the following:

$$(\Delta T)_{total} = W_5(\epsilon'_{xx} + \epsilon'_{yy})$$

$$(\Delta R)_{total} = W_6(\epsilon'_{xx} + \epsilon'_{yy}) \qquad (3.29)$$

where

W_5 = proportionality constant associated with total transmittance

W_6 = proportionality constant associated with total reflectance

The factors proposed in Section 3.0.2.3 as influencing the change in central image transmittance include changes in the film effective thickness, the development of microfractures, and the effect of diffraction. Film effective thickness changes resulting from area changes increase transmittance corresponding to a positive strain. Determination of the effect of changes in effective film thickness due to changes in the light path caused by wrinkle geometry requires additional study. The effect of diffraction is to deflect energy into lateral side bands and therefore to decrease central image transmittance. It is compressive wrinkling, of course, which causes diffraction, and in the event that none of the principal strains are negative, then the effect of diffraction may be ignored. Diffraction, when present, probably contributes the strongest influence of these factors. Based on these considerations, the following relationships are proposed between the change in central image transmittance (or central image reflectance) and strain.

$$(\Delta T)_{\text{central image}} = W_1 \epsilon'_{xx} + W_2 \epsilon'_{yy} - J_1 \epsilon'_{xx} - J_2 \epsilon'_{yy} \tag{3.30}$$

$$(\Delta R)_{\text{central image}} = W_3 \epsilon'_{xx} + W_4 \epsilon'_{yy} - J_3 \epsilon'_{xx} - J_4 \epsilon'_{yy}$$

where

W_1, W_2 = proportionality functions associated with total transmittance

W_3, W_4 = proportionality functions associated with total reflectance

J_1, J_2, J_3, J_4 = proportionality functions associated with diffraction

$J_1, J_3 = 0$ if ϵ'_{xx} is positive

$J_2, J_4 = 0$ if ϵ'_{yy} is positive

$\epsilon'_{xx}, \epsilon'_{yy}$ = principal strains

The sum of the first two terms in each of the expressions of equation (3.30) are expressions for the change in total transmittance or total reflectance, respectively. Making this substitution, one obtains

$$(\Delta T)_{\text{central image}} = (\Delta T)_{\text{total}} - J_1 \epsilon'_{xx} - J_2 \epsilon'_{yy}$$

$$(\Delta R)_{\text{central image}} = (\Delta R)_{\text{total}} - J_3 \epsilon'_{xx} - J_4 \epsilon'_{yy} \qquad (3.31)$$

In other words, the change in central image transmittance (or central image reflectance) is equal to the change in the total transmittance (or total reflectance) reduced by the influence of diffraction.

Assuming that the above proposed empirical relationships are correct, it is seen possible to completely determine the strain field for a general biaxial problem by making two sets of experimental measurements (either total and central image transmittance or total and

central image reflectance) and by substitution of the changes in these quantities into the appropriate expressions from equations (3.28) and (3.31).

The proportionality functions used in these expressions (W_1,W_2, J_1, and J_2 for transmittance experiments, and W_3,W_4,J_3, and J_4 for reflectance experiments) are determined from calibration tests on uniaxially loaded specimens. From a practical standpoint, it is desirable to select coatings for which these functions are linear and which have a large sensitivity for the strain range expected in the problem. The transmittance response of some typical metallic coatings is presented in the next section.

3.1 Experimental

The purpose of the experimental portion of this investigation was to experimentally establish the relationship between the mechanical state of the structure and the change in total and central image transmittance of the thin metallic film deposited on it, to determine the physical mechanisms responsible for the change in optical properties; and to check experimental data against analytical models for a biaxial case of loading. Most of the study was done on uniaxially loaded specimens in order to isolate the variables.

Several metals were used as thin films in this study in order to survey the response of a range of both optical and mechanical properties. All were deposited on the same substrate material, a silicone rubber.

The biaxial problem selected for investigation was the problem of a uniaxially loaded rectangular plate with a centrally located hole.

This particular problem was selected for comparative study because the problem has been studied both analytically and experimentally, and therefore, solutions are available; and because the problem is simple to set up experimentally.

3.1.1 Apparatus and Instrumentation

3.1.1.1 Thin Film Deposition System

The most commonly used thin film coating technique is the thermal evaporation process in which a metal is vaporized and condensed on a substrate material. This process, also called vapor deposition, is easily controlled and results in films of high puri For further information on this coating technique as well as of ot commonly used today, see references 16, 19, and 34.

A new technique was used to coat the specimens used in this study. The technique shown schematically in figure 9 involves the vaporization of the coating material by a hot tungsten filament in an electrostatic field. A 6-volt dc potential existed between the coating material and the tungsten filament. The coating material was driven into the filament by a motor-driven screw. Thus, in addition to thermal vaporization, the resulting electric arc also excited the material into an ionic state. The specimens to be coated were located on two aluminum plates separated by approximately 6 inches. An electric potential of 310.5 volts was applied between the two plates. This set up an electrostatic field between the plates, which tended to accelerate the vaporized ions of the coating material into the substrate. Deposition was conducted in a vacuum at a pressure of approximately 10^{-6} torr

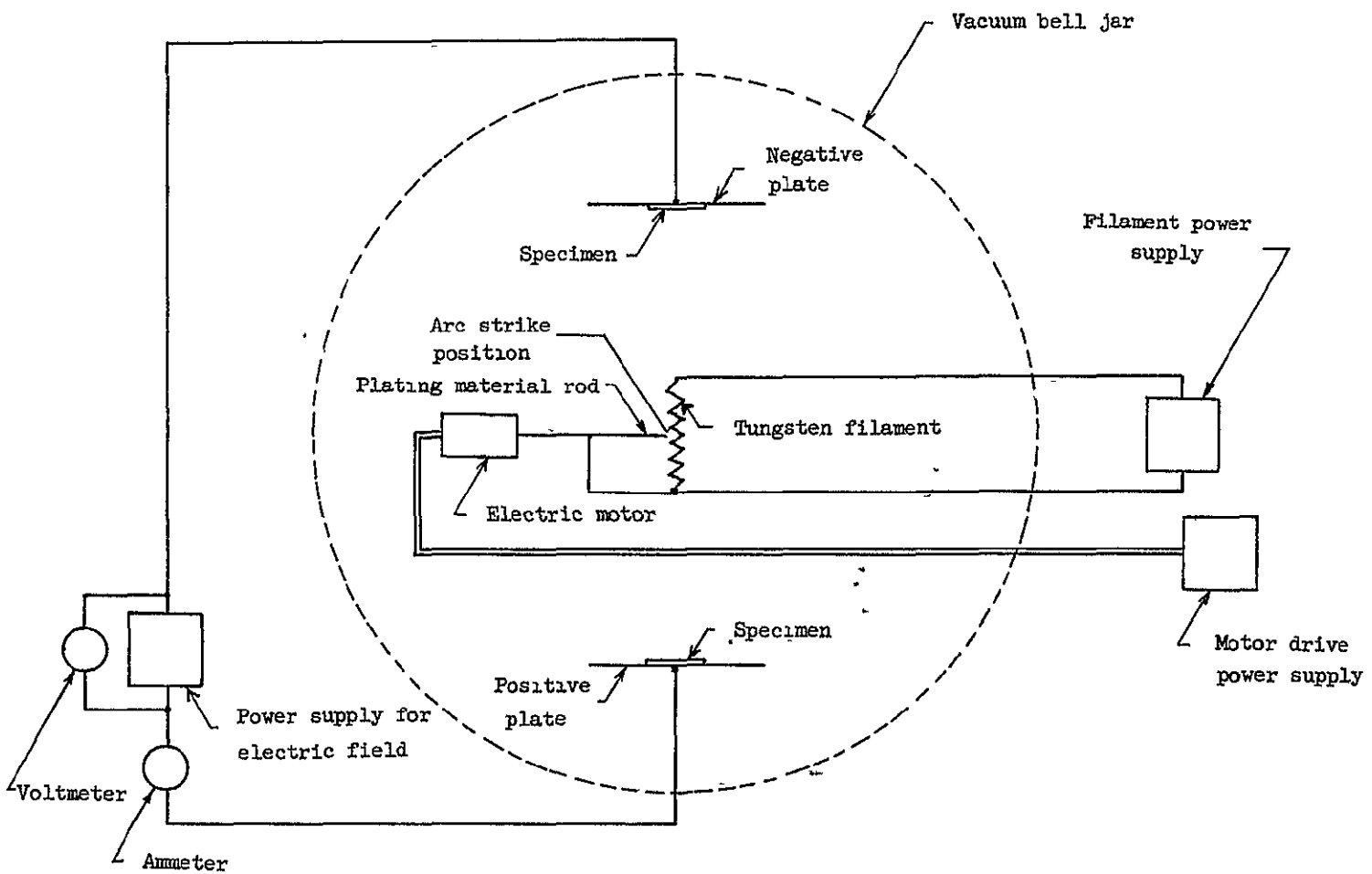

Figure 9.- Schematic of thin film deposition system.

and the substrate material was cleaned in each case before deposition by arcing in the corona by back streaming with argon. Using this thin film deposition technique, the writer was able to obtain better adhesion and an apparent reduction in the size of microfractures developed in the coating due to substrate deformation than using conventional coating techniques.

3.1.1.2 Test Setup

The basic experimental test setup is shown in figure 10. It includes a load-displacement instrument and recorder; a fiber optics light system; an optical system consisting of filters, lenses, and apertures, a photomultiplier tube, amplifier, and recorder; a kinematic optical bench; an X-Y axis optics transporter; and a test specimen. Tests were conducted with the room darkened and with shields strategically located to mask out stray light from the light source. The load instrument applied a load by advancing the crosshead (to which is attached the lower specimen clamp) at a constant displacement rate. The upper specimen clamps attach via a coupling to a strain-gage type load cell and can be considered to maintain a fixed position. The load response is recorded graphically on a strip chart recorder which advances the paper at a constant rate (1 inch per minute in these tests). Consequently, the distance from the starting position is uniquely related to the crosshead displacement.

The light source is a 150-watt tungsten filament bulb, the visible light spectral response of which is shown in figure 11. Line

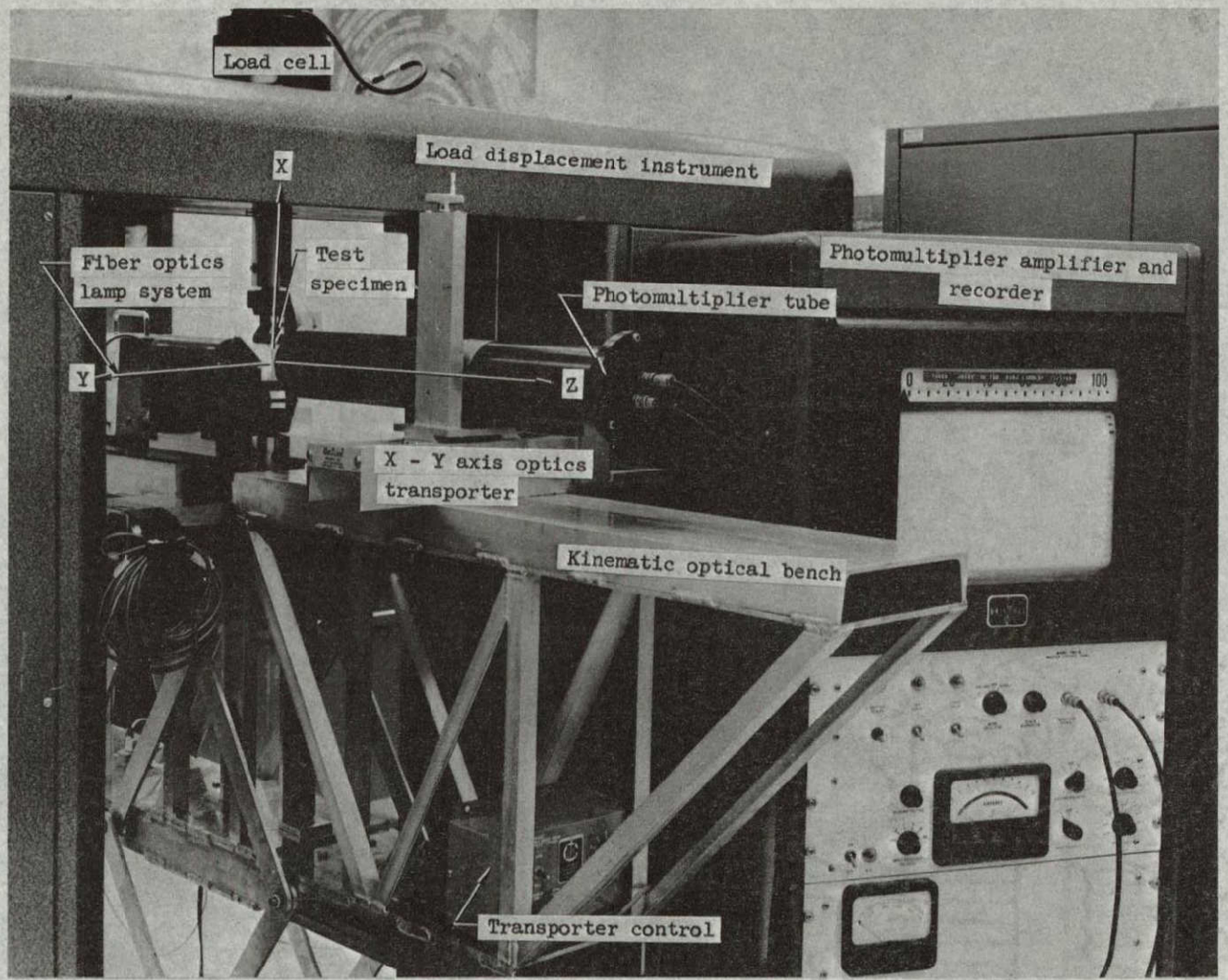

Figure 10.- Experimental test setup.

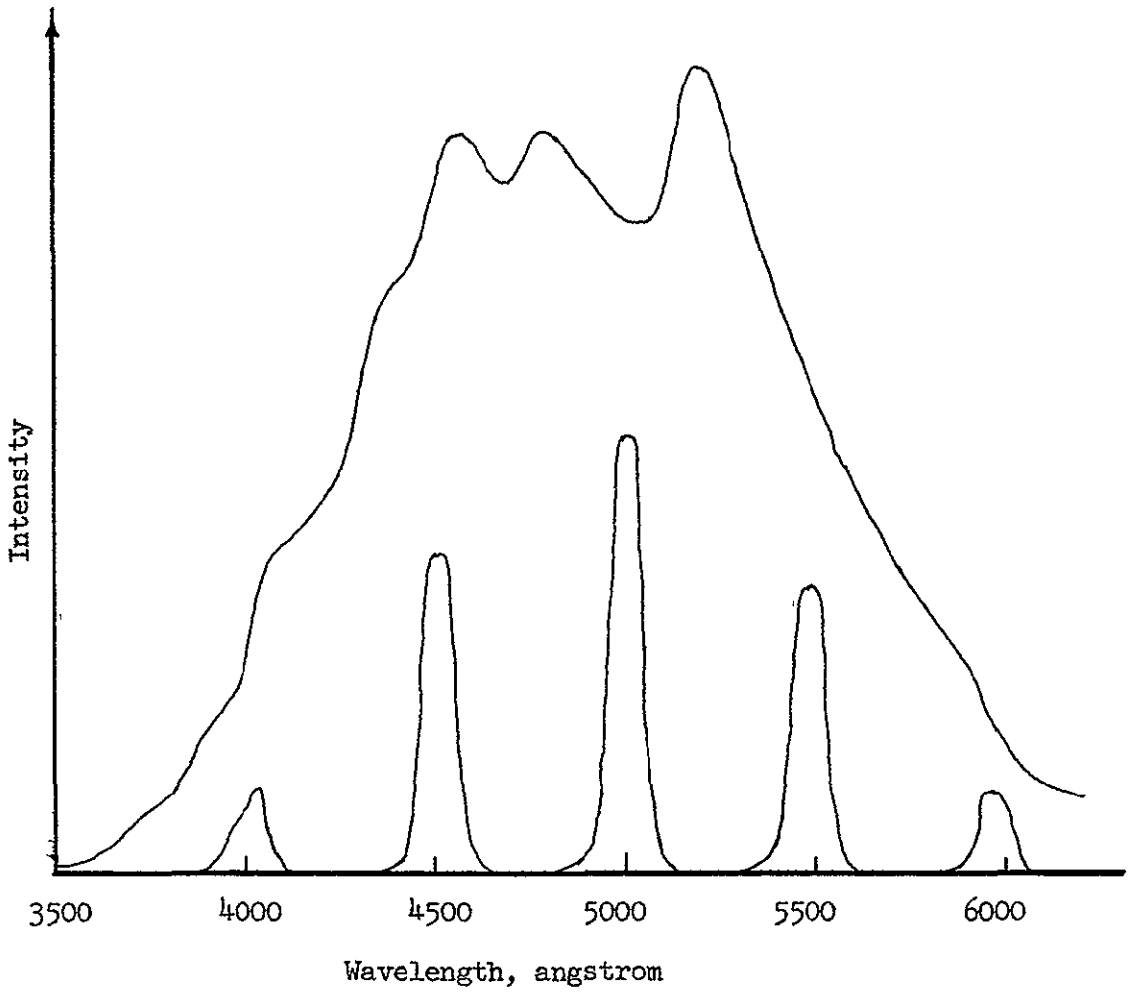

Figure 11.- Spectral response of fiber optics lamp system with and without selected filters.

voltage is conditioned by an ac voltage regulator (110 ±1 volt) in order to provide a constant intensity output. The light is channeled to the light source tube by a 0.125-inch-diameter bundle of 50-micron-diameter glass fibers. The light source tube contains a collimator lens and a circular aperture to control the size of the beam. Various narrow band filters were available to place in front of the light source tube aperture in order to select a specified wavelength of light for study. The spectral response of the fiber optics lamp when used in combination with these filters is also shown in figure 11.

The photomultiplier tube is housed within a circular 3-inch-diameter, 24-inch-long tube. The face of the photomultiplier tube is located 6-1/4 inches from one end of the circular tube. The electrical leads from the photomultiplier tube connect to an amplifier and the response is recorded graphically on a strip chart recorder. A constant chart advance rate of 1 inch per minute was used in these tests.

The optical system mounts on a kinematic optical bench. The function of the kinematics of the bench is to allow continuous monitoring of the same area of a specimen during a load test. The lower mount of the bench is attached to the fixed base of the load instrument and the upper mount is attached to the moving crosshead. The kinematic optical bench translates at a ratio of 1 to 2 relative to the crosshead.

The X-Y axis optics transporter is motor driven in the Y-direction at a constant displacement rate and hand driven in the X-direction. The transporter motor control allows a continuous range

of speeds of from zero to 2 inches per minute. Both axes have a millimeter scale and a vernier.

Three variations of this basic setup were used in this investigation corresponding to tests in which the total intensity, central image intensity, and scan data were recorded.

Total intensity transmittance test measurements required an optical system which would collect not only the central image, but also diffracted side bands. This was accomplished by mounting a 2-inch-diameter collector lens on the end of the circular tube housing the photomultiplier tube. The lens, located approximately 1.5 inches from the specimen, collected all of the light striking it and focused it in the plane of the face of the photomultiplier tube. The total intensity of light incident upon the specimen was limited by a 0.004-inch-diameter circular aperture located approximately 0.15 inch from the specimen. This distance was reduced to 0.04 inch for the test measurements on the rectangular plate with a circular hole. The first-order diffraction ring from this aperture fell well outside the collection area of the lens.

In the setup for central image transmittance measurements, the collector lens used in total intensity measurement tests was removed and a pair of circular apertures 1/32 inch in diameter were placed approximately 16 inches apart in the circular tube housing the photomultiplier tube. These collimated apertures restricted the view of the photomultiplier tube to permit measurement of the central image response. They were large enough, however, to insure that the

dimensions of the area for which transmittance was measured was large relative to the period of the wrinkle so as to obtain an averaging effect rather than some local anomaly.

In tests where scan capability was desired (transmittance in the region of the hole in a uniaxially loaded rectangular plate containing a centrally located hole), the two test setups described above were used to make total and central image measurements, respectively; with the exception that the light source tube was mounted on the X-Y axis transporter.

3.1.1.3 Microdensitometer

Before and after each transmittance and microscopic surface examination test, the transmittance of the specimen was measured on a microdensitometer. A scan was made in the region of the specimen center in both the X and Y directions. Specimens showing large variations in this region were discarded. The result of this measurement was assumed as the initial transmittance of the specimen and was used to calibrate the transmittance response of the photomultiplier measurement system. The instrument reads optical density directly and has a zero to two full-scale range.

3.1.1 4 Optical Microscope Examination of Loaded Specimen

Specimens were uniaxially loaded to selected magnitudes of strain in the test frame shown in figure 12 and examined using a research microscope to study the microscopic effect of loading on the metallic thin film. Manual rotation of the micrometer dial applied the load to the specimen and the scale gave an accurate measurement of the

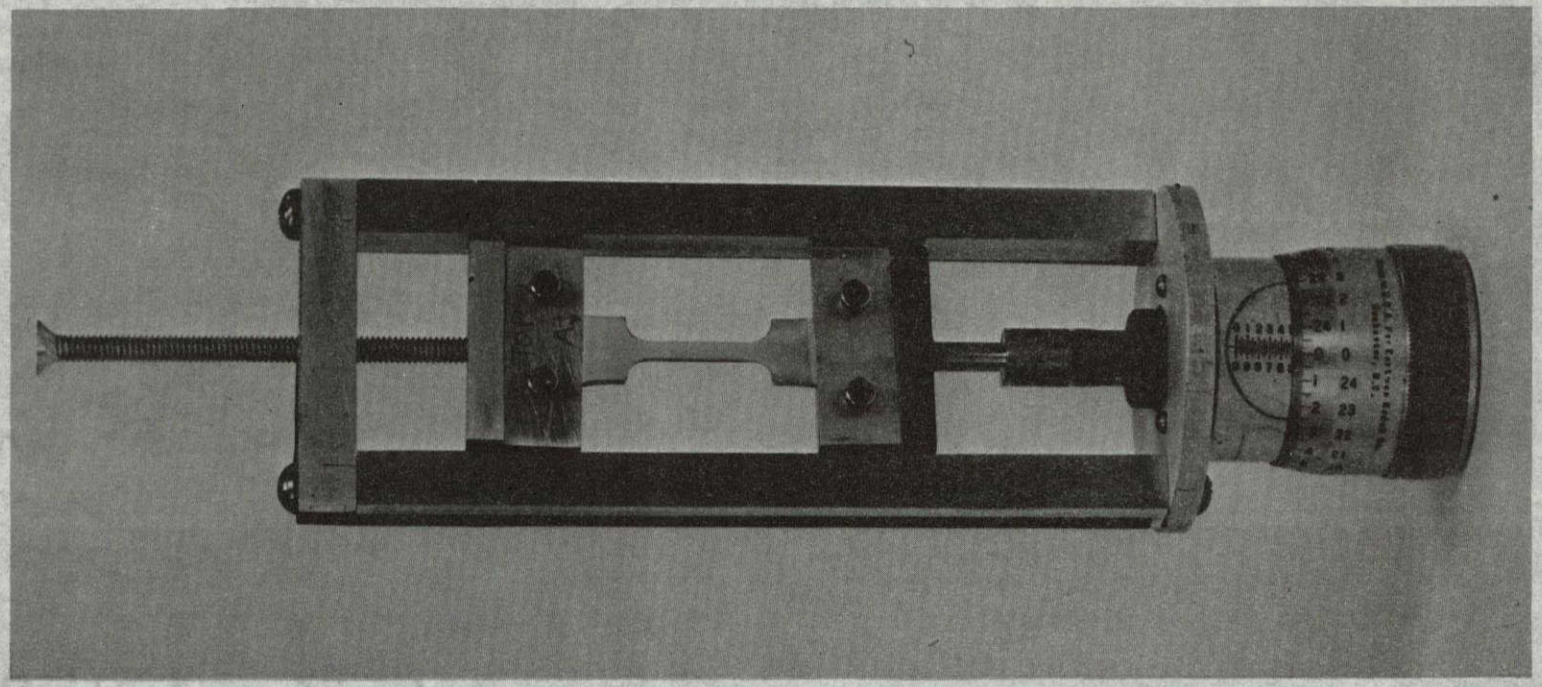

Figure 12.- Stretch test frame used in optical microscope surface examinations.

displacement (read to 0.001 inch). Initial distance between clamps was 1.5 inches, as was the case in transmittance tests.

The microscope used was equipped with transmitted brightfield, reflected brightfield, reflected darkfield, and polarizing accessories. Microscope optics permitted 110, 220, and 450 times magnification. A xenon lamp was used to illuminate the specimen. Photomicrographs were taken at each magnitude of strain examined for a permanent record.

3.1.1.5 Electron Microscope Examination of Loaded Specimen

Electron microscope studies of the surface of uniaxially loaded specimens were performed using a Materials Analysis Company Combination Scanning and Electron Microprobe Microscope Model 400 S. This instrument measures backscattering of primary electrons with an energy of 20,000 electron volts. The angle of incidence was approximately 27-1/2° from the normal to the specimen.

3.1.1.6 Monochrometer

The spectral response of the fiber optics lamp system by itself and in combination with selected filters was measured using a McPherson monochrometer. This instrument slowly rotates a 1,200 line per inch reflection-type diffraction grating to obtain the wavelength separation.

3.1.1.7 Discussion of Accuracy

The accuracy of key measurement systems utilized in this investigation are summarized below.

The accuracy of the load measurement system is better than ±0.5 percent. The crosshead displacement scale is graduated in units

of 0.005 inch and can be interpolated to 0.001 inch. Errors in specified chart advance speeds in both the loading and photomultiplier recorders were negligible.

The total transmittance measurement system was found to be capable of resolving better than 500 lines per inch when scanning a moiré grid transmission grating located in the position of the specimen. Similarly, the central image transmittance measurement system was found capable of resolving approximately 75 lines per inch.

The system for measuring both total and central image transmittance was found (using calibrated standard neutral density filter accurate to within ±1 percent) to indicate true transmittance magnitudes to within ±5 percent. The system is capable, however, of sensing and recording a change in magnitude of approximately ±0.2 percent of full scale. An effort was made to select the recorder scale and voltage so as to record data at the upper regions of the scale in order to take advantage of this sensitivity. The microdensitometer was also found to indicate the true transmittance magnitude to within ±5 percent of the indicated value.

Since accurate measurements also required the lamp system to provide a steady intensity output, its intensity was measured for periods of 2 hours and longer. It showed negligible change in this time period, which is much longer than required for any of the tests of this investigation. The lamp output can, of course, be expected to decrease with use, but this change occurs so slowly as not to be a factor in any one set of measurements.

3 1.1.8 Setup For Photographing Diffraction Grating Spectrum

Color photographs of the diffraction grating spectrum produced by normally incident light striking the wrinkle pattern set up in the transverse direction of uniaxially stressed specimen were taken with the basic test setup shown schematically in figure 13. The entire assembly including camera was mounted on the kinematic optical bench.

3.1.1.9 Strain-Crosshead Displacement Calibration

The dumbell shaped specimen used in uniaxial load tests were clamped using a spring loaded roller which pressed the specimen against a smooth jaw surface. The separation distance between rollers was 1.5 inches. This was not a true gage length, however; since this included part of the dumbell transition section in addition to the constant width test section. A calibration technique was, therefore, employed to experimentally relate the principal conventional Lagrangian strains to the crosshead displacement. The technique is described below.

Gage marks were placed on the specimen along principal X and Y directions and the u and v displacements were measured at selected levels of crosshead displacement. Principal conventional Lagrangian strains are then the ratio of the u or v displacements to the gage length in the X and Y directions, respectively. Poisson's ratio was calculated as the ratio of the Y direction strain (ϵ^L_{yy}) to X direction strain (ϵ^L_{xx}).

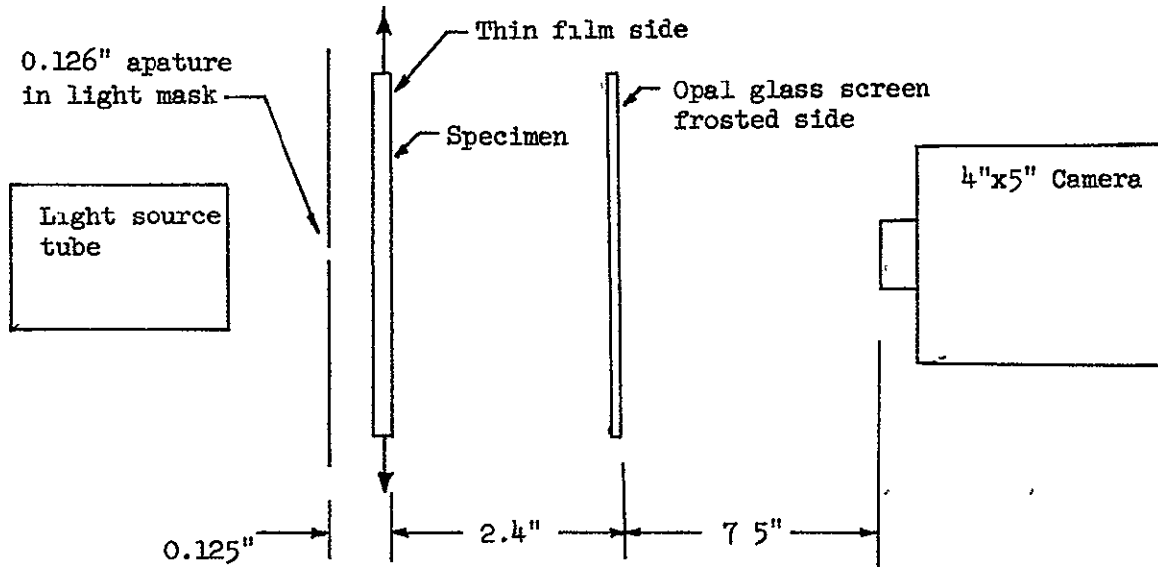

Figure 13.- Setup for taking photographs of diffraction grating spectrum

The results of this determination were used to relate the strains to crosshead displacement for all of the uniaxial load tests of this investigation. This extension is justified on the basis of the close repeatibility of load-crosshead displacement curves for the silicone rubber material used in these tests both with and without thin film metallic coatings.

3.1.2 Test Materials

3.1.2.1 Substrate

The substrate material used in this investigation was Sylgard 184, a room temperature vulcanizing silicone rubber manufactured by the Dow Corning Corporation. This material hereafter referred to as silicone rubber was gravity cast into sheet stock (approximately 0.1 inch thick) against highly polished chrome plated steel plates having a 1/2 rms finish. This produced sheets with two smooth clear parallel surfaces. All of the material used as specimens was cast at the same time and from the same batch. A standard ASTM die D-1708 was used to cut tensile test specimens. The circular hole was drilled in the rectangular plate using an end mill type bit and with the temperature of the silicone rubber reduced to below its glass transition temperature for clean milling purposes by immersion of the material in liquid nitrogen.

Silicone rubber is highly transparent throughout the entire wavelength range of the visible spectrum as shown in figure 14 (from ref. 8). Silicone rubber is a dielectric (k = 0) and has an index of refraction of 1.430 (ref. 48).

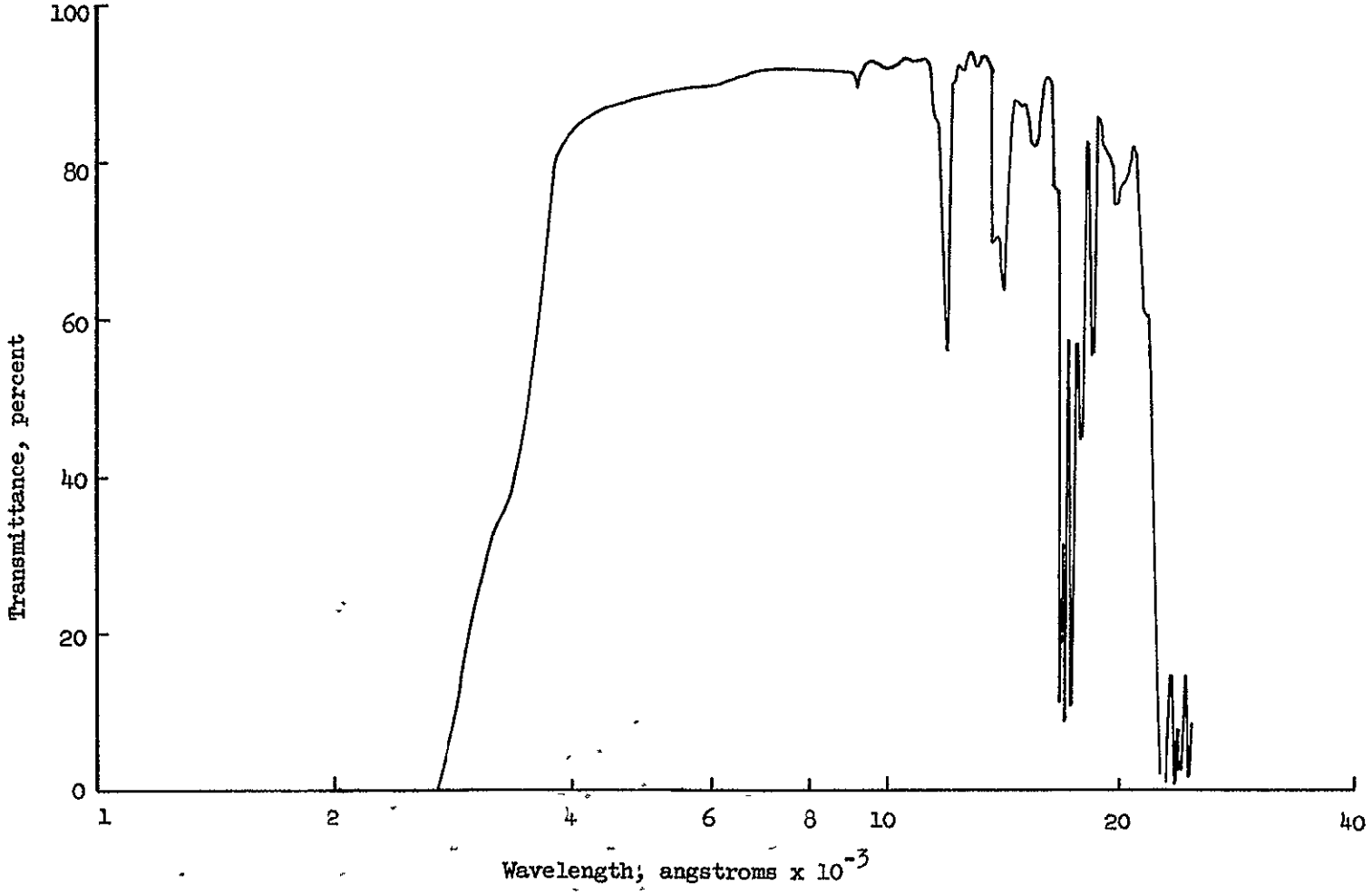

Figure 14.- Transmittance versus wavelength for Sylgard 184 silicone rubber (from Williams and Judd (ref. 5)).

The stress-strain curve for this material using conventional and natural strain/true stress definitions is presented in figure 15. The response is approximately linear using conventional definitions for strains of up to approximately 40 percent. The material exhibits very little creep at room temperature and is highly resilient as can be seen by the near coincidence of the load and unload portions of the curve. Poisson's ratio is also plotted on this graph based on both conventional and natural strain defintions.

3 1.2.2 Metallic Thin Films

Bulk metals deposited in this investigation as thin films included aluminum, copper, gold, indium and silver. The supplier and purity of each of these metals used is listed in table 2.

Selected mechanical properties of each of these metals in bulk form are presented in table 3 (refs. 36, 37). A stress-strain curve for 99.995 percent pure bulk aluminum (from ref. 38) is presented in figure 16. Reference 17 presents a similar plot for polycrystalline copper.

The physical properties of metals in thin film form frequently differ from those of the parent bulk form (refs. 18, 31, 40). Quarrell (ref. 41) has shown that even the basic crystal form of the bulk material may be violated in very thin films. For example, silver and gold which in bulk form have a face centered cubic crystal exhibit a close-packed hexagonal crystal in very thin film form.

A stress-strain curve for a 5000 Å thick gold film subjected to uniaxial loading is presented in figure 17 (from ref. 42). The

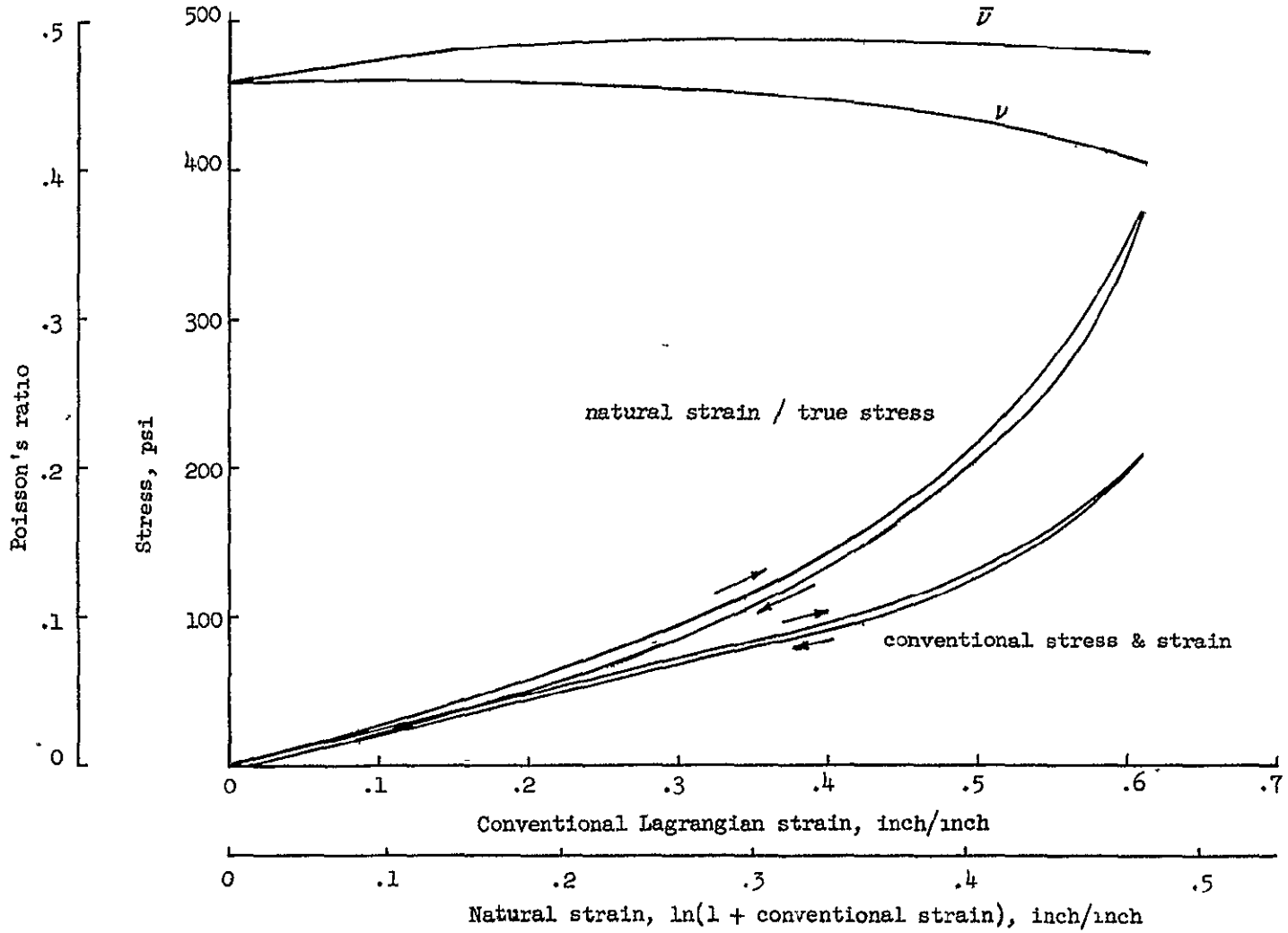

Figure 15.- Stress-strain graph and Poisson's ratio variation for Sylgard 184 silicone rubber.

TABLE 2.- RAW MATERIALS USED IN THIN FILM DEPOSITION

Material	Supplier	Purity, percent
Aluminum	Fisher Scientific	99.7
Copper	Fisher Scientific	99.9
Gold	Goldsmith Brothers	99.99
Indium	Electronic Space Products, Inc.	99.999

TABLE 3.- TYPICAL MECHANICAL PROPERTIES OF SELECTED BULK METALS

Material	Modulus of elasticity, psi	Ultimate tensile strength, ksi	Ultimate elongation, percent	Yield strength, ksi	Poisson's ratio
Aluminum*					
99.996 percent pure sheet					
Annealed	9×10^6	6.8	60	1.7	---
Cold-rolled (75 percent of original thickness)	9×10^6	16.3	5	15.4	---
Copper*					
Annealed	17×10^6	32-37	46	4.6-12.0	0.33
Drawn	---	55-61	--	50.0-55.0	0.33
Gold*					
Annealed 300° C	11.2×10^6	18-20	39-45	---	0.42
Cold-worked (60 percent)	11.2×10^6	30-32	4	---	0.42
Indium*	1.57×10^6	0.38	22	---	---
Silver+					
Annealed	11×10^6	22	48	8	

*Encyclopedia of the Chemical Elements (ref. 36).
+Material Engineering Materials Selector Issue (ref. 37).

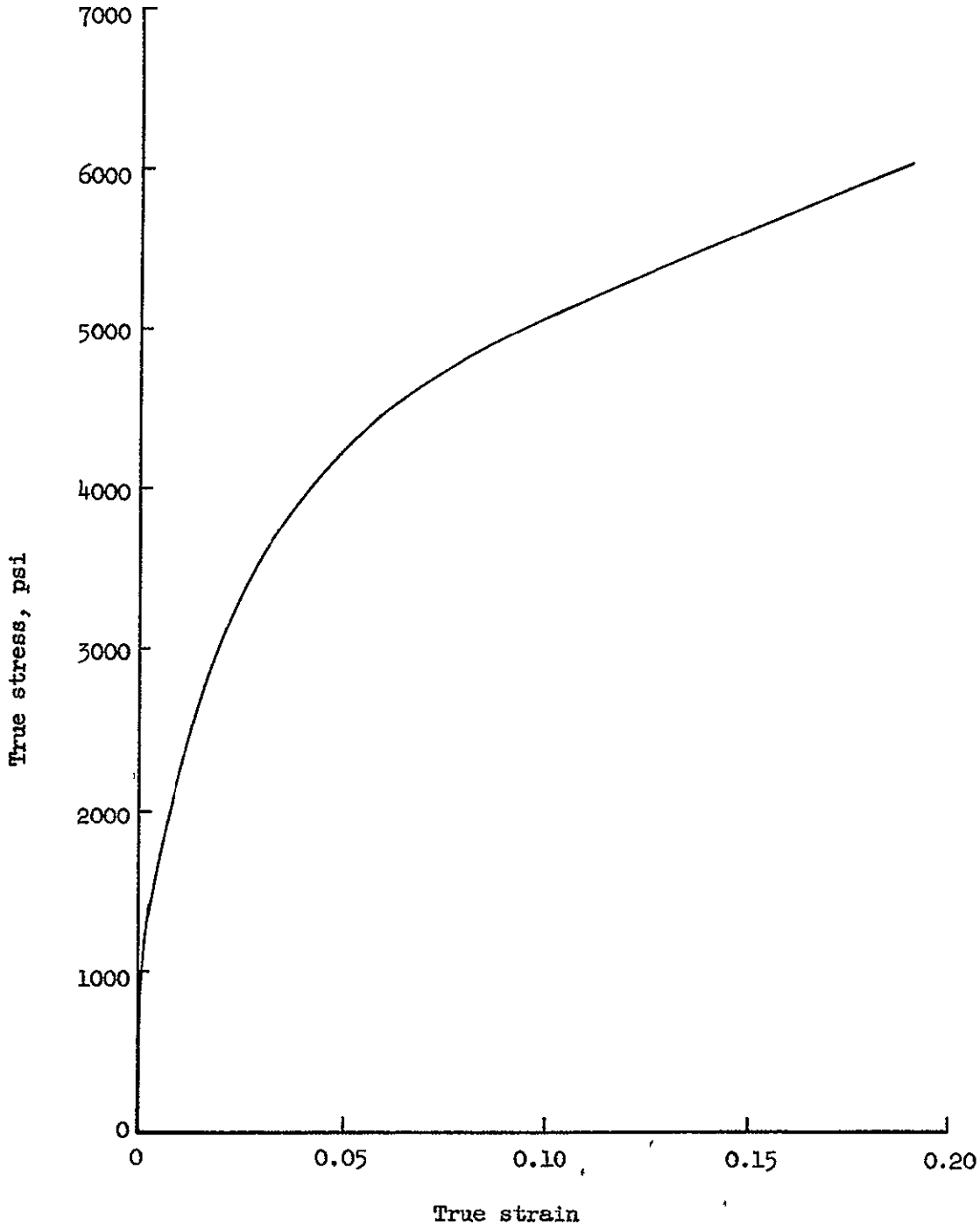

Figure 16.- Stress-strain graph for 99.995 percent pure aluminum (from Tietz, Meyers, and Lytton (ref. 38)).

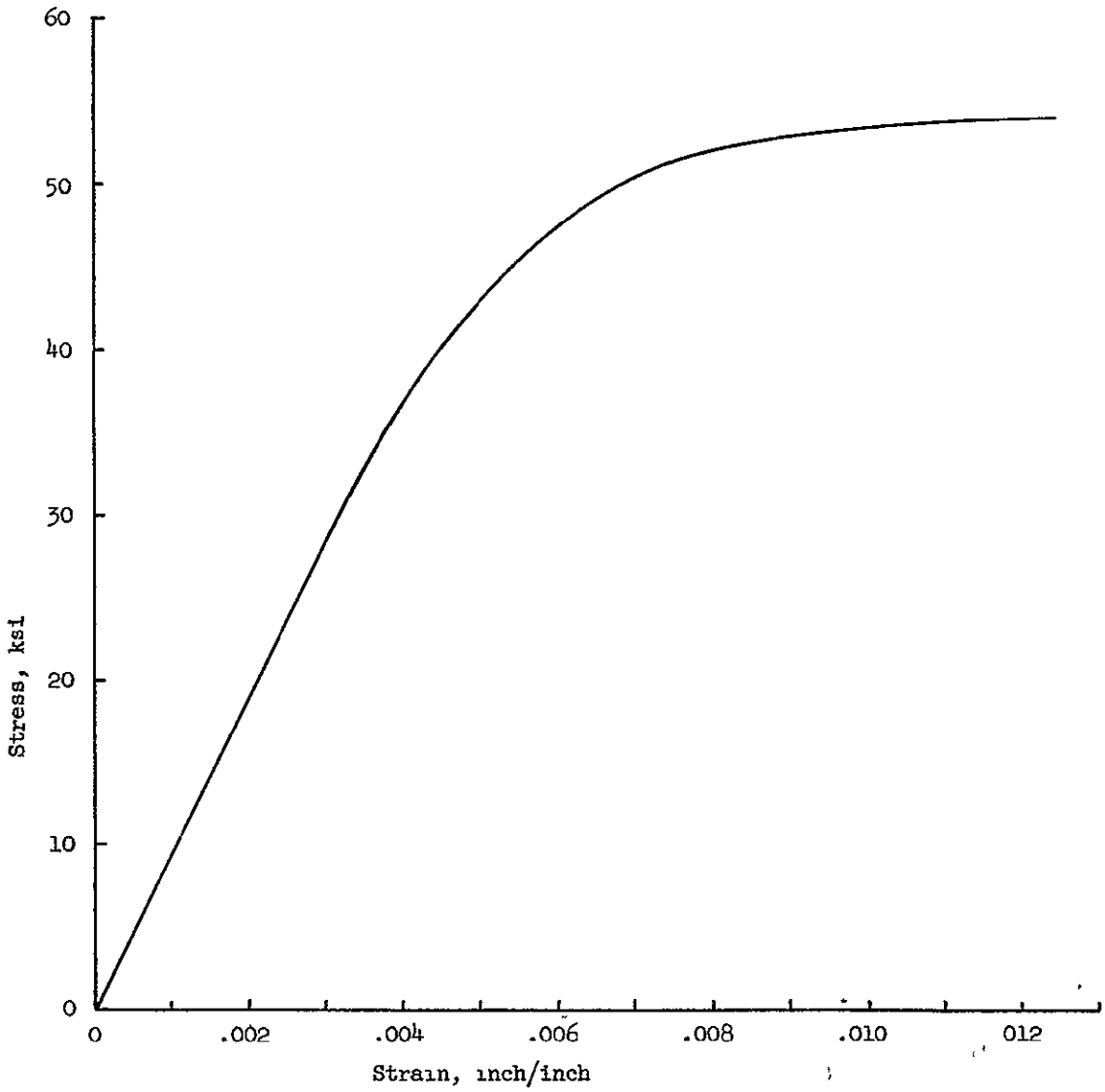

Figure 17.– Stress–strain graph for an evaporated gold film 5000 angstroms thick (after Neugebauer (ref. 42)).

fracture stress for a 200 Å thick gold film was experimentally found by Beams (ref. 43) to be 75,400 psi. This data for gold indicates that the ultimate elongation is smaller and the ultimate stress greater for the thin film form than for the bulk form. Young's modulus was found to be approximately the same for both forms (ref. 43). Gold in thin film form exhibits creep and plastic deformation even at relatively low magnitudes of strain.

A discussion of proposed physical explanations for the difference in mechanical properties between bulk and thin film forms may be found in references 42, 44, 45, and 46. The conditions of the deposition process itself such as temperature, pressure, and rate of deposition are important parameters which influence the resulting physical and optical properties. Slow rates of deposition encourage aggregation of the metal which Sennett and Scott (ref. 40) suggest explains the difference in properties from that of the bulk form. For a discussion of the influence of these and other factors see references 34, 42, and 47.

3.1.3 Test Results

3.1.3.1 Total and Central Image Transmittance Measurements for Uniaxially Loaded Specimen

Results of measurements of the total and central image transmittance versus the conventional and natural Lagrangian strains in the direction of the applied uniaxial load are given in figures 18, 19, 20, and 21, for specimens of silicone rubber with aluminum, copper, and indium thin film coatings. Total and central image transmittance data for each coating material was measured for the same specimen but on separate load cycles. Arrows denote the correlation of data with the load and unload portion of each cycle. It was found that the load portion of the initial load cycle for coatings with thicknesses greater than that corresponding to an initial transmittance of approximately 10 percent gave data which was either noncontinuous (i.e., finite changes in transmittance over a very short strain interval) or nonrepeatible on successive cycles. The unload portion of the first cycle and load cycles thereafter gave very good repeatibility of results (within the normal load hysteresis of the specimen). For coatings initially thinner than that corresponding to an initial transmittance of approximately 20 percent, the entire first cycle was closely duplicated on successive cycles. This irregular phenomena exhibited on the first cycle of thick films is probably related to the development of microfractures. The anomaly noted at the start of loading in figure 18(a) is characteristic of starting errors introduced in these tests due to initially poorly alined specimen. This problem is self-correcting with the application of loading.

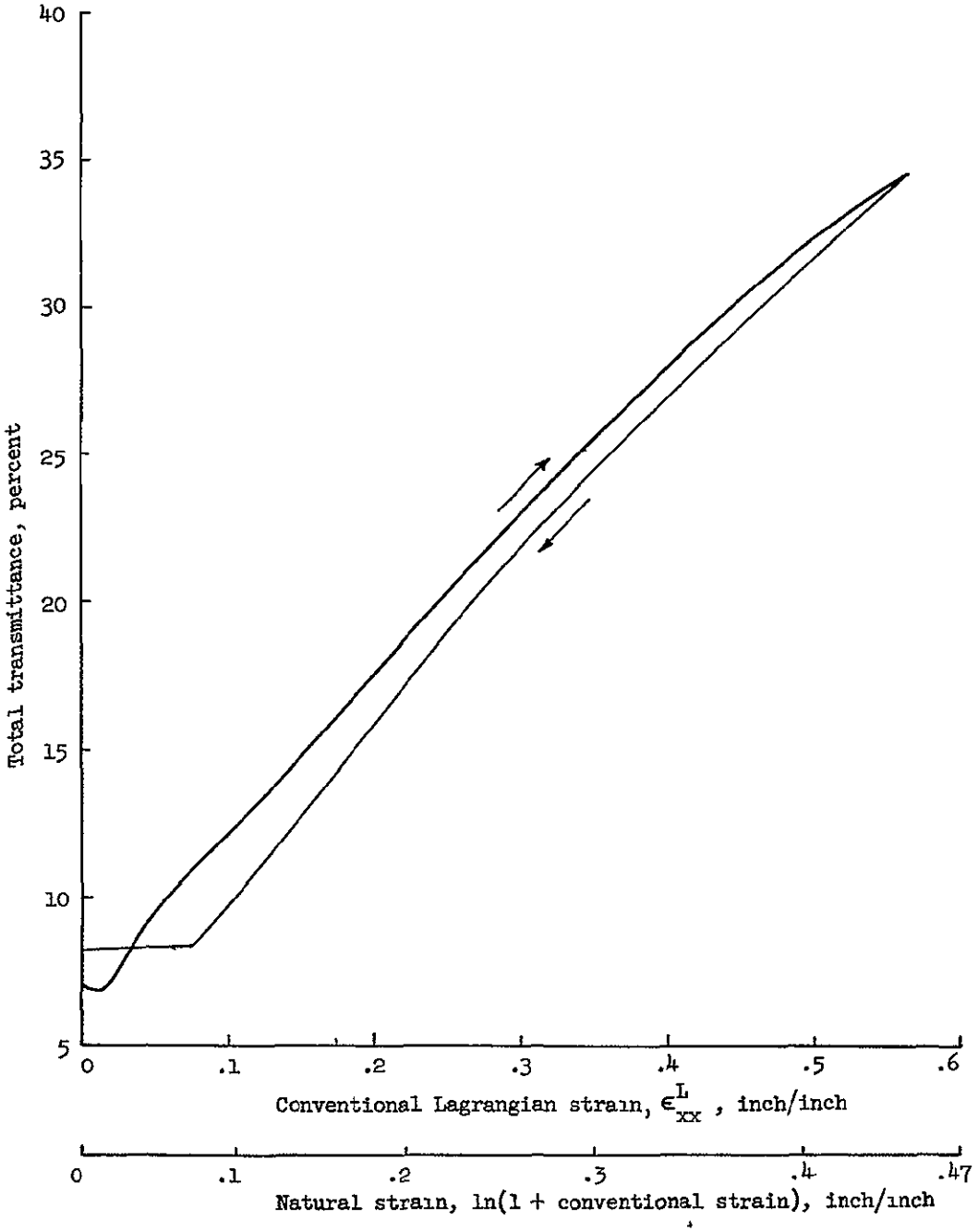

(a) Total transmittance.

Figure 18.- Transmittance response versus strain for uniaxially loaded specimen of silicone rubber with aluminum thin film coating.

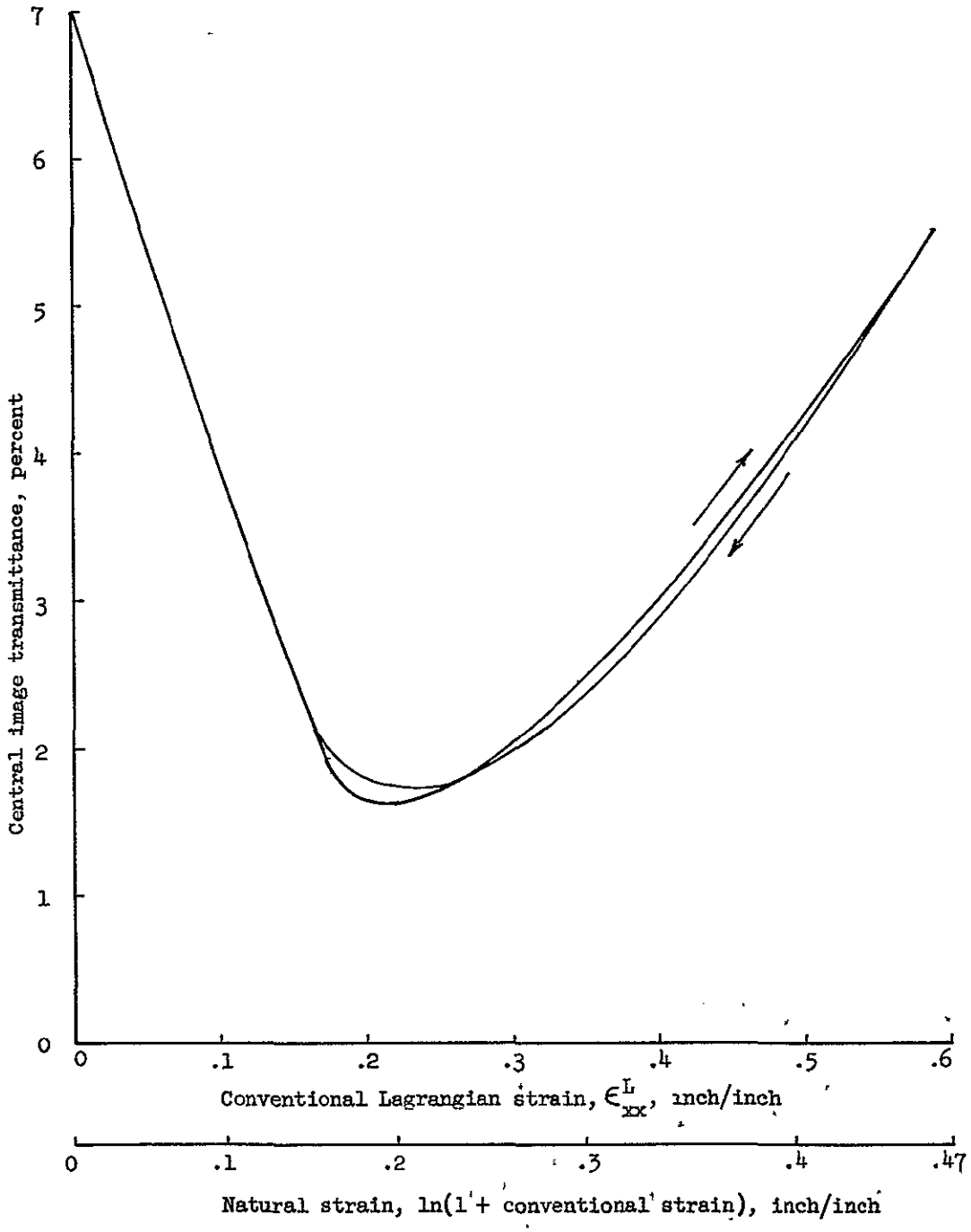

(b) Central image transmittance.

Figure 18.- Concluded.

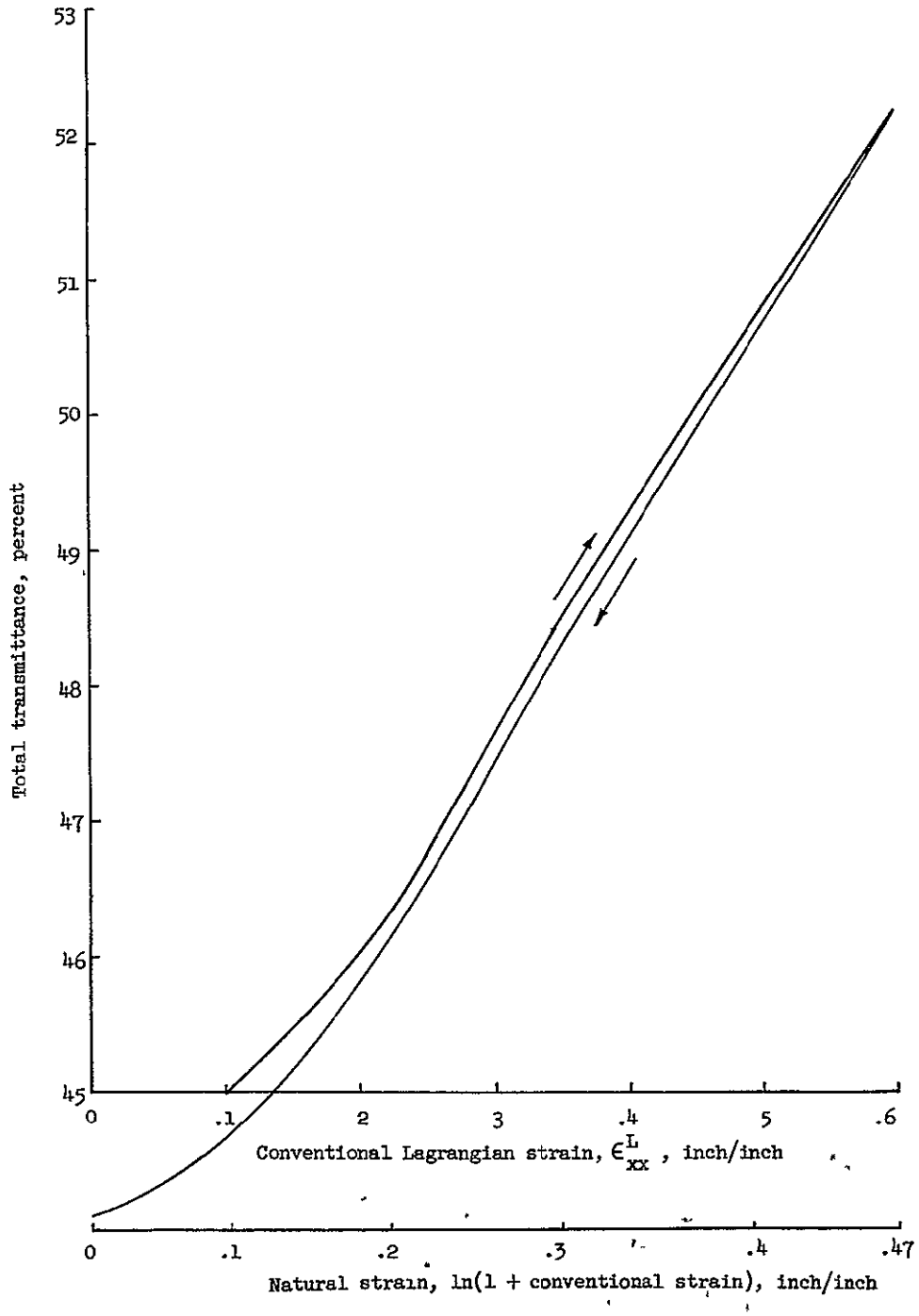

(a) Total transmittance.

Figure 19.- Transmittance response versus strain for uniaxially loaded specimen of silicone rubber with copper thin film coating.

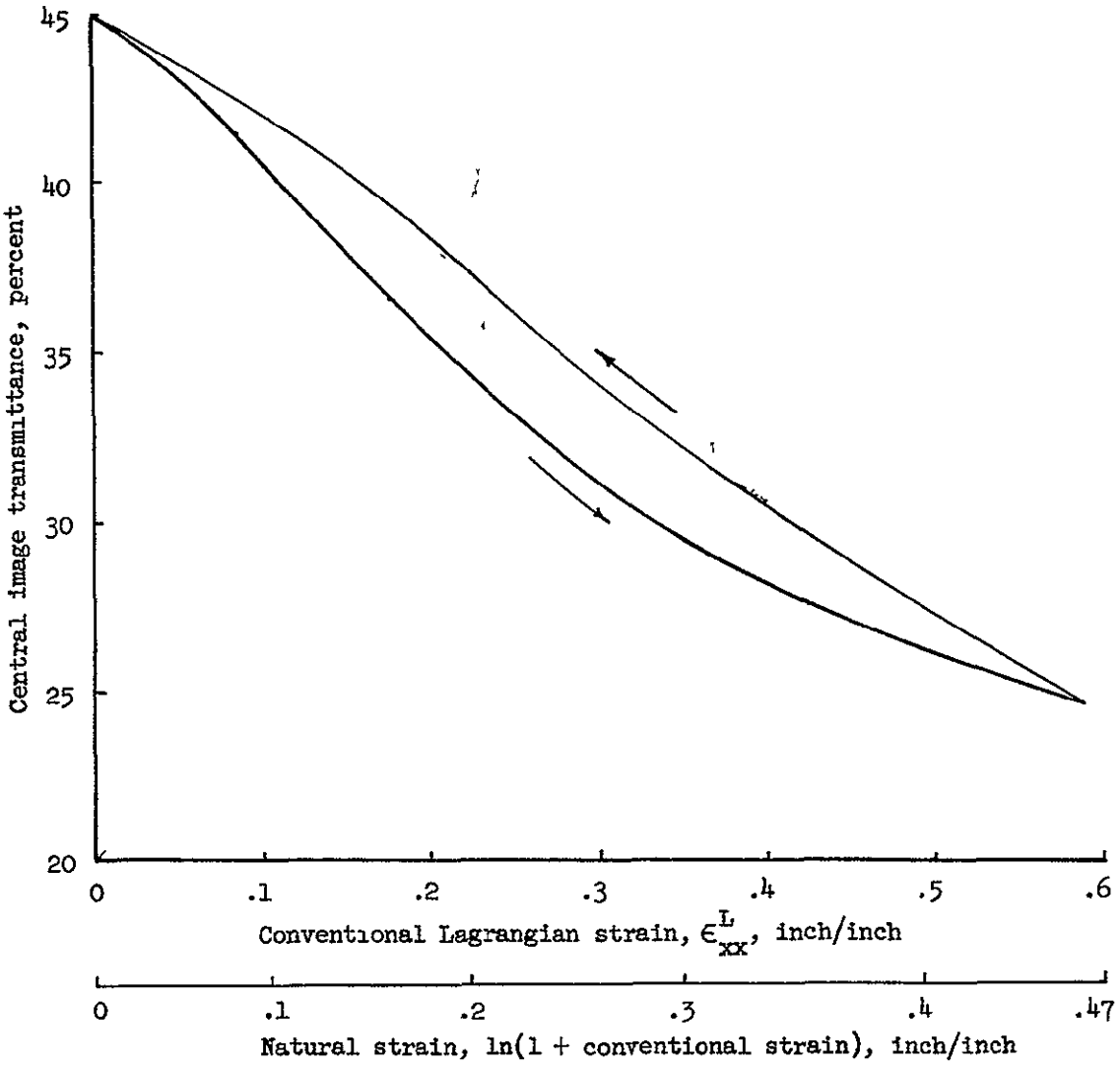

(b) Central image transmittance.

Figure 19.- Concluded.

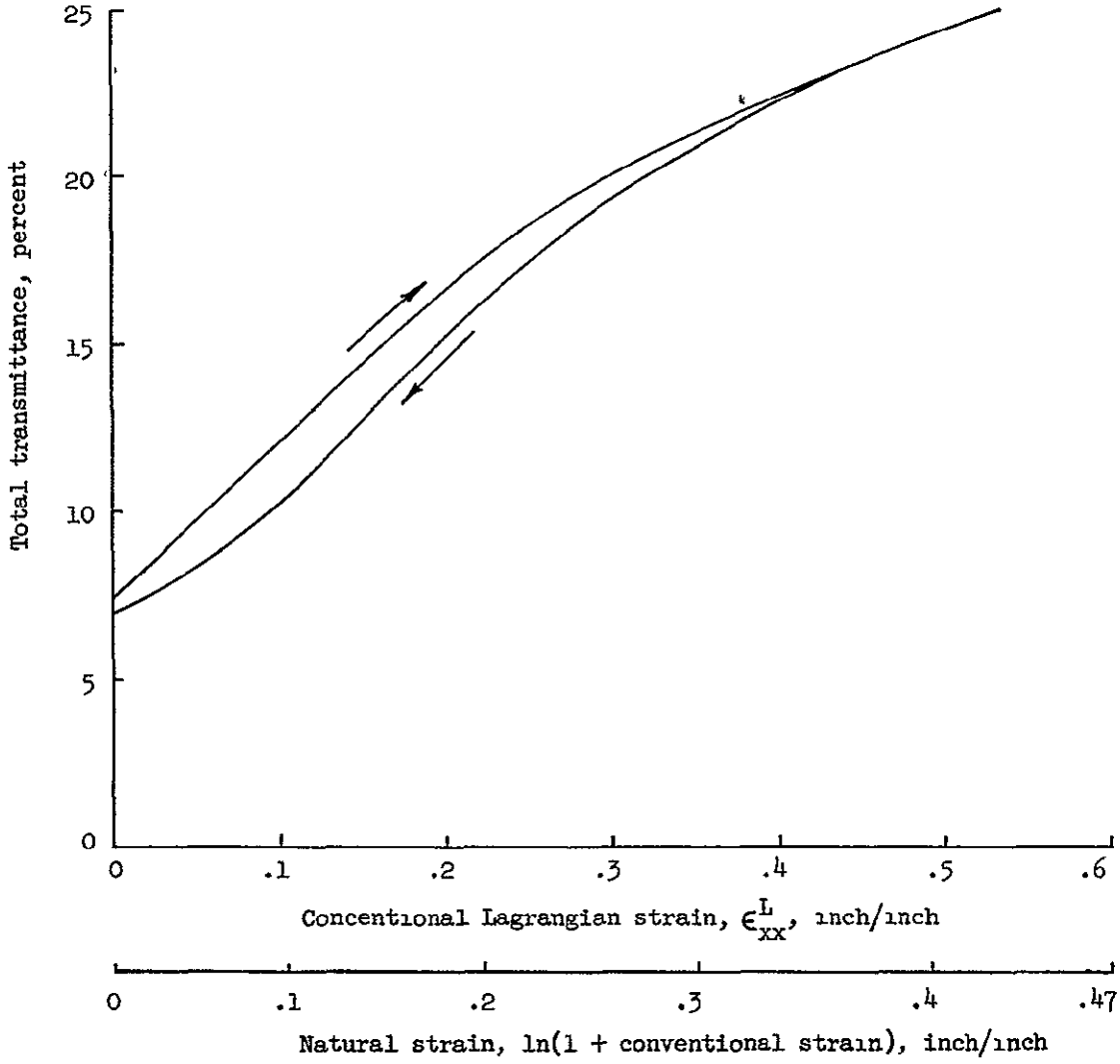

(a) Total transmittance.

Figure 20.- Transmittance response versus strain for uniaxially loaded specimen of silicone rubber with indium thin film coating (initial transmittance = 7.5 percent).

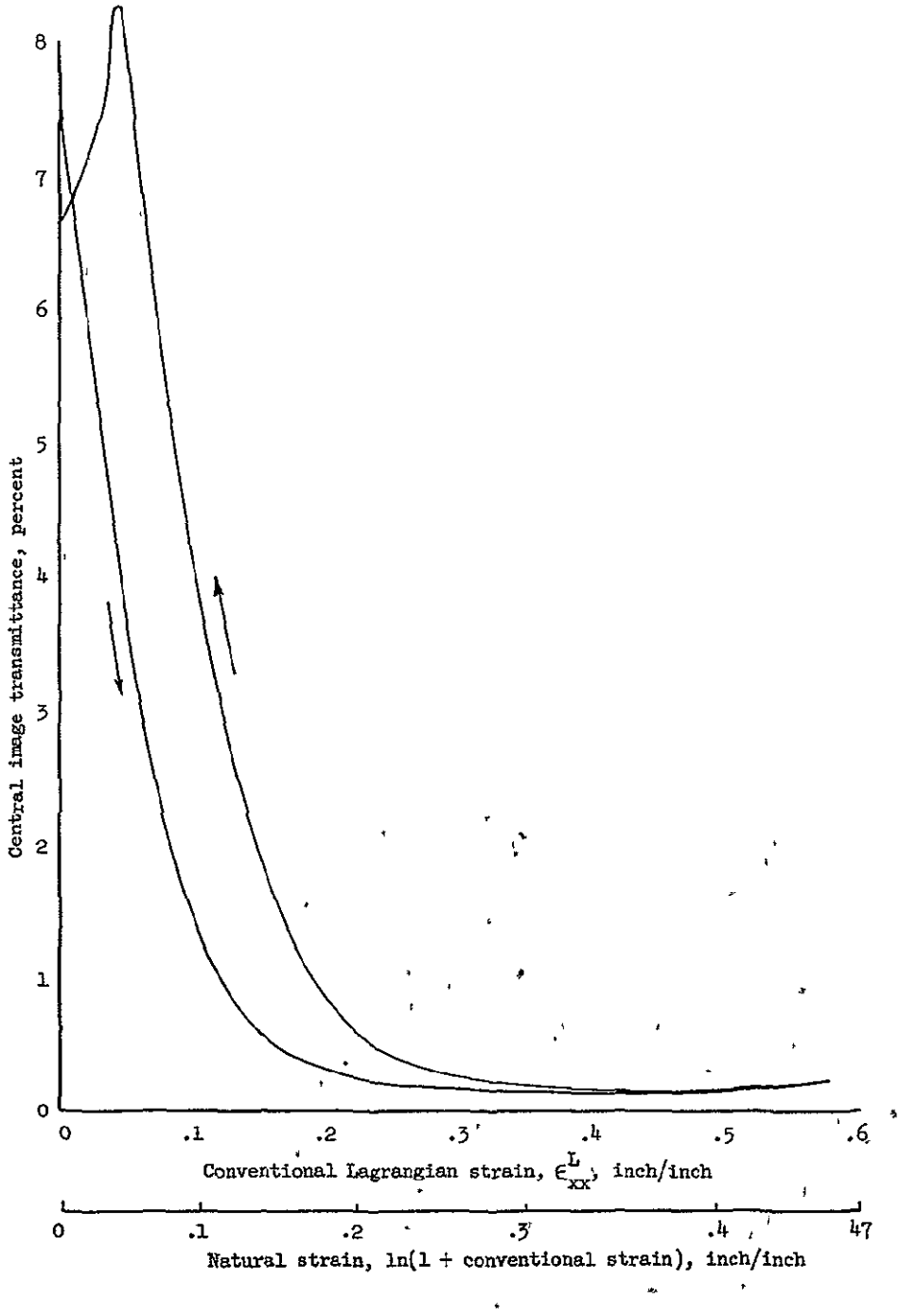

(b) Central image transmittance.

Figure 20.- Concluded.

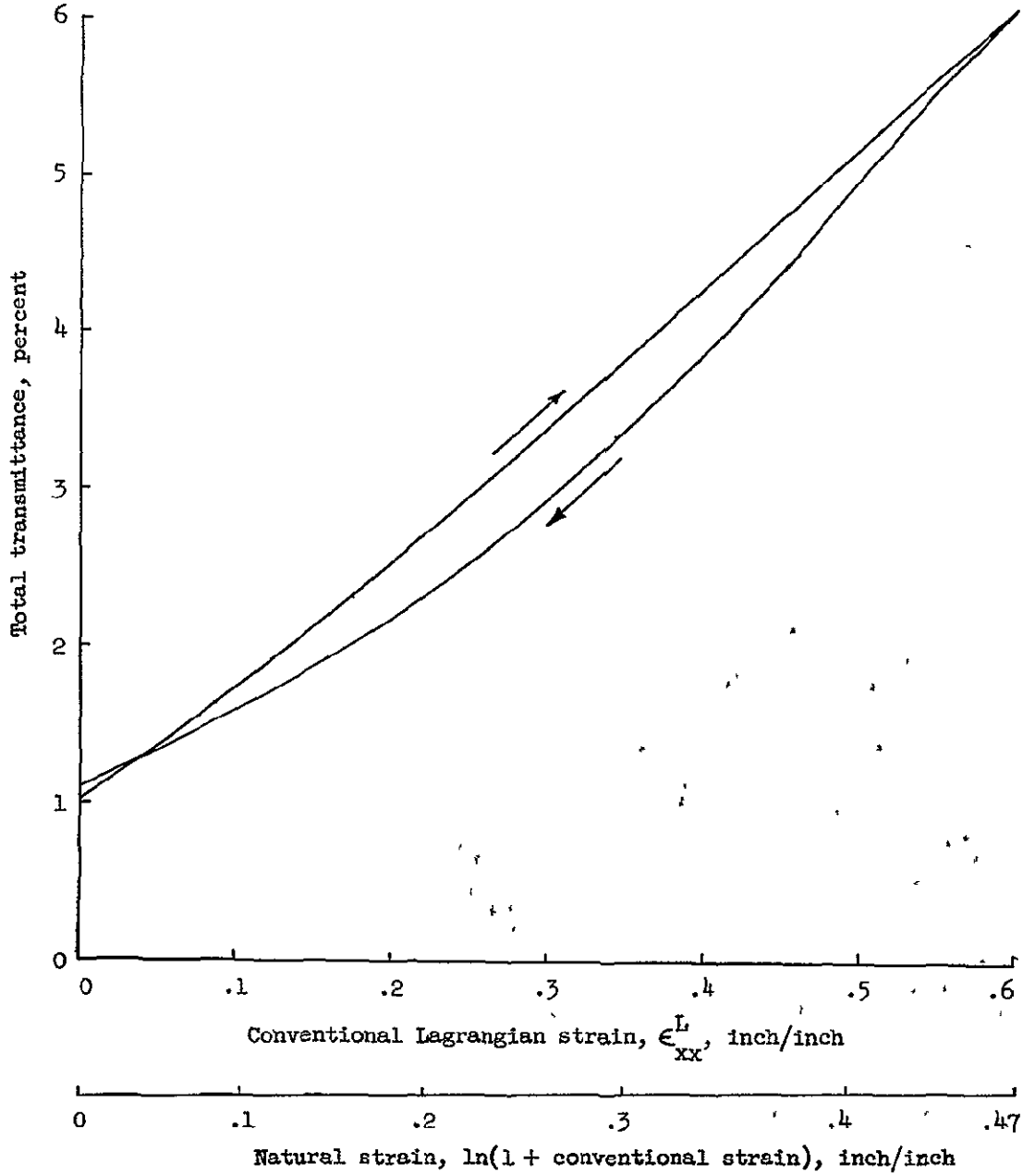

(a) Total transmittance.

Figure 21.- Transmittance response versus strain for uniaxially loaded specimen of silicone rubber with indium thin film coating (initial transmittance = 1 percent).

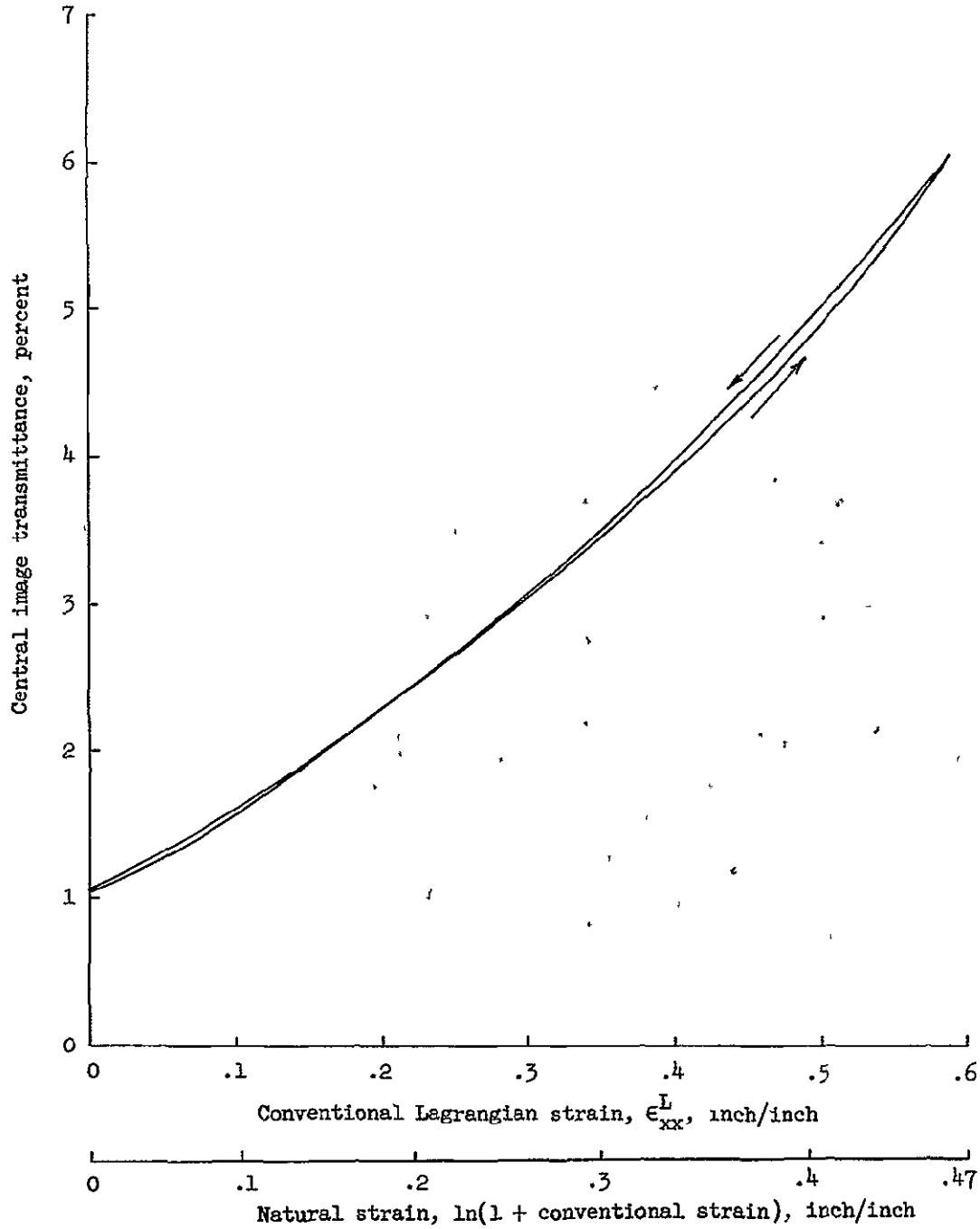

(b) Central image transmittance.

Figure 21.- Concluded.

All specimens were approximately 0 1 inch thick. The strain rate for the data presented was approximately 0.038 inch/inch/minute. Tests were also conducted at strain rates of approximately 0.38 and 3.8 inch/inch/minute, but without any apparent change in the results. All data presented is for specimens illuminated with white light. Tests conducted at selected narrow bands of light wavelength indicated shifts in the magnitude of transmittance but gave in general the same basic form for the data.

To insure that the changes recorded were not due to the substrate; total and central image transmittance tests were conducted on uncoated silicone rubber specimens. The results showed strain to exercise negligible influence on either of these two properties. It was also determined by comparing load-displacement curves for specimens with a variety of coatings and coating thicknesses that the thin film coating had no significant influence on stress-strain history. A similar transmittance response to that presented here was recorded for other materials tested in this investigation including gold and silver. In general, the total transmittance continuously increases with increasing strain and is in some cases nearly linear. The central image transmittance versus strain usually exhibits an initial decrease in transmittance which may reverse itself and become an increasing function as was the case for the relatively "thick" thin film of aluminum (fig. 18(b)) or it may continuously decrease as was the case for the thin film of copper (fig. 19(b))

The central image transmittance for a specimen with a thin film coating of indium having an initial transmittance of 7.5 percent (figure 20(b)) decreases rapidly with increasing magnitudes of strain up to a conventional strain of approximately 15 percent at which point the specimen is nearly opaque (less than 0.5 percent central image transmittance). This is exactly opposite to the response of a slightly thicker coating of indium (with an initial transmittance of approximately 1 percent) as presented in figure 21(b). The central image transmittance of this specimen continuously increases with increasing magnitudes of strain. In fact, the total and central image transmittance responses of this specimen are almost identical indicating a negligible influence of diffraction. Indeed, spectral wavelength separation (discussed in Section 3.1.3.3) was almost indistinguishable for this specimen. More will be said about the differences in these two specimens with thin film coatings of indium when the results of microscopic surface examinations of these same two specimens are presented in the next section.

3.1.3.2 Microscopic Surface Examination of Uniaxially Loaded Specimen

A series of photomicrographs is presented in figure 22 of the surface of a uniaxially loaded specimen of silicone rubber with a gold thin film coating whose undisturbed transmittance was approximately 25 percent. The specimen was examined in transmitted brightfield and reflected brightfield lighting at magnitudes of conventional Lagrangian strain ranging from zero to 60 percent. The specimen was initially clear and without surface irregularities as shown in figure 22(a).

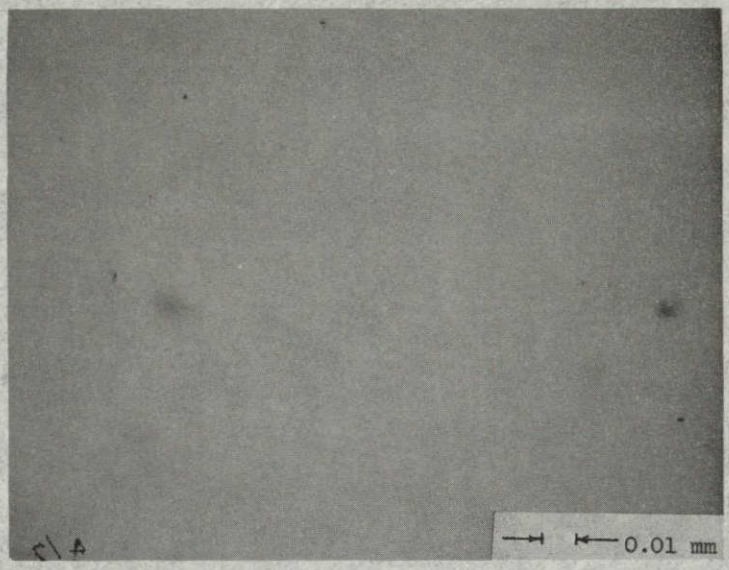

Transmitted brightfield

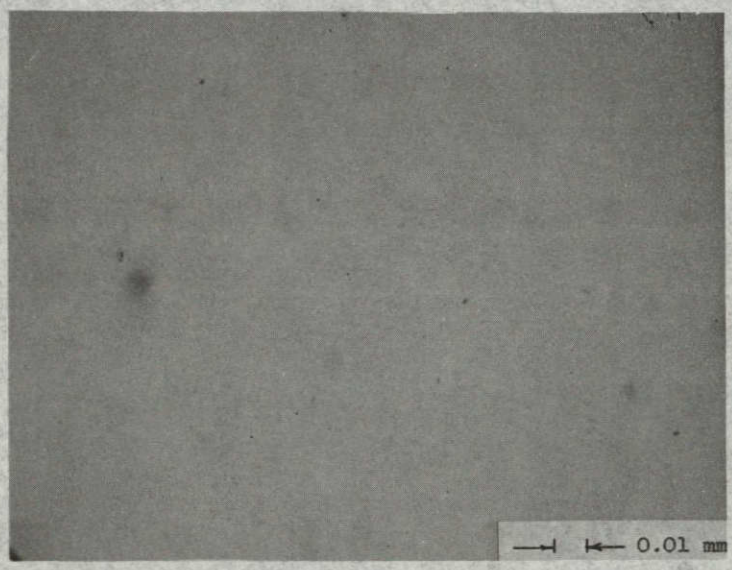

Reflected brightfield

(a) As deposited, $\epsilon^{L}_{xx} = 0.$

Figure 22.- Photomicrographs of thin gold film deposited on silicone rubber substrate for selected magnitudes of strain corresponding to uniaxial loading. Transmittance (as deposited) = 25 percent.

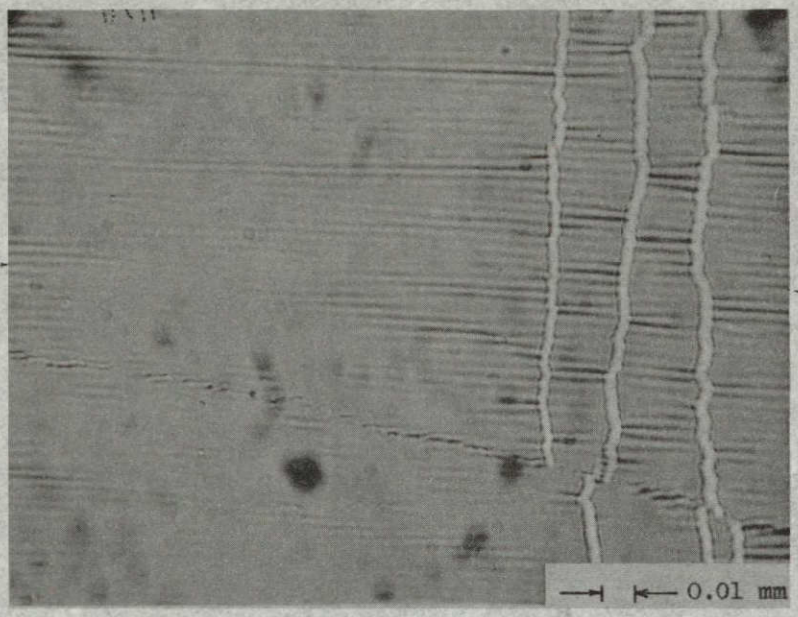

Transmitted brightfield

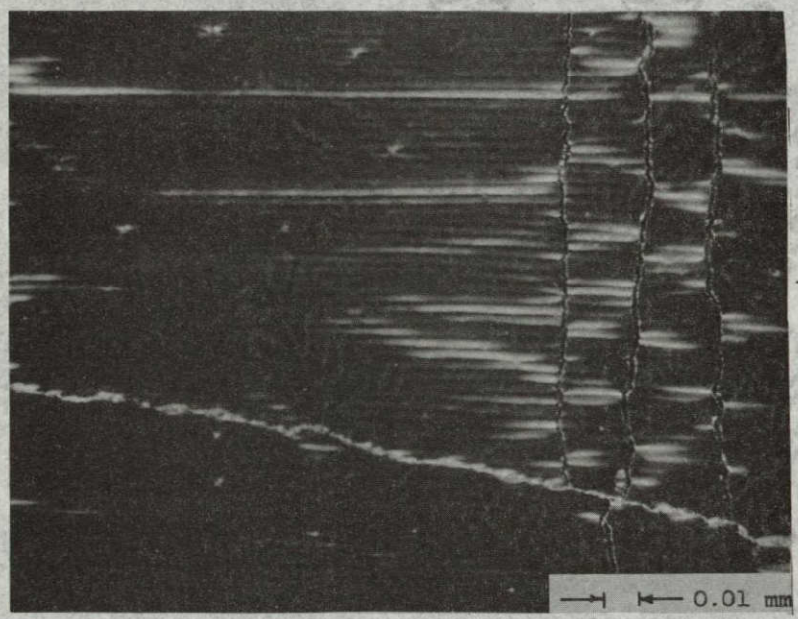

Reflected brightfield

(b) Wrinkle pattern clearly established, $\epsilon^{L}_{xx} = 0.04$.

Figure 22.- Continued.

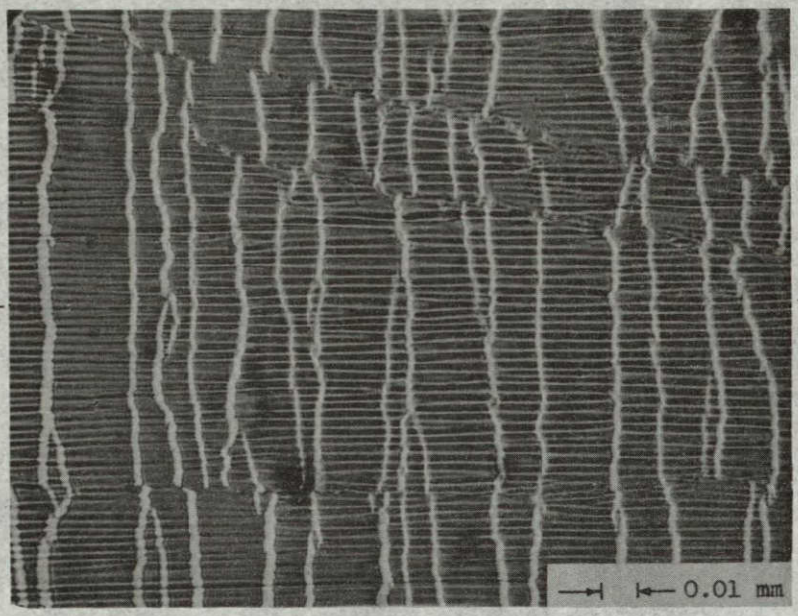

Transmitted brightfield

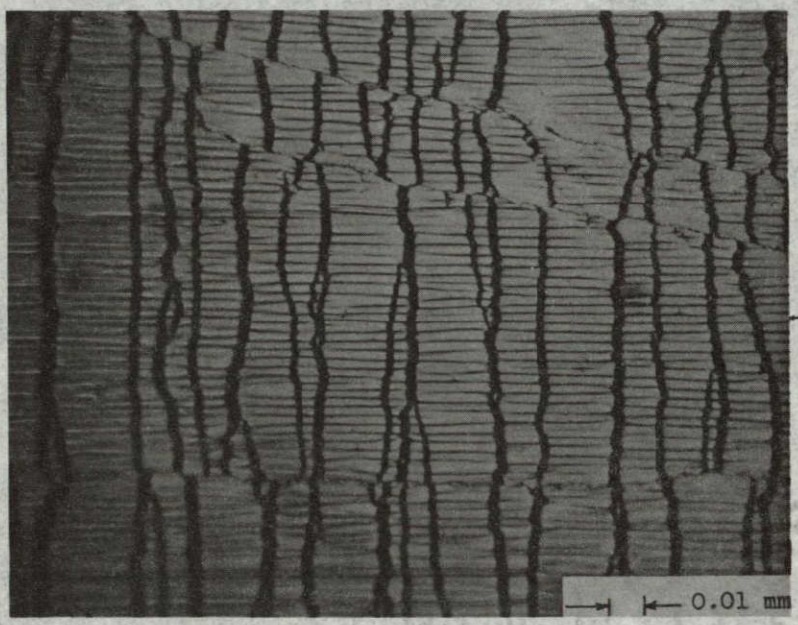

Reflected brightfield

(c) $\epsilon_{xx}^{L} = 0.21.$

Figure 22.- Continued.

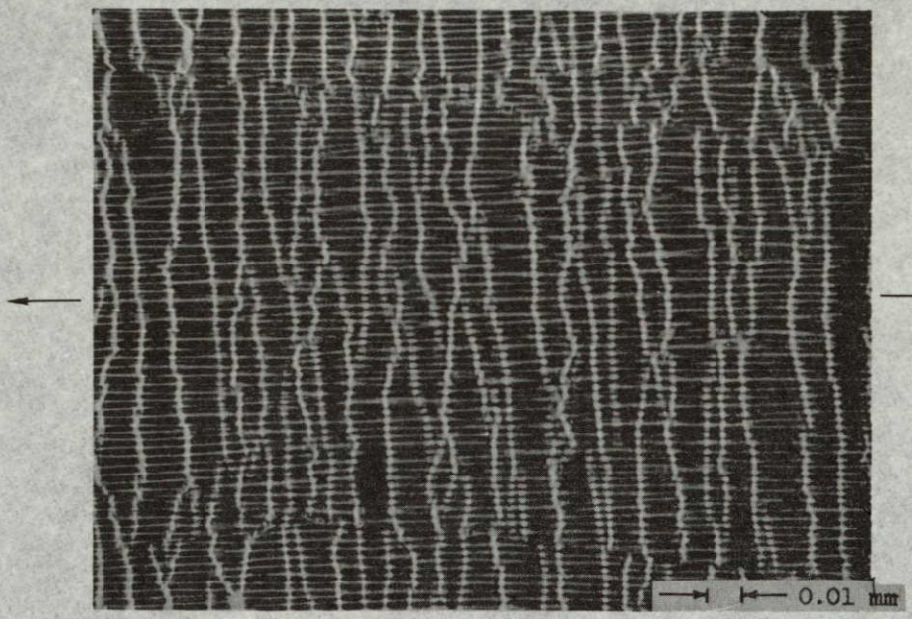

Transmitted brightfield

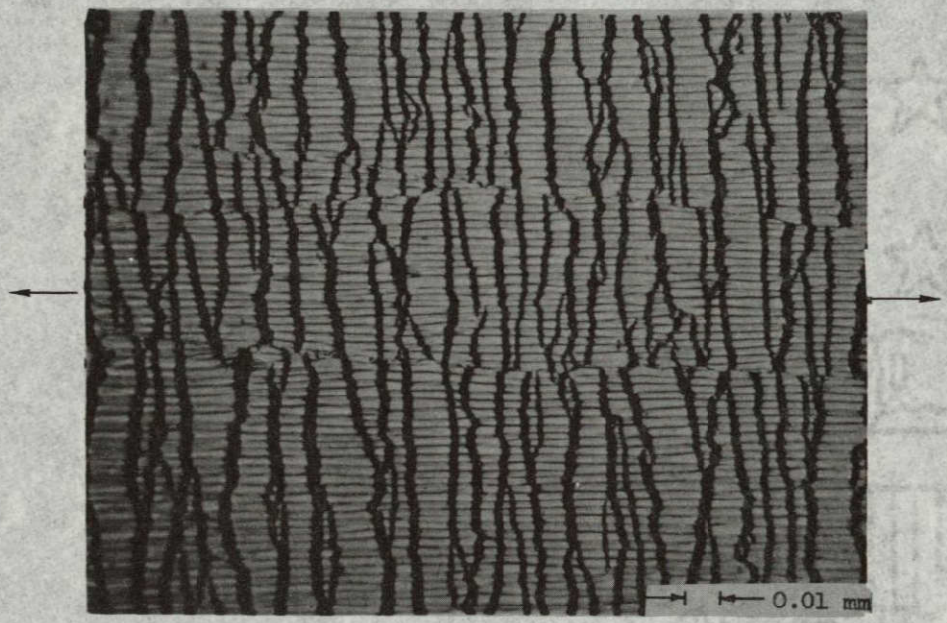

Reflected brightfield

(d) $\epsilon_{xx}^{L} = 0.42.$

Figure 22.- Continued.

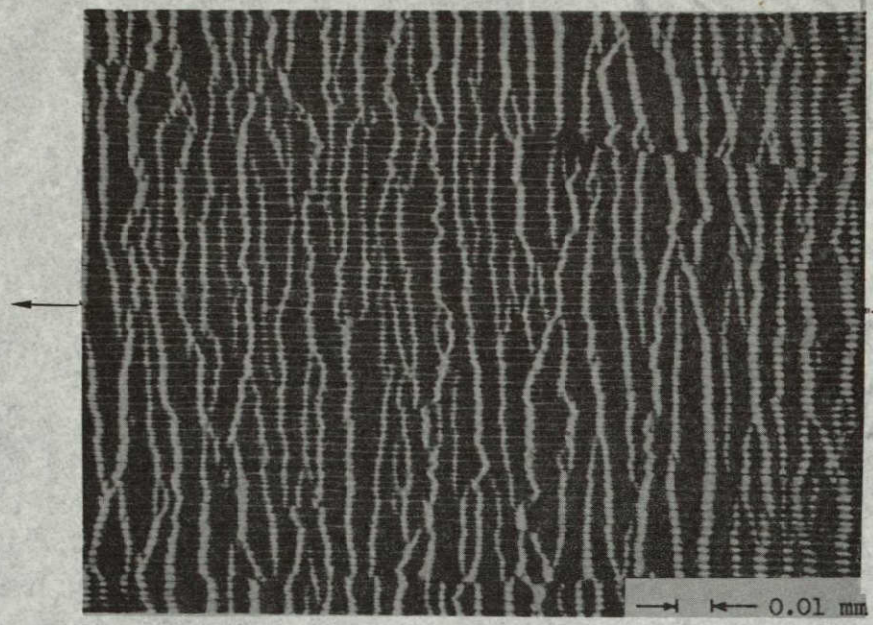

Transmitted brightfield

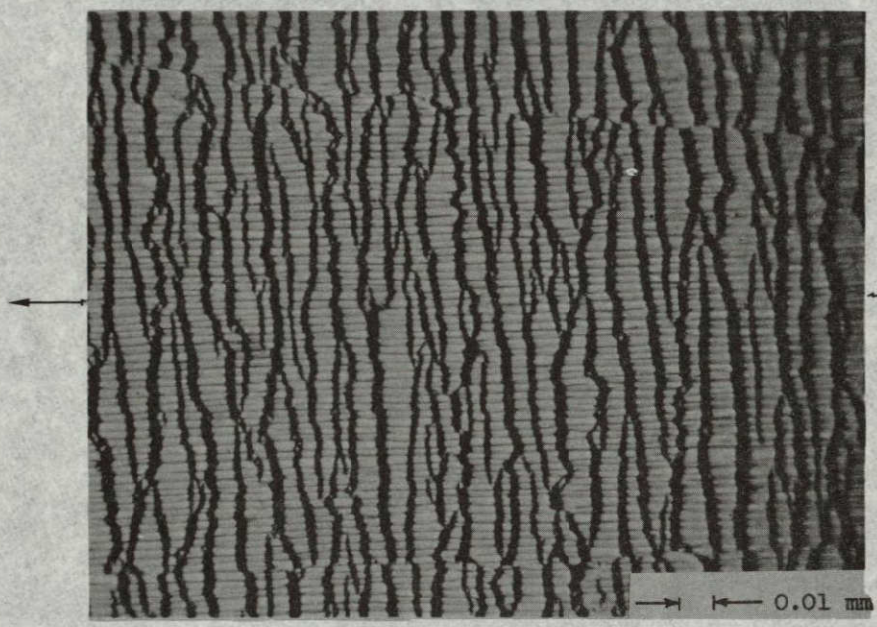

Reflected brightfield

(e) $\epsilon_{xx}^{L} = 0.60.$

Figure 22.- Continued.

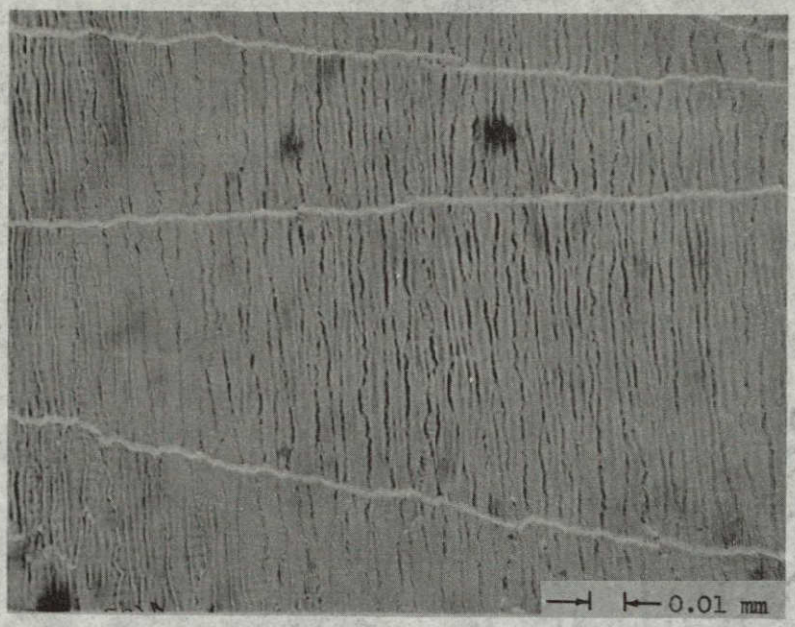

Transmittance, percent

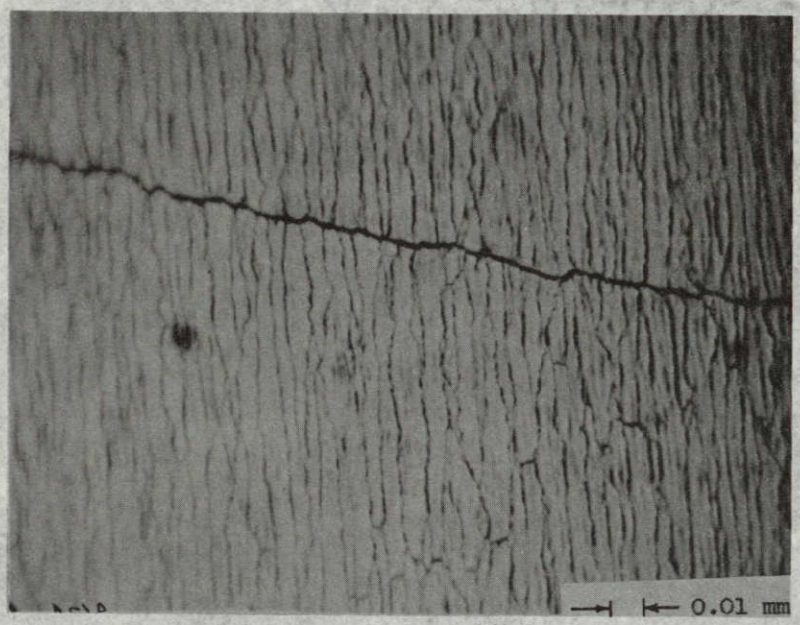

Reflected Brightfield

(f) Imposed deformation released, $\epsilon_{xx}^{L} = 0$.

Figure 22.- Concluded.

As strain was applied an orthogonal set of lines developed which in general were alined along and perpendicular to the direction of the applied load (i.e., along principal directions). These lines began to assume definition at a strain of approximately 4 percent. Slip lines are also evident in certain regions.

The lines perpendicular to the direction of the applied load are irregular. The lines appear light in transmitted brightfield and dark in reflected brightfield lighting, thus indicating that there is physical separation of the thin film; i.e., the development of microfractures. The number of microfractures per unit length progressively increases with increasing magnitudes of strain.

The lines parallel to the direction of the applied load are straight and have a common frequency even across slip lines and microfractures. When transmitted and reflected brightfield photomicrographs are compared, one still observes light and dark lines, respectively. These lines are not, however, due to microfractures; but are due to the interaction of light with a nonplanar surface, i.e., a series of wrinkles in the thin film. The frequency of these wrinkles increases as a function of increasing strain. A plot of a microdensitometer scan across a typical wrinkle pattern of the film used to print figure 22(c) is presented in figure 23. The shape is observed to be periodic and roughly sinusoidal. Minor variations in the shape of such a curve can be induced by the focus of the microscope during the exposure of the negative.

Figure 23.- Microdensitometer scan across typical wrinkle pattern of film used to print figure 22(c).

A listing of the accumulative width of microfractures per unit length and of the frequency of wrinkles versus strain for this specimen is presented in table 4.

Microscopic examination of specimens of silicone rubber with thin film coatings of copper and aluminum showed these specimens to respond to loading in a manner similar to that of the gold specimen described above (with minor variations such as wrinkle frequency). Figure 24 presents a set of photomicrographs for three specimens with aluminum coatings, each with different initial thickness (i.e., different initial transmittance). The strain imposed was identical for each of these tests and of magnitude $\epsilon^{L}_{xx} = 0.42$. From these photomicrographs, it is difficult to establish a general rule concerning the coating thickness and the magnitude of the corresponding wrinkle frequency. The frequency for the aluminum thin film with an initial transmittance of 59 percent is much greater than that for thin films with an initial transmittance of either 10 or 80 percent. A possible explanation for

TABLE 4.- ACCUMULATIVE WIDTH OF MICROFRACTURES AND WRINKLE FREQUENCY VERSUS STRAIN FOR SPECIMEN OF SILICONE RUBBER WITH GOLD THIN FILM COATING

	Strain, ϵ_{xx}^{L}, inch/inch				
	0	0.04	0.21	0.42	0.60
Accumulative width of microfractures per unit length, inch/inch	0	0.08	0.14	0.24	0.34
Wrinkle frequency, wrinkles/inch	0	8400	10200	11100	11800

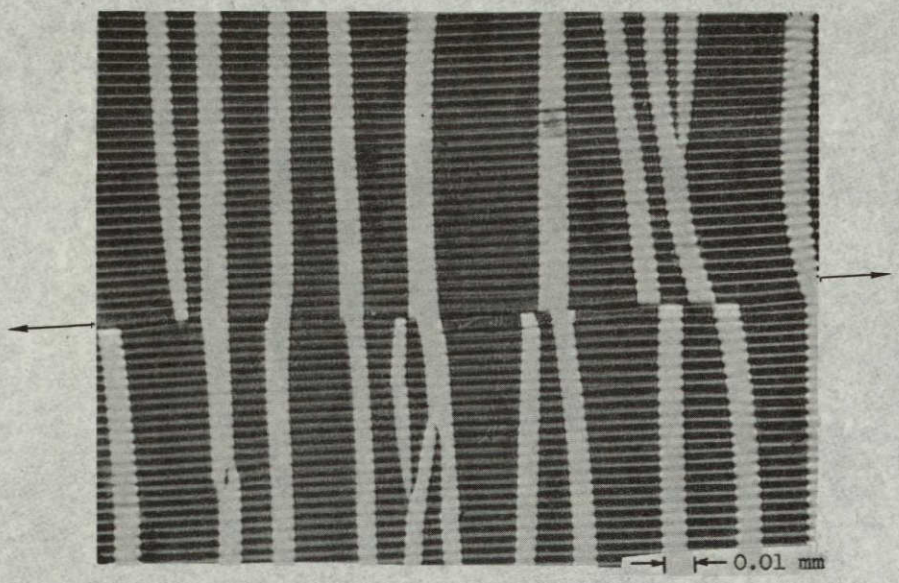

Transmitted brightfield

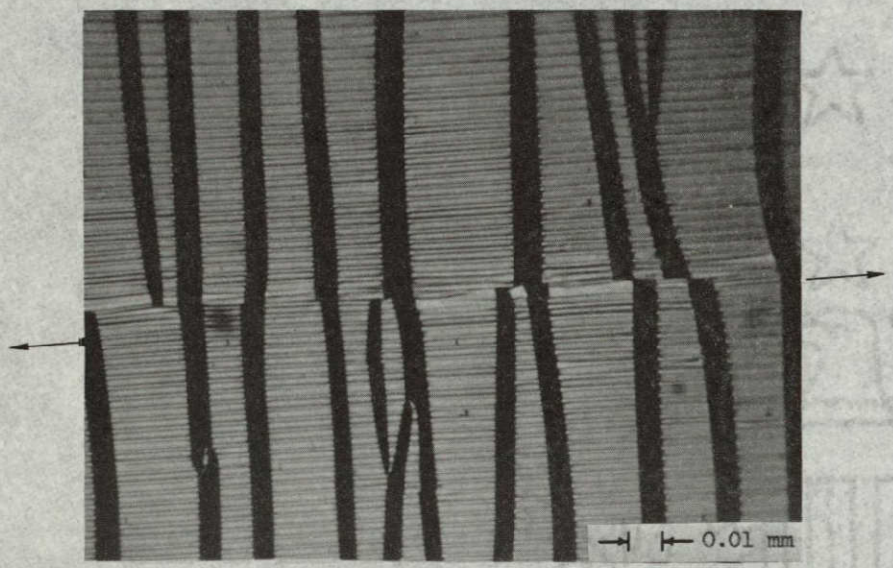

Reflected brightfield

(a) Transmittance (as deposited) = 10 percent.

Figure 24.- Photomicrographs of thin film of aluminum deposited on a silicone rubber substrate uniaxially loaded to impose a conventional strain of 42 percent (ϵ^{L}_{xx} = 0.42).

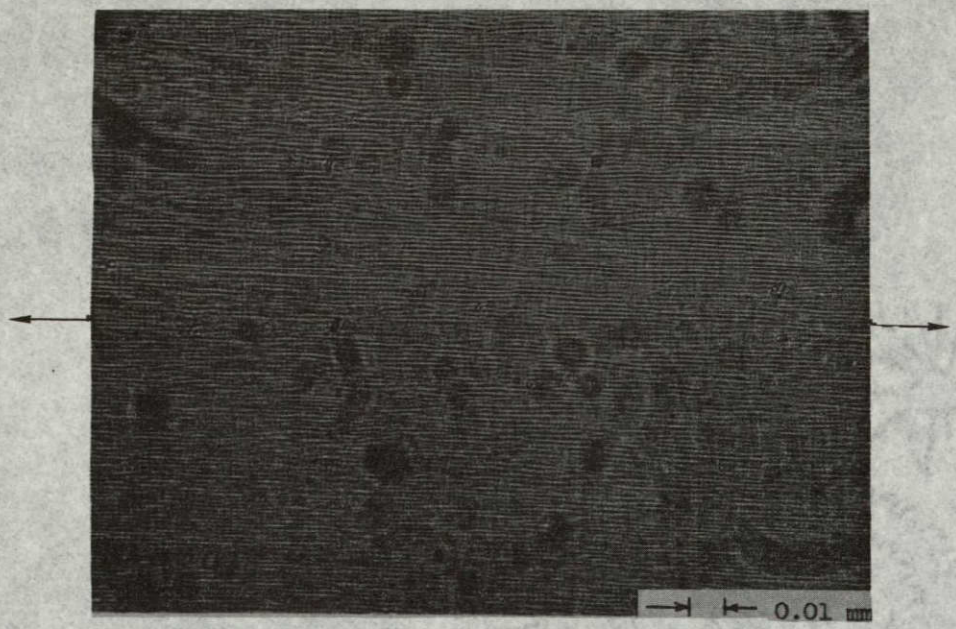

Transmitted brightfield

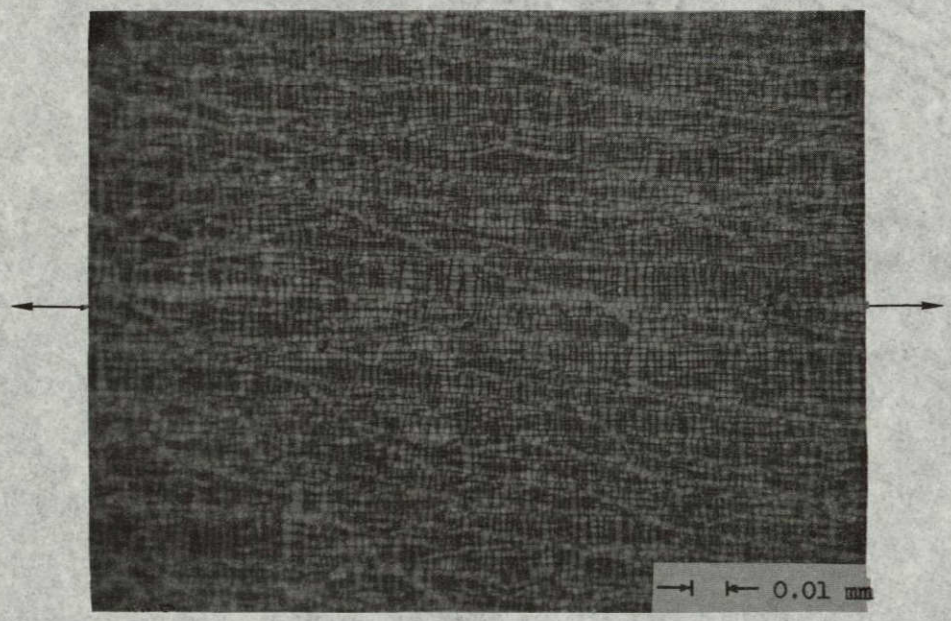

Reflected brightfield

(b) Transmittance (as deposited) = 59 percent.

Figure 24.- Continued.

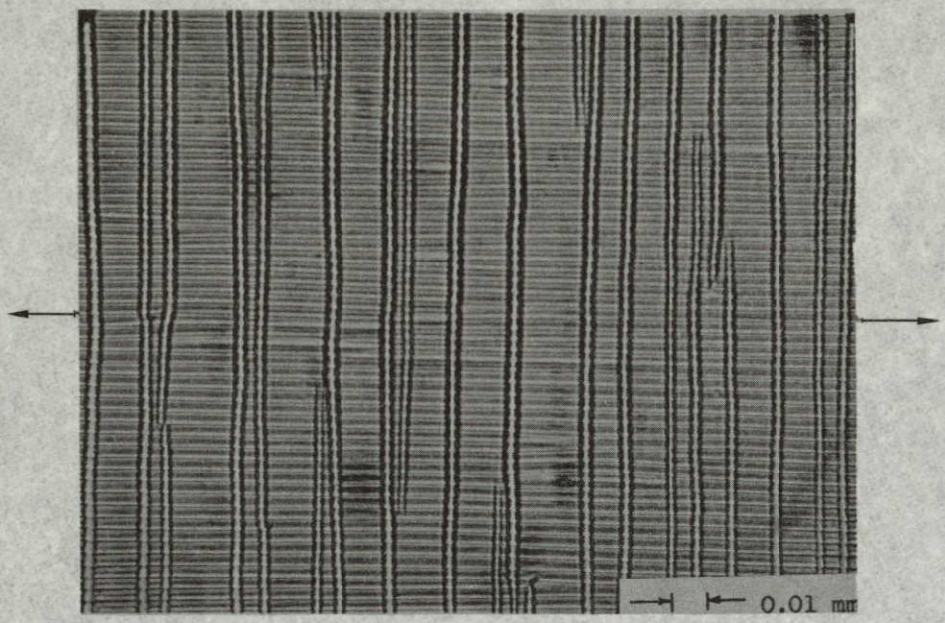

Transmitted brightfield

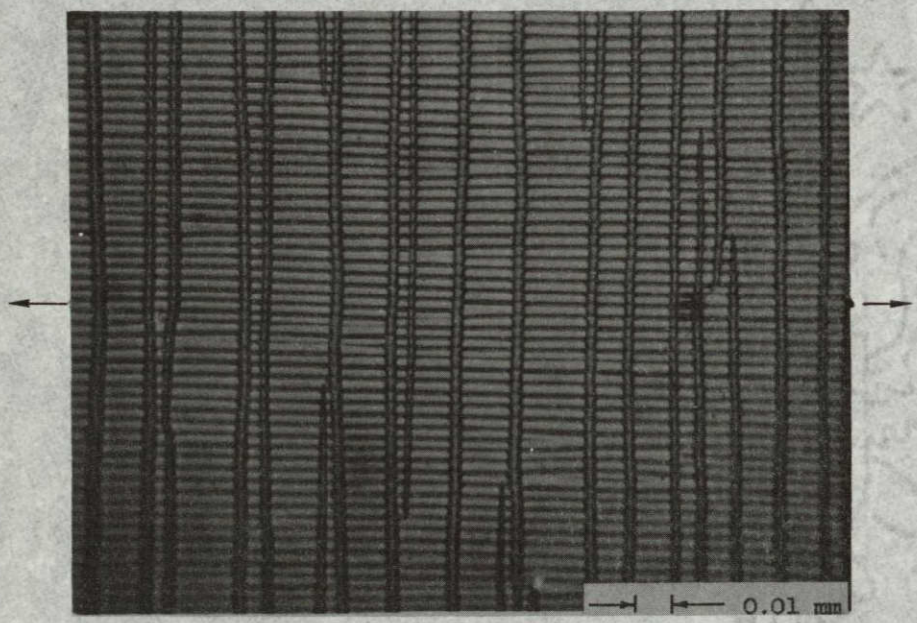

Reflected brightfield

(c) Transmittance (as deposited) = 80 percent.

Figure 24.- Concluded.

this anomaly is the different crystal structure (close packed hexagonal) observed by Quarrell (ref. 41) for very thin films. Such a crystal structure would be expected to have different mechanical properties than the normal face centered cubic form of aluminum.

The metal indium is a very ductile, highly plastic, and easily deformed material. It has a very low ultimate tensile strength (380 psi) and other unique mechanical properties as shown in table 3. The results of microscopic examinations of the surfaces of two specimens with thin film coatings of indium uniaxially loaded to impose a conventional strain in the direction of loading of 42 percent is presented in figure 25. The specimens for which the photomicrographs were taken were the same specimens used in total and central image transmittance measurements, the results of which were presented in figures 20 and 21. Figures 25(a) and 25(b) correspond to figures 20 and 21, respectively. The microfracture and wrinkle patterns of figure 25(a) are regular and clearly defined. Both microfracture and wrinkle patterns are distinguishable in figure 25(b) at this same level of magnification, but with less regularity and definition. Recalling the results of central image transmittance measurements for these two specimens, it is perhaps the breaking up of the regularity of the wrinkle pattern by such a high frequency of microfractures in combination with the unusual mechanical properties of indium which caused the limited influence of diffraction in the test results reported in figure

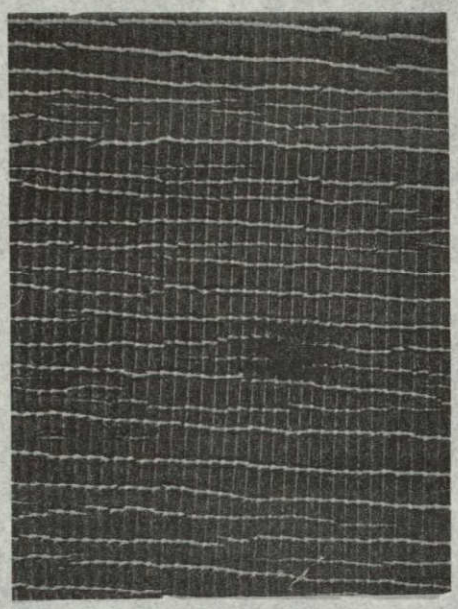

Transmitted brightfield

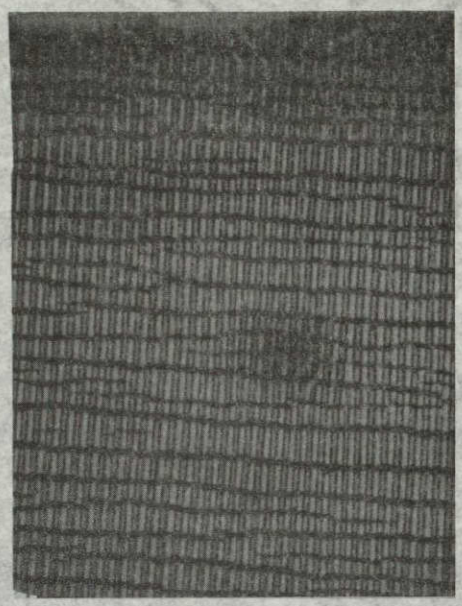

Reflected brightfield

(a) Initial transmittance = 7.5 percent.

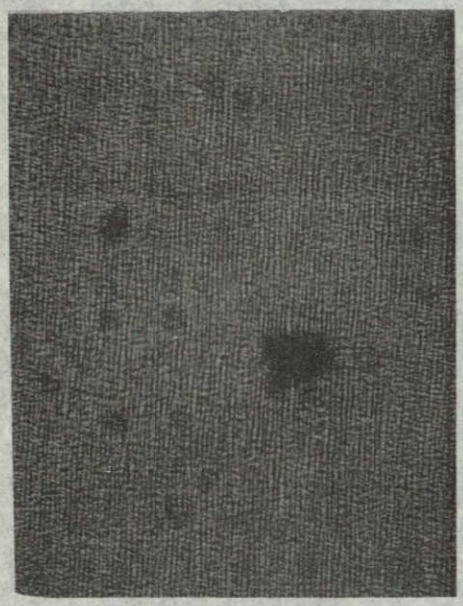

Transmitted brightfield

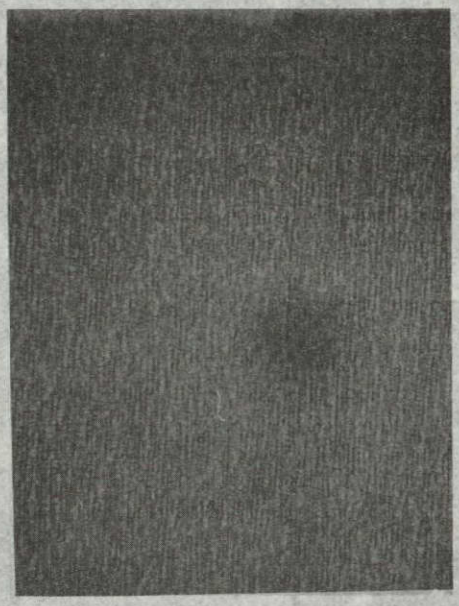

Reflected brightfield

(b) Initial transmittance = 1 percent.

Figure 25.- Photomicrographs of thin films of indium deposited on a silicone rubber substrate uniaxially loaded to impose a conventional strain of 42 percent ($\epsilon^{L}_{xx} = 0.42$).

21(b). In comparison, the frequency of wrinkles and microfractures for aluminum (figure 24(b)) are roughly of the same order of magnitude, but in this case excellent spectral separation was exhibited as will be shown in Section 3.1.3.3.

The microscopic examination of metallic thin films deposited on structural substrates subjected to uniaxial loading, all exhibited characteristic wrinkling along the direction transverse to the direction of loading. The strain in the direction transverse to the direction of loading for a case of uniaxial loading is, of course, negative. Uniaxial loading therefore, subjects the thin film in this direction to a state of compressive loading. Wrinkling in the direction of loading therefore confirms the physical model proposed in Section 3.0.2.1 for the compressive wrinkling of a thin metallic film deposited on a thick low modulus substrate.

To further confirm this model, a specimen of silicone rubber was subjected to a uniaxial preload ($\epsilon^{L}_{xx} = 0.62$) and then deposited with a thin film of aluminum (initial transmittance = 36 percent). Upon release of the preload the specimen was observed microsopically. Photomicrographs of the response for this case are presented in figure 26. In this case, line elements characteristic of microfractures developed parallel to the direction of prestretch; and line elements characteristic of wrinkling developed transverse to the direction of prestretch. Strains imposed on the coating by the release of preload are negative (compressive) along the direction parallel to the direction of prestretch and positive (tensile) in the direction

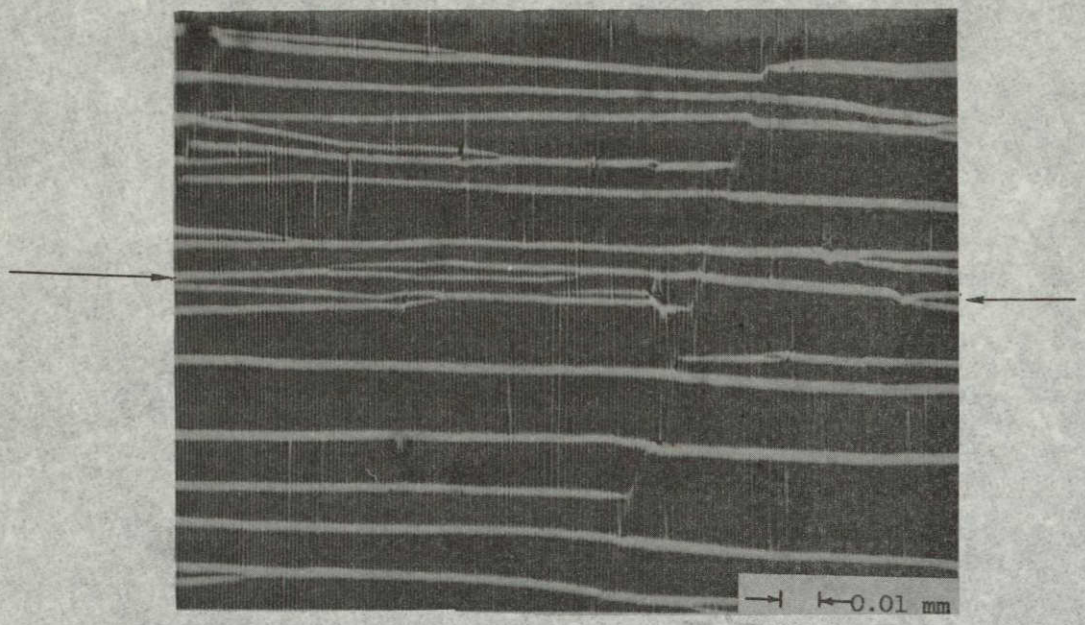

(a) Transmitted brightfield.

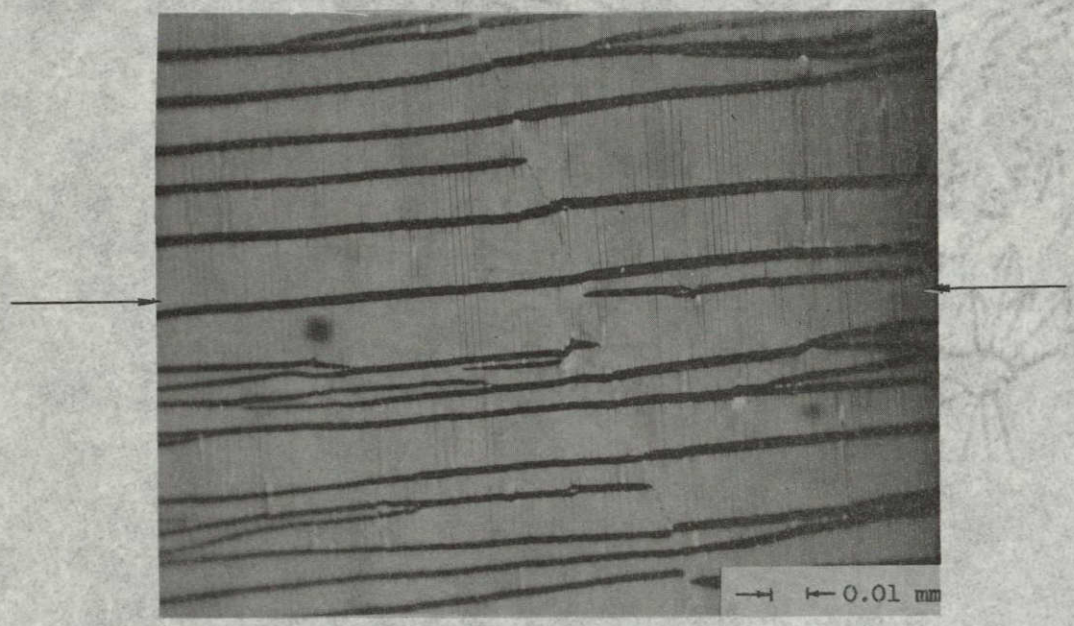

(b) Reflected brightfield.

Figure 26.- Photomicrographs of thin films of aluminum deposited on prestressed silicone rubber substrate (ϵ^{L}_{xx} = 0.62) taken after imposed prestress released. Transmittance as deposited = 36 percent, central image transmittance after release of prestress = 25 percent.

perpendicular to it. As predicted by the wrinkling and microfracture models, one observes wrinkling due to compressive loading along the direction of preload and microfractures due to failure of the film in tension along the direction transverse to the direction of the applied prestress.

The nature of the surface irregularities for a specimen subjected to a uniaxial load was also examined using a scanning electron microscope which measures backscattering of primary electrons. The photomicrographs presented in figure 27 show the results obtained in this study for specimens of silicone rubber with aluminum thin film coatings. Figures 27(a) and 27(b) are for two separate specimens with initial transmittances of 34 and 3.4 percent, respectively. The pictures clearly show the regular pattern of ridges and valleys characteristic of thin film compressive wrinkling. Characteristic microfractures are also exhibited although less clearly in figure 27(a) because of the orientation of the specimen for this particular photomicrograph. A slight rotation of the specimen during this test did show this feature to clearly be that characteristic of microfractures. The exact orientation of the specimen was not defined in these tests relative to the photograph, but it was observed that these are the same irregularities exhibited in optical microscope observations. Therefore, the direction of loading for these tests is indicated on the photomicrographs by association.

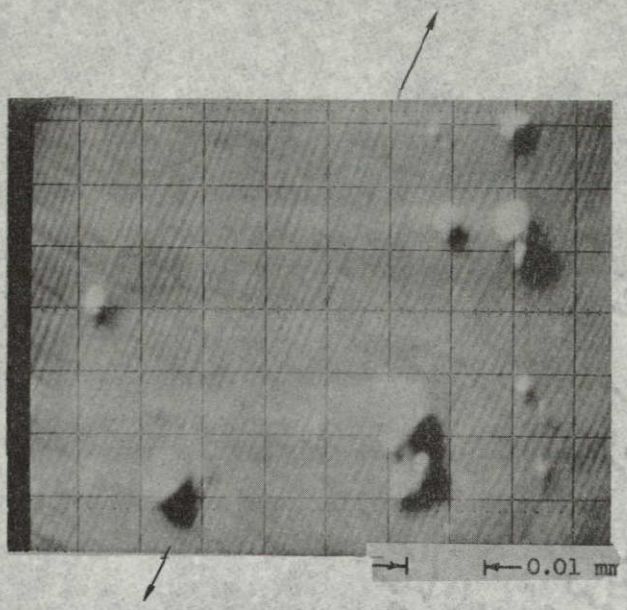

(a) Initial transmittance = 34 percent
Imposed conventional Lagrangian strain = 37 percent.

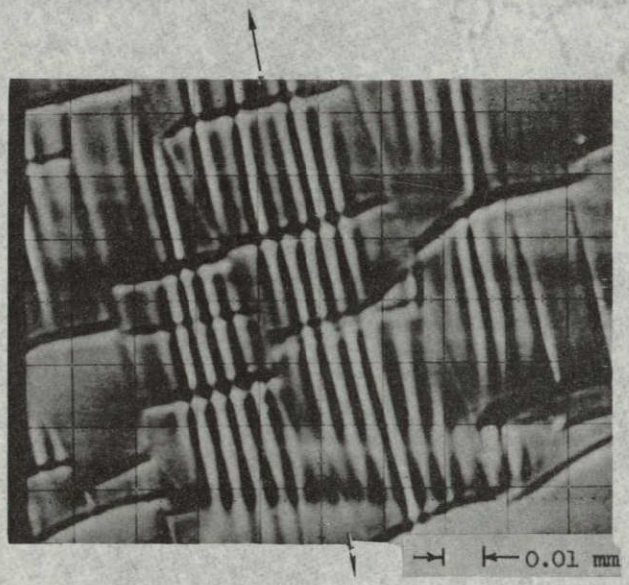

(b) Initial transmittance = 3.4 percent
Imposed conventional Lagrangian strain = 16 percent.

Figure 27.- Electron microscope photomicrographs of uniaxially loaded specimens of thin films of aluminum deposited on a silicone rubber substrate.

3.1.3.3 Diffraction Grating Spectrum

The theory proposed in Section 3.0.2 predicts that a closely spaced system of wrinkles which result in a sinusoidal type transmission pattern will create a diffraction grating which provides spectral separation. The results of Section 3.1.3.2 clearly establish the existence of a periodic and roughly sinusoidal type transmission pattern as a result of metallic thin film compressive wrinkling.

As predicted by theory, spectral separation was exhibited in uniaxial load tests (beginning at a strain of on the order of 2 percent) in which collimated light struck the wrinkled thin film surface. The light was diffracted radially from the area of illumination (both in front of and behind the specimen) into a region bounded by two planes drawn perpendicular to the direction of the applied load. The separation distance between planes was approximately equal to the length the specimen was illuminated along the axis of loading (with minor spread beyond those planes).

The test setup described in figure 13 was used to take photographs of the spectral distribution. Photographic results of two of these tests are presented as figures 28 and 29. The photographs of figures 28 and 29 were taken using the same aluminum coated specimens as were used in microscopic surface studies; the results of which were presented in figures 24(a) and 24(c), respectively. The circular image is due to the circular light aperture. The central image of figure 28 is very bright (so bright a mask had to be used to shut off its image to avoid burning out the image for the first and second order components).

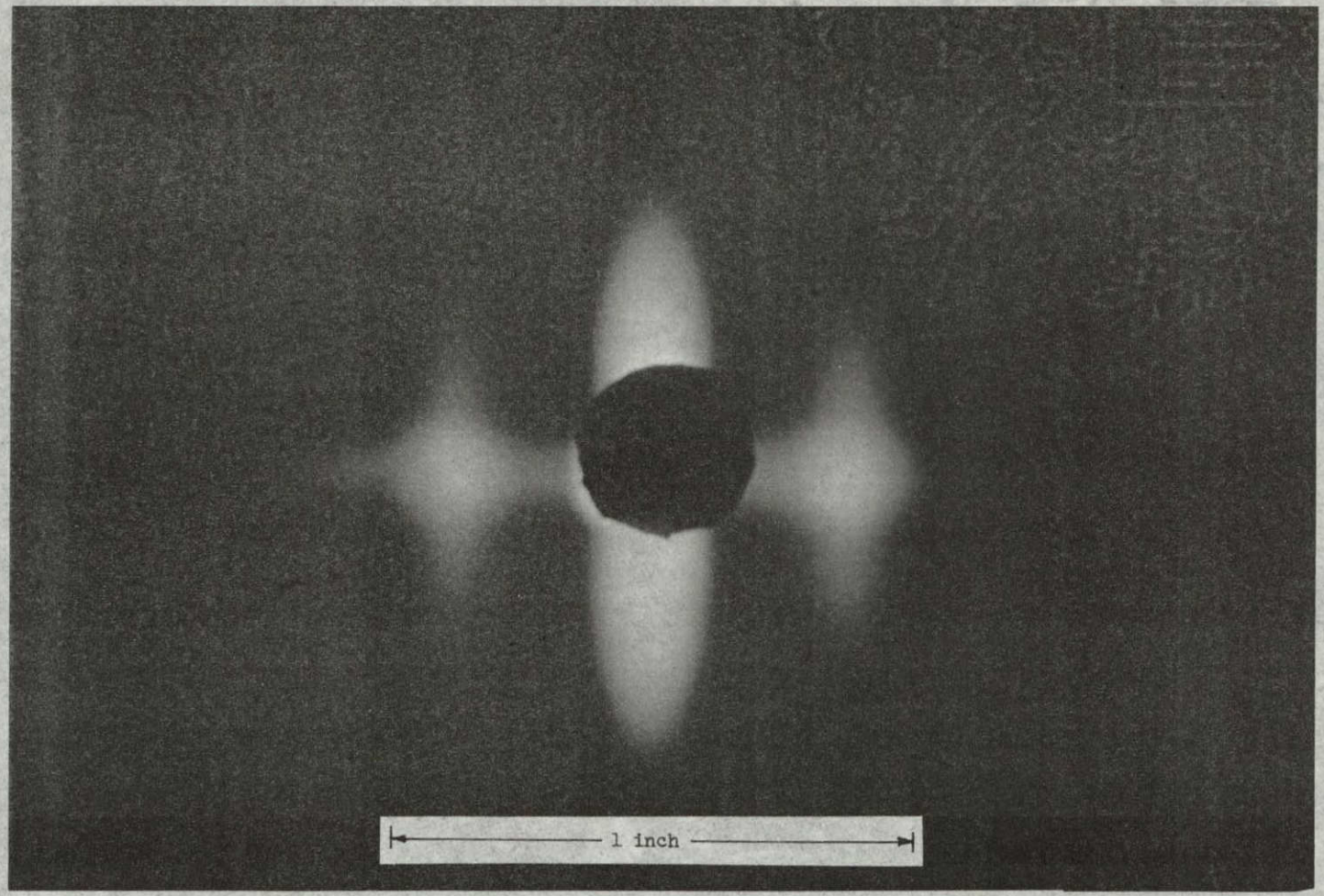

Figure 28.- Diffraction grating spectrum set up by collimated light beam striking uniaxially loaded specimen (ϵ_{xx}^{I} = 0.42) of aluminum thin film deposited on silicone rubber substrate. Initial transmittance = 10 percent.

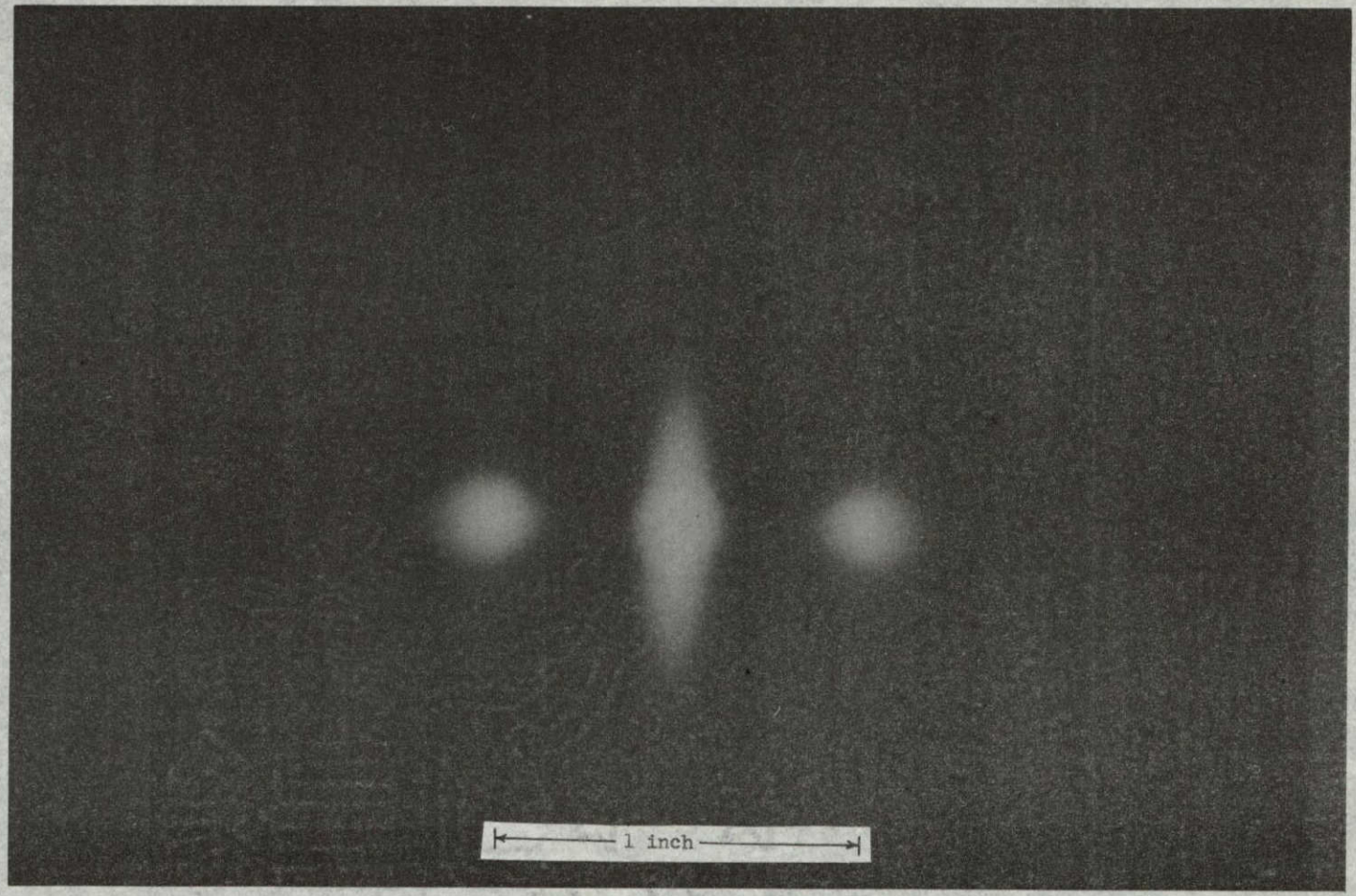

Figure 29.- Diffraction grating spectrum set up by collimated light beam striking uniaxially loaded specimen (ϵ_{xx}^{L} = 0.60) of aluminum thin film deposited on silicone rubber substrate. Initial transmittance = 80 percent.

This was typical of all of the tests conducted except for the one shown in figure 29. In this photograph the central image is of the same order of magnitude as the first order component. It also contains a distinct (although less intense) second order component. Some specimens in which the wrinkle frequency was very large (for example, that of the specimen for which the photomicrographs of figure 24(b) were made) did not exhibit detectable second order components. In such cases the angle over which the spectrum was spread approached 90°. This fact made total transmittance measurements unattainable for certain specimens because of the limitation of the collecting ability of the lens used.

It would appear that the change in spectral distribution and corresponding displacement of collimated light energy into side components set up by the wrinkled thin film diffraction grating, in general, fits fairly well the theory for Fraunhofer diffraction due to a sinusoidal type transmittance function. Both the sinusoidal amplitude grating and the sinusoidal phase grating (for $q = 1$) predict that the first order component will be displaced a distance of $f_o \lambda z$ from the central image. Computing this value for the tests of figures 28 and 29 by measuring f_o from the photomicrographs of figure 24, assuming a wavelength of 5000 $\mathring{A}$, and taking $z = 2.4$-inch from figure 13; one obtains computed values of 0.376 inch and 0.388 inch; respectively. The measured values from figures 28 and 29 are 0.36 inch and 0.41 inch; respectively.

3.1.3.4 Uniaxially Loaded Rectangular Plate With Centrally Located Circular Hole

Kirch published in 1898 (ref. 48) an exact elasticity solution subject to infinitesimal deformation assumptions for the stress in the vicinity of the hole of an infinitely wide plate with a centrally located hole subject to pure tension. This solution showed the principal stresses along the cross section located radial from the hole and perpendicular to the direction of the applied load to be of the following form:

$$\sigma_{xx} = \frac{\sigma_a}{2}\left(2 + \frac{r^2}{y^2} + \frac{3r^4}{y^4}\right)$$

$$\sigma_{yy} = \frac{3}{2}\sigma_a\left(\frac{r^2}{y^2} - \frac{r^4}{y^4}\right)$$

where

σ_a - uniformly applied stress in x-direction

r - hole radius

In recent years, because of an interest in nonlinear theories and in materials capable of large deformations; this problem has been reexamined assuming both physical and geometric nonlinearities. Adkins, Green, and Shield (ref. 49) were the first to publish an approximate solution (accurate to a second approximation) of Kirch's problem. Koifman (ref. 50) presents an approximate solution (accurate to the second approximation) for the stress concentration at the contour of the hole which is circular before deformation and becomes oval as a

result of deformation. Kirch's solution predicts a stress concentration of 3 0 at this point whereas the large deformation solution of Koifman results in stress concentrations less than this value. For a review of the literature on nonlinear problems of stress concentrations near holes in plates see reference 51.

It was proposed in Section 3.0.3 that the change in total transmittance under certain conditions (for an isotropic coating with a linear response) was related to the sum of the principal strains (eq. (3.28)). In addition, it was proposed that the change in central image transmittance was the difference between the total transmittance and the transmittance change induced by diffraction where diffraction effects were related to a compressive principal strain field (eq. (3.31)). The problem of a uniaxially loaded rectangular plate with a centrally located hole was experimentally studied in this investigation using transmittance measurement techniques to determine if the mathematical models were of the correct general form.

Three types of measurements were obtained in this study. These included total and central image transmittance data which were used to calculate the strain values presented in figure 30 and microscopic surface examinations of the specimen in the vicinity of the hole; the results of which are presented in figure 31. Separate specimens were used for the data of each of these two figures. Geometry for both of these specimens is shown in figure 31(a). Both specimens were composed of silicone rubber with an aluminum thin film coating. The load was applied along the longitudinal axis (x-direction)

and transmittance data was obtained for a scan along an imaginary line drawn radially from the center of the hole and perpendicular to the free edge. Measurements were made before the application of loading and with the specimen loaded sufficiently to impose an average conventional strain of approximately 8 percent.

The experimental solution for the sum of principal strains presented in figure 30(a) is based on substitution of the measured change in total transmittance between initial and final conditions into equation (3.29) where the proportionality constant W_5 is taken from the graph of figure 18(a) to be 0.53 percent change in total transmittance per percent strain. Kirch's solution to this problem for small deformations and Koifman's solution at the hole edge for large deformations are presented for comparison. The value from Koifman's solution is calculated using interpolation of data presented in reference 51 for a ratio of the uniformly applied stress in the x-direction to the substrate material shear modulus for the subject specimen of 0.279. The Koifman stress concentration factor thus determined is equal to 2.79 as opposed to 3.0 for the Kirch solution. The results obtained by the experimental solution at the hole edge are in agreement with the Koifman solution and the general shape of the curve across the section agrees with the Kirch solution.

The experimental solution for the principal compressive strain "ϵ^L_{yy}" presented in figure 30(b) is based on substitution of the difference in the change in total and central image transmittance measurements into equation (3.31) where J_2 is determined again using the

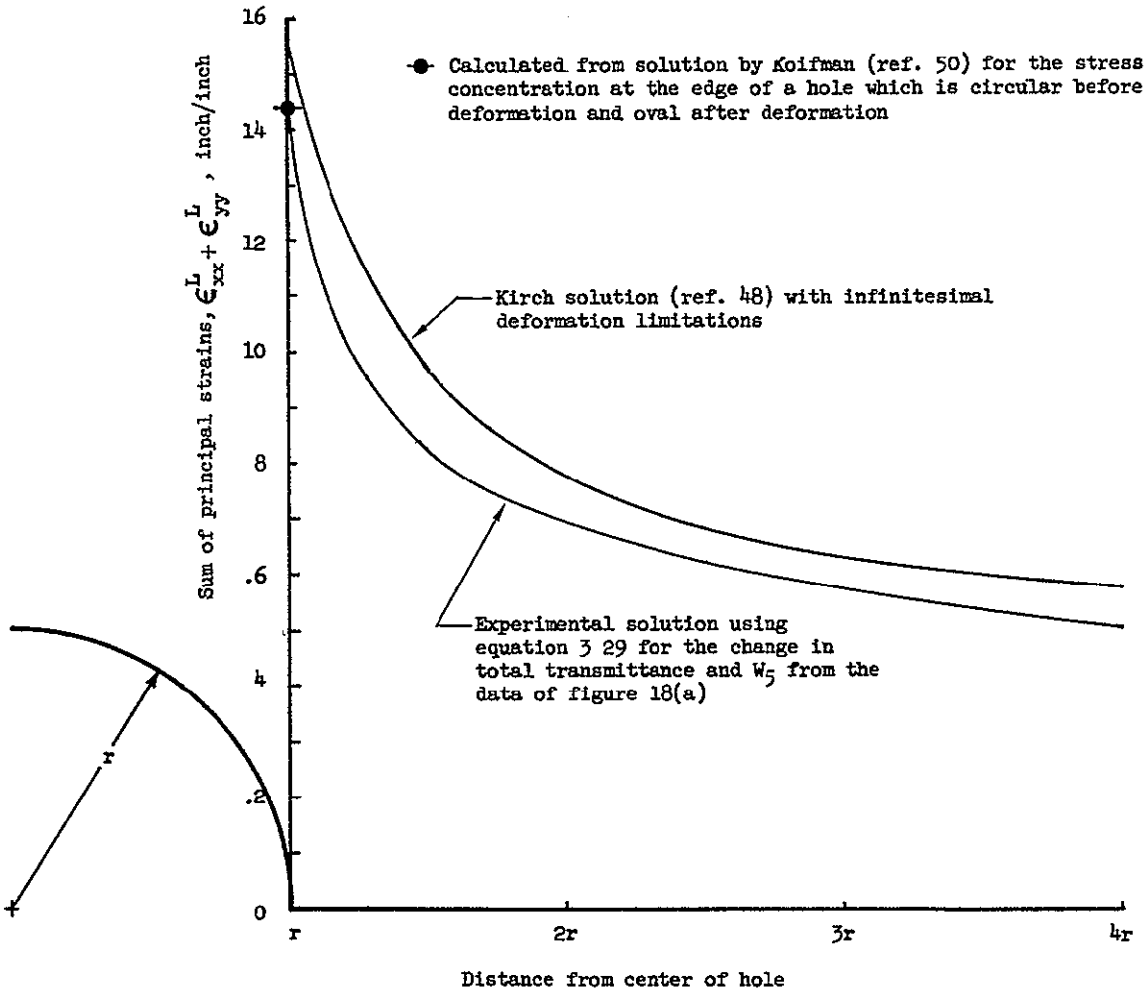

(a) Sum of principal strains, $\epsilon^L_{xx} + \epsilon^L_{yy}$

Figure 30.– Sum of principal strains and principal compressive strain plots for the section of minimum cross section of a rectangular plate with a centrally located hole subjected to loading along the longitudinal axis sufficient to impose an average conventional Lagrangian strain of approximately eight percent. Specimen composed of silicone rubber with a thin film coating of aluminum having an initial transmittance of approximately eight percent.

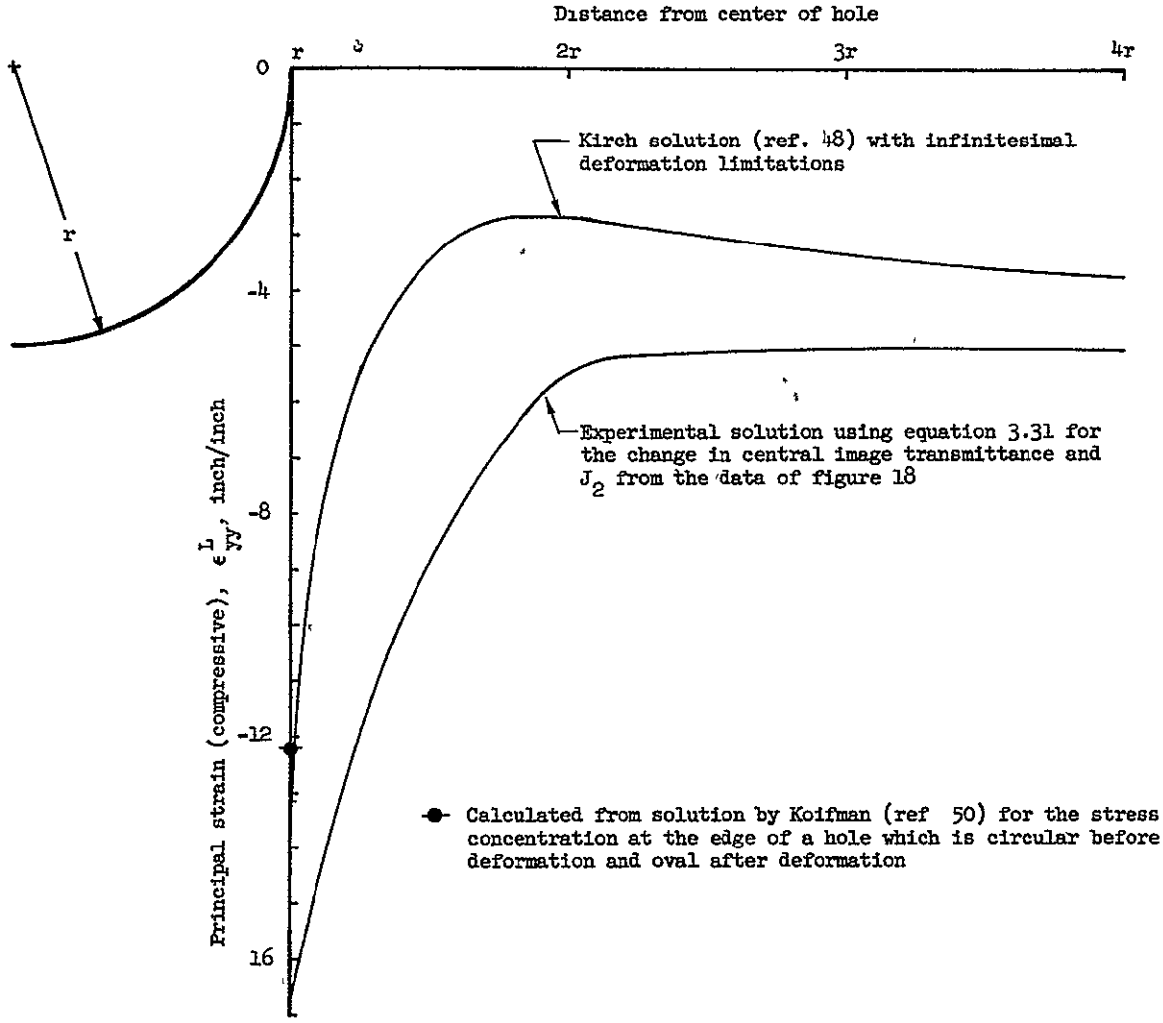

(b) Principal (compressive) strain, ϵ^{L}_{yy}

Figure 30.– Concluded.

calibration data of figure 18. The proportionality function "J_2" is taken as 0.824 and is the difference between the total and central image transmittances per unit strain. For an imposed compressive strain ϵ^L_{yy} of less than approximately 8 percent (which according to the Kirch solution is the case in this problem for all except very close to the hole), J_2 is by the data of figure 18 very nearly a constant (i.e., constant slope for both total transmittance and central image transmittance versus strain). The Kirch solution at the hole for large deformations is conservative as shown in figure 30(b) by the value plotted for ϵ^L_{yy} from Koifman's solution.

The experimental solution for ϵ^L_{yy} at the edge of the hole is too large by approximately 4 percent strain. It is believed that the difference is a result of applying the results of a similar, yet different, test specimen (aluminum coating deposited at a different time and with slightly different thickness) for the calibration of the proportionality functions. The total transmittance response for this material as well as for others tested (see figs. 18, 19, 20, and 21), in general, assumes an increasing and sometimes linear relationship with the imposed strain. The central image transmittance response, however, as shown in these same figures; exhibits both decreasing and increasing relationships to the imposed strain and is linear only within certain narrow regions. It is also influenced by a number of factors including wrinkle frequency. The results presented earlier have shown that considerable more study is required to establish the

exact relationship between the mechanical and physical properties of the coating and substrate and the corresponding wrinkle frequency.

In summary, the experimental results for the sum of principal strains (using the data of figure 18(a) total transmittance measurements for the calibration of the proportionality function W_5) agree well with theory. The experimental results for the principal compressive strain (using the results presented in figure 18 for the variation of the central image as well as total transmittance for the calibration of the proportionality function J_2) were greater than that predicted by theory, but the data for the section of minimum cross-sectional area had approximately the correct relative variation. The results therefore indicate that the empirical mathematical models proposed in Section 3.0.3 for the relationship between the change in total and central image transmittance and the strain field for a general biaxial problem are basically of the correct form. The application of these relationships with confidence, however, will require more experimental verification using models for which the proportionality factors are measured for specimens identical to the model. The application of the equations and especially the role of diffraction should be examined for other types of strain fields such as the case in which both principal strains are negative.

The set of photomicrographs presented in figure 31 show the surface irregularities created for this problem for several different locations in the vicinity of the hole. Position 1 at the top edge of the hole clearly exhibits thin film wrinkling but no microfractures.

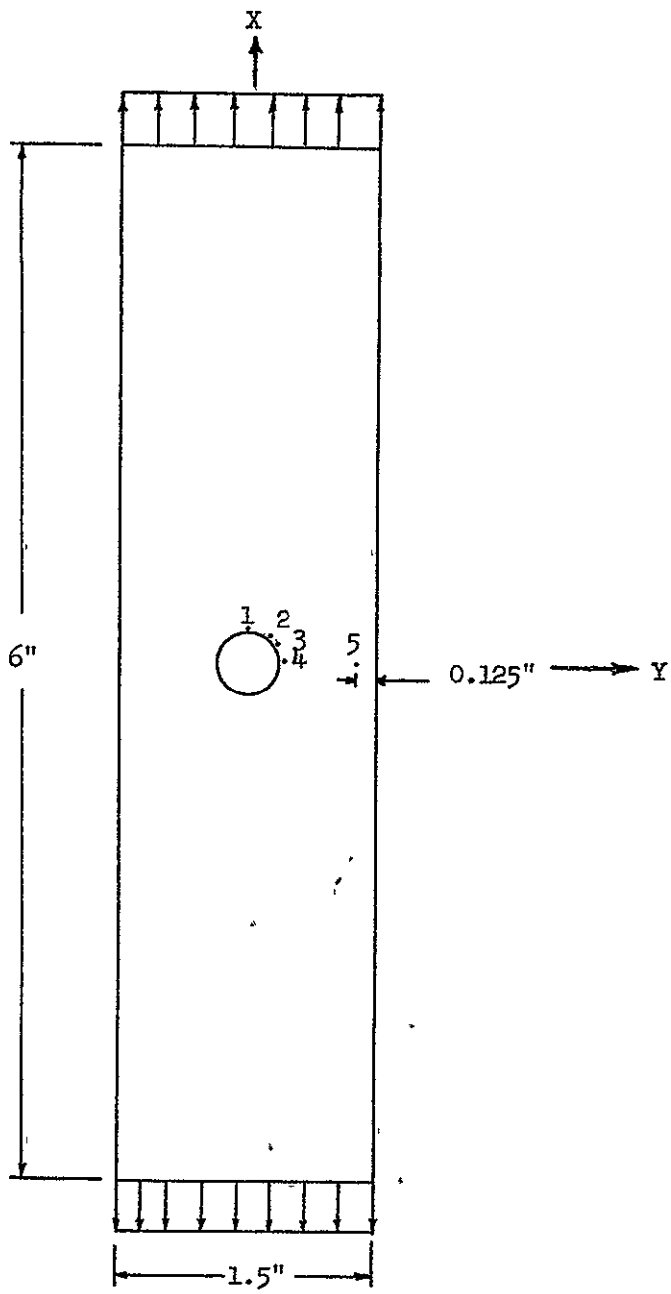

(a) Specimen geometry and photomicrograph position designation, specimen thickness = 0.106 inch.

Figure 31.– Surface study of wrinkle and microfracture pattern for rectangular plate with centrally located circular hole subjected to uniaxial loading. Silicone rubber substrate with thin aluminum coating with an initial transmittance of approximately 12 percent.

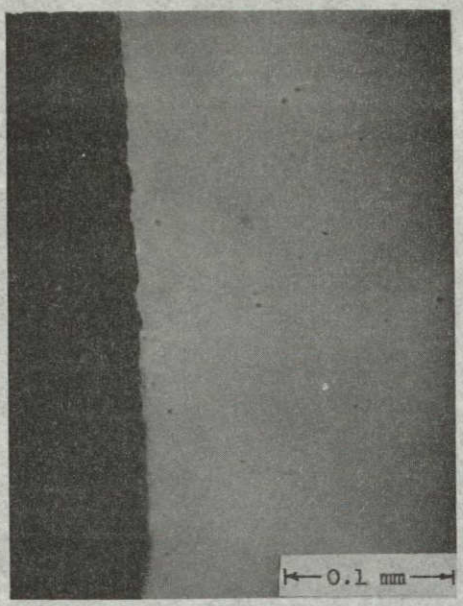

(b) Position 4, unstressed.

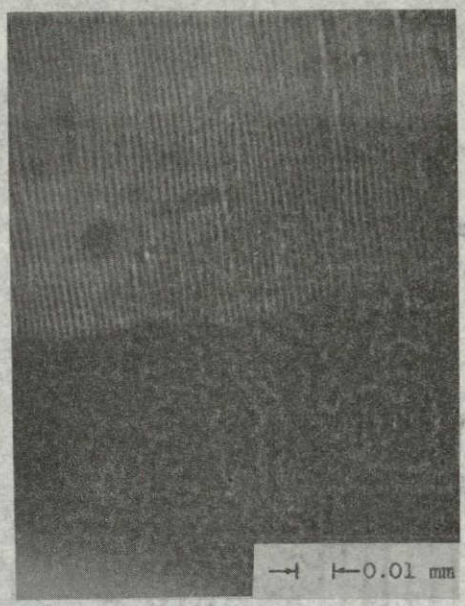

(c) Position 1, $(\epsilon^{L}_{xx})_{avg} = 0.08$.

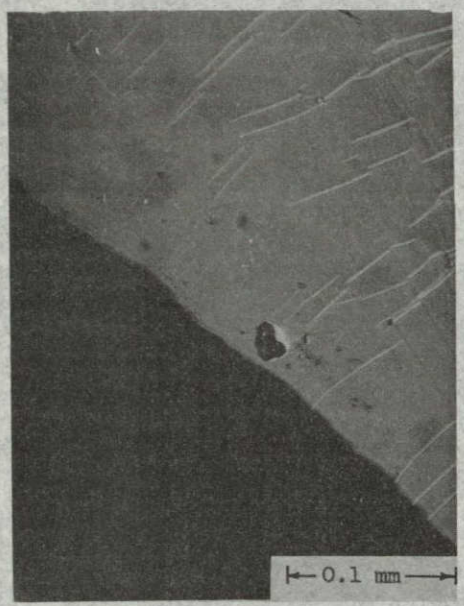

(d) Position 2, $(\epsilon^{L}_{xx})_{avg} = 0.08$.

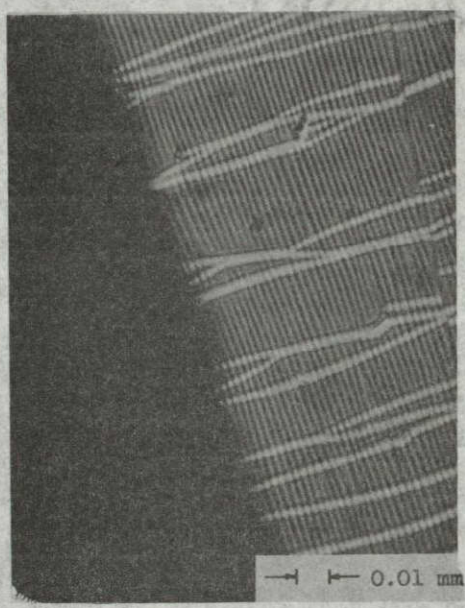

(e) Position 3, $(\epsilon^{L}_{xx})_{avg} = 0.08$.

Figure 31.- Continued.

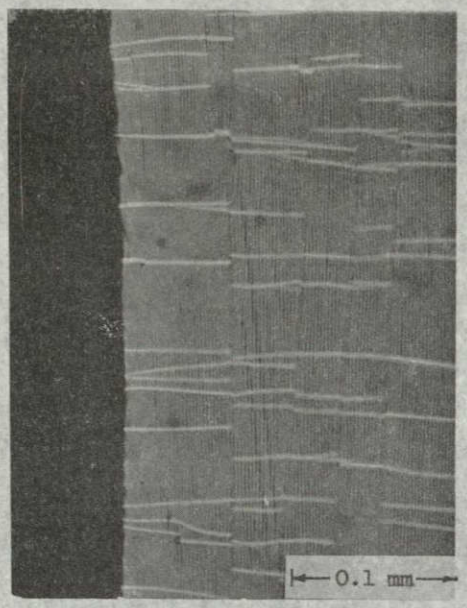

(f) Position 4, $(\epsilon^{L}_{xx})_{avg} = 0.025$.

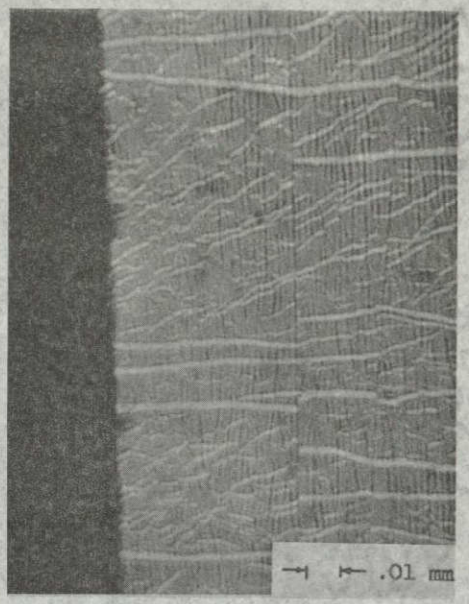

(g) Position 4, $(\epsilon^{L}_{xx})_{avg} = 0.08$.

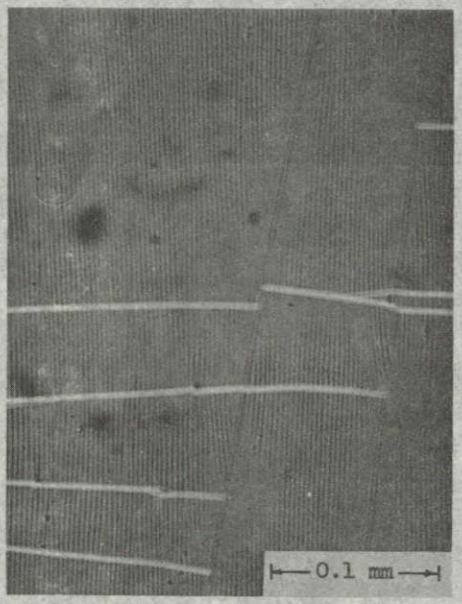

(h) Position 5, $(\epsilon^{L}_{xx})_{avg} = 0.025$.

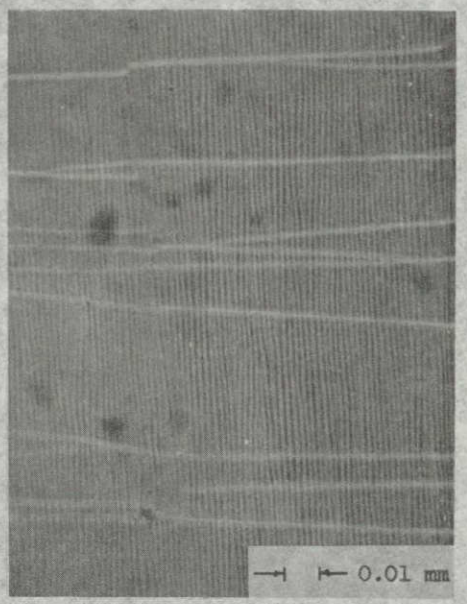

(i) Position 5, $(\epsilon^{L}_{xx})_{avg} = 0.08$.

Figure 31.- Concluded.

The Kirch solution for the stress at this point for an infinitely wide plate predicts that the σ_{yy} stress at this point is compressive and that the σ_{xx} stress is zero. Consequently, the strains at this point in the y and x directions are negative and positive, respectively, with the latter being of low magnitude. The development of the wrinkle pattern and absence of microfractures is thus in agreement with this result.

Position 4 at the right edge of the hole is shown for two different magnitudes of strain. These photomicrographs illustrate that at a low level of strain, lines characteristic of both wrinkling and microfracture are evident, but that at higher levels of strain, the wrinkle pattern seems to be less clearly defined. Spectral separation resulting from diffraction is clearly visible at this point, however, thus indicating a regular pattern of wrinkles. As one traverses from position 4 to 5, one begins to clearly pick up the regular pattern of both wrinkles and microfractures.

The photomicrograph of position 2 is presented to illustrate the transition area in which wrinkles seem to disappear. Immediately below this region (position 3), wrinkles and microfractures are clearly visible. This result is in agreement with the solution for the circumferential stress at position 2, which is zero.

IV. DISCUSSION OF RESULTS

Experimental studies of the total and central image transmittance properties of thin metallic films deposited on a low modulus substrate establish that a measurable variation in these properties occurs as a result of uniaxial loading of the substrate In general, the total transmittance increases with increasing magnitudes of imposed strain and in some cases the relationship is linear. It is proposed that the change in total transmittance response is caused by two factors: (1) by a change in the thin film effective thickness and (2) by the development of microfractures. Microscopic surface examination studies show that the accumulative width of microfractures per unit length increases with increasing magnitudes of positive strain. Data would also indicate the influence of effective thickness changes as well. The central image transmittance exhibits both increasing and decreasing relationships to an imposed strain field which is compressive in one of the principal directions. It is influenced by diffraction effects which are a result of the response of light to a set of closely spaced wrinkles which develop in the thin film coating along the direction of the principal compressive strain. Microscopic surface examination studies confirm the existence of these closely spaced wrinkles and also that the wrinkle frequency, in general, increases with increasing magnitudes of compressive strain Visual observations and photographic results also demonstrate the spectral wavelength separation resulting from this closely spaced wrinkle diffraction grating.

Change in transmittance properties are detectable for a range of strains of from on the order of 1 percent or less to very large magnitudes of on the order of 100 to 200 percent. The upper limit is dependent among other things on the materials used and on the initial film thickness A wide range of sensitivities are available through judicious selection of the materials and test conditions used.

The results of studies of the strain field in the vicinity of the hole of a uniaxially loaded plate containing a centrally located hole appear, in general, to obey the general biaxial optical-mechanics' laws proposed for the relationship between total and central image transmittances and the imposed strain field. A more thorough study is needed, however, to establish if these relationships are general and if calibration inaccuracies are the cause of the high magnitudes of compressive strain reported for this biaxial strain problem

The discussion to this point has dealt primarily with the form of the relationship between light intensity properties and the mechanical state of the structure. The complete identification of the mechanical state at any point requires that the direction of these principal strains be identified as well as there magnitude. Two techniques evolved out of this investigation applicable to the solution of this problem. The first technique is the microscopic examination of the wrinkles and microfractures which apparently aline themselves along principal directions. The second technique is related to the first, but does not require microscopic detection It is visual observation of the diffraction spectrum which is oriented along the direction of a

principal compressive strain. In uniaxial tests the axis of this spectrum was perpendicular to the direction of the applied load. In the biaxial problem of the rectangular plate with a centrally located hole, lines associated with the diffraction spectrum were also observed. At positions 1, 4, and 5 (fig. 31), the axis of the spectrum was transverse to the direction of the applied stress. At position 3 the axis of the spectrum was perpendicular to the hole edge. Each of these results agrees with the theoretical predictions of the principal directions at these positions.

V. CONCLUDING REMARKS

The results of this investigation establish that one can relate changes in the mechanical state of a structure as a result of loading to the optical properties of a thin metallic film deposited on it. Two fundamental types of optical responses occur. These include: (1) changes in the total intensity and (2) changes in the central image intensity of light energy transmitted or reflected by the material. The theoretical relationships developed in this paper have been developed for both transmittance and reflectance types of measurements. Experimental studies, however, were concentrated on the transmittance type. It is believed that parallel results also exist for reflectance types of measurements. The latter is important if one wishes to determine the mechanical response of opaque structures using this technique.

The results of experimental studies of the strain field in the vicinity of the hole in a uniaxially loaded rectangular plate containing a centrally located initially circular hole demonstrate that the technique is potentially useful for the determination of the strain field of a general biaxial problem. More study of the problem is needed, however, to establish the validity of proposed empirical optical-mechanics laws for a more general strain field. Also, thorough characterization of the optical response of thin metallic films used in this technique is required to accurately calibrate the proportionality functions used.

Although a set of total and central image measurements appear to be sufficient to completely define the strain field, it may be desirable in certain applications to combine the total transmittance technique with existing experimental techniques such as photoelasticity or holography for the solution of a problem. Also, the regularity of wrinkles and manner in which their frequency varies with strain suggests that a moiré approach could be developed in which fringes are created by the superposition of a set of photomicrographs of the same specimen area taken at successive levels of strain.

It should be pointed out that this new experimental strain analysis approach is most applicable to the study of problems with large deformations. The limited sensitivity of the technique for very small strains makes it noncompetitive with existing techniques for this problem. For the solution of large deformation problems; however, with development, it is seen as a valuable new approach.

It is interesting to note that this strain analysis approach, although new, ties together in a logical manner long-established optical and physical principles and techniques The variation of transmittance and reflectance properties with the thickness of a thin metallic film, for example, has been known and applied in the field of optics for years. Also, the approach is an optical one and therefore experimentally shares much with photoelasticity; and the development of microfractures in the thin film coating is closely related to the development of fractures in brittle coating techniques It is perhaps three factors which make the appearance of this new

approach now timely. (1) the relatively recent development of thin film deposition techniques; (2) the current interest in large deformation problems and associated nonlinearities; and (3) the availability and utilization in structural applications of modern plastics which because of their low modulus relative to metals may experience relatively large deformations.

VI. REFERENCES

1. Rivlin, R. S. Large Elastic Deformations. Chapter 10 of Rheology, vol. I, F. R. Eirich, ed., Academic Press, Inc., 1956, pp. 351-385.

2. Durelli, A. J., Parks, V. J.; and Feng, H.: Experimental Methods of Large Strain Analysis. Int. Jnl. Non-Linear Mech., vol. 2, no 4, Pergamon Press, Dec. 1967, pp 387-404.

3. Dally, James W.; and Riley, William F.. Experimental Stress Analysis. McGraw-Hill Book Co., Inc., 1965.

4. Williams, Jerry G. Flexible Reinforced Composite Window Material. Third Aerospace Expandable and Modular Structures Conference, AFAPL TR 68-17, May 1967, pp. 63-88. (Also available as NASA TM X-60137.)

5. Williams, Jerry G.; and Judd, Joseph H.: Measurement of the Effect of Factors of the Space Environment on the Properties of Some Flexible Transparent Polymers. Prospective NASA TN.

6. Novozhilov, V. V.. Foundations of the Nonlinear Theory of Elasticity. Graylock Press, 1953.

7. Green, A. E.; and Zerna, W.: Theoretical Elasticity. Oxford University Press, 1960.

8. Green, A. E.; and Adkins, J. E.: Large Elastic Deformations and Non-Linear Continuum Mechanics. Oxford University Press, 1960.

9 Biot, Maurice. Mechanics of Incremental Deformations. John Wiley and Son, Inc., 1965.

10. Durelli, A. J., and Mulzet, A. P.: Large Strain Analysis and Stresses in Linear Materials. J. Engng. Mech., Div. Am. Soc. Civ. Engrs, 91, June 1965, pp. 65-91.

11. Parks, V. J.; and Durelli, A. J. On the Definitions of Strain and Their Use in Large-Strain Analysis. Experimental Mech., 7 (6), June 1967, pp. 279-280.

12 Parks, V. J.; and Durelli, A. J.: Natural Stress. Int. J. Non-Linear Mech., vol. 4, Pergamon Press, 1969, pp. 7-16.

13. Frederick, Daniel; and Chang, Tien Sun: Continuum Mechanics, Allyn and Bacon, Inc., 1965.

14. Newton, Sir Issac Optics. Great Books of the Western World, vol. 34, R. M. Hutchins, ed., Encyclopedia Britannica, Inc., 1952, pp. 375-544.

15. Faraday, Michael The Bakerian Lecture. Phil. Trans. Roy. Soc. of London, vol. 147, 1857, pp. 145-181.

16. Anders, Hugo Thin Films in Optics. The Focal Press, 1967.

17. Born, Max, and Wolf, Emil· Principles of Optics, Macmillan Co., 1964.

18. Hass, George: Physics of Thin Films. Vol. 2, Academic Press, 1964.

19. Heavens, O. S.: Optical Properties of Thin Films. Butterworths Scientific Publications, 1955.

20. Vasicek, A.: Optics of Thin Films. North-Holland Publishing Company, 1960.

21. Schulz, L. G.· The Optical Properties of Silver, Gold, Copper, and Aluminum. I. The Absorption Coefficient "k." J. of the Optical Society of America, vol. 44, no. 5, May 1954, pp. 357-362.

22. Schulz, L. G.; and Tangherlini, F. R.: Optical Constants of Silver, Gold, Copper, and Aluminum. II. The Index of Refraction "n." J. of the Optical Society of America, vol. 44, no. 5, May 1954, pp. 362-368.

23. Hadley, L. N., and Dennison, D. M.:. Reflection and Transmission Interference Filters. J. of the Optical Society of America, vol. 37, no. 6, June 1947, pp. 451-465.

24. Berning, Peter H.· Theory and Calculation of Optical Thin Films. Vol. 1 of Physics of Thin Films, George Hass, ed., Academic Press, 1963, pp 69-121.

25. Heavens, O. S.· Measurement of Optical Constants of Thin Films. Vol. 2 of Physics of Thin Films, George Hass and Rudolf Thun, ed., Academic Press, 1964, pp. 193-238.

26. Harris, Louis, Beasley, John K.; and Loeb, Arthur L.· Reflection and Transmission of Radiation by Metal Films and the Influence of Nonabsorbing Backings. J. of the Optical Society of America, vol. 41, no. 9, Sept. 1951, pp. 604-614.

27. Jenkin, Francis A.; and White, Harvey E.: Fundamentals of Physical Optics. McGraw-Hill Book Co., Inc., 1937.

28. Harris, Louis, and Loeb, Arthur L · Evaluation and Analysis of Optical and Electrical Constants of Thin Films as Functions of Reflectance and Transmission Data by Electronic Digital Computation. J. of the Optical Society of America, vol. 45, no. 3, March 1955, pp. 179-188.

29. Huygens, Christiaan: Treatise on Light. Great Books of the Western World, vol. 34, R. M. Hutchins, ed., Encyclopedia Britannica, Inc., 1952, pp. 547-619. (Originally published 1690.)

30. Goodman, J. W. Introduction to Fourier Optics. McGraw-Hill Book Company, 1968.

31. Hartman, Thomas E.: Density of Thin Evaporated Aluminum Films. J. of Vacuum Science and Technology, vol. 2, no. 5, Sept.-Oct. 1965, pp. 239-242.

32. Hetenyi, Miklos. Beams on Elastic Foundations. The University of Michigan Press, 1946.

33. Budiansky, Bernard, Seide, Paul; and Weinberger, Robert A.: The Buckling of a Column on Equally Spaced Deflection and Rotational Springs. NACA TN No. 1519, 1948.

34. Holland, L.. Vacuum-Deposition of Thin Films. Chapman and Hall, Ltd., Fourth printing, 1961.

35. Anon.· Sylgard 184 Potting and Encapsulating Resin. Dow Corning Bulletin 07-066, August 1963.

36. Hampel, Clifford A., ed.: Encyclopedia of the Chemical Elements. Reinhold Book Company, 1968.

37. Anon.. Materials Engineering Materials Selector Issue. Material Engineering, vol. 70, no. 5, 1969.

38. Tietz, T. E.; Meyers, C. L.; and Ly Hun, J. L.: The Effect of Concurrent Straining and a 1-Percent Magnesium Addition on the Recovery Behavior of Aluminum. WADD Technical Report 61-138, May 1961.

39. Hayden, Wayne; Moffatt, William G.; and Wulff, John: Structure and Properties of Materials, vol. III, Mechanical Behavior. John Wiley and Sons, Inc., 1965.

40. Sennett, R. S., and Scott, G. D.: The Structure of Evaporated Metal Films and Their Optical Properties. J. of the Optical Society of America, vol. 40, no. 4, April 1950. pp. 203-211.

41. Quarrell, A. G : Structural Changes During the Growth of Metal Films. Phys. Soc. of London, Proc., vol. 49, 1937, pp. 279-293.

42. Neugebauer, C. A : Structural Disorder Phenomena in Thin Metal Films. Vol. 2 of Physics of Thin Films, George Hass and R. E. Thun, ed., Academic Press, 1964, pp. 1-62.

43 Beams, J W.: Structure and Properties of Thin Films. John Wiley and Sons, Inc , 1959, p. 183.

44. Thun, Rudolf E.: Structure of Thin Films. Vol 1 of Physics of Thin Films, George Hass, ed., Academic Press, 1963, pp. 187-232.

45. Menter, J. W.; and Pashley, D. W.: Structures and Properties of Thin Films. John Wiley and Sons, Inc., 1959, p. 111.

46. Andrade, E N. Da C.; and Martindale, J G · The Structure and Physical Properties of Thin Films of Metal on Solid Surfaces. Phil. Trans. Roy. Soc. London, vol. CCXXXV - A747, 1935, pp. 69-107.

47. Levinstein, Henry: The Growth and Structure of Thin Metallic Films. J. of Applied Physics, vol. 20, April 1949, pp. 306-315.

48. Kirch, G.: Die Theorie der Elastizität und die Bedürfnisse der Festigkeitslehre Zeitschrift der Vereines deutscher Ingenieure, vol. 42, 1898, p. 797.

49. Adkins, J. E., Green, A. E ; and Shield, R. T.: Finite Plane Strain. Philosophical Transactions of the Royal Society of London, series A, no. 910, vol. 246, October 29, 1953, pp. 181-213.

50. Koifman, Yu. I.· Reshenie ploskoi zadachi nelineinoi teorii uprugosti (A Solution to the Two-Dimensional Problem of the Nonlinear Theory of Elasticity for an Infinite Plate With a Curvilinear Hole). Izvestiya Vysshikh Uchebnykh Zavedenii, Seriya Stroitel'stvo i Arkhitektura, no. 1, 1962.

51 Savin, G. N.: Nonlinear Problems Of Stress Concentration Near Holes In Plates. Theory of Shells and Plates - Proceedings of the 4th All-Union Conference On Shells and Plates Held at Erevan; S. M. Durgar'yan, editor, October 24-31, 1962. Translated from Russian by the Israel Program for Scientific Translations. (available as NASA TT F-341)

V. ACKNOWLEDGEMENTS

For making this graduate study possible, the writer wishes to express his gratitude and appreciation to the following individuals and organizations:

To God for creating the Universe subject to an orderly set of laws and for giving the writer a healthy mind and body with which to pursue knowledge.

To the National Aeronautics and Space Administration for giving the writer the financial support necessary to make this graduate program possible.

To Dr. Daniel Frederick for his guidance and inspiration both as an instructor and as the writer's adviser.

To the other members of the writer's Graduate Program Committee for their helpful comments and suggestions.

To the staff of the National Aeronautics and Space Administration for giving assistance and providing services instrumental to the success of this program including preparing specimen, making test equipment, and preparation of this manuscript. A special expression of gratitude is due Mr. Joseph Judd for his suggestions and review of the writer's work from the very outset of this investigation.

To the writer's wife and family for their encouragement and patience during the course of this study.

VI. VITA

The author was born in 1939 in Ponca City, Oklahoma. He attended public schools in Oklahoma and graduated from Muskogee Central High School in 1957. He attended Oklahoma State University from 1957 through 1962 and received both B.S. and M S. degrees in civil engineering from this institution.

He has been an employee of the National Aeronautics and Space Administration, Langley Research Center since 1962 where he has been involved in research programs in the areas of materials, mechanics, and structures with special emphasis on manned expandable structures applications. He has published numerous papers in these fields.

The author is a member of the Society for Experimental Stress Analysis and is a registered Professional Engineer in the state of Virginia. As an undergraduate he was active in Chi Epsilon, Omicron Delta Kappa, Phi Eta Sigma, and Pi Mu Epsilon and was elected to Who's Who in American Colleges and Universities and Phi Kappa Phi.

Jerry Gene Williams